Steady State Modelling of Solid Oxide Cells

Modelling the steady state operational performance of solid oxide electrolysers/fuel cell systems in order to answer economic questions

Master Thesis

Andrew Spekreijse

Delft University of Technology

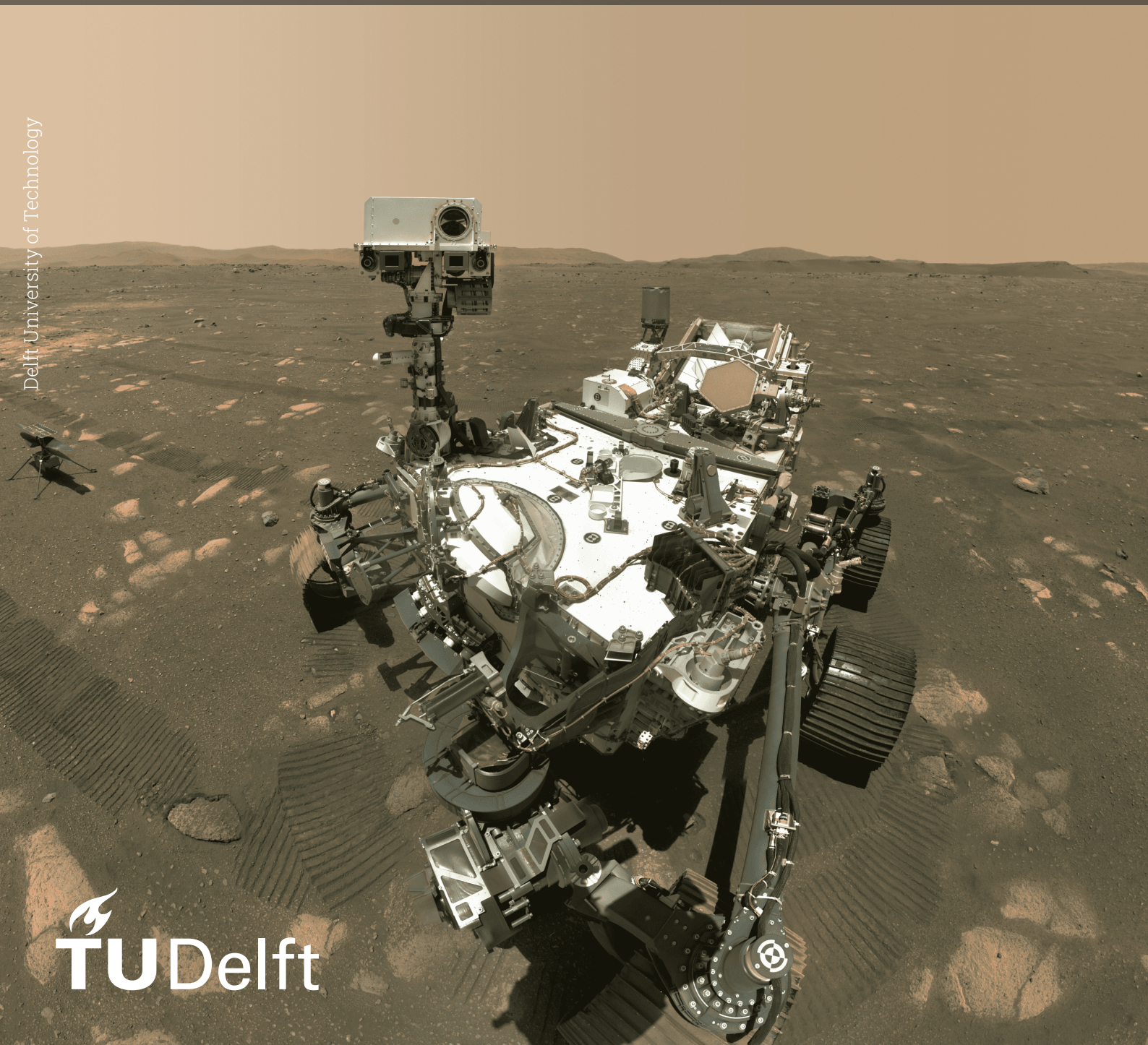

TU Delft

Steady State Modelling of Solid Oxide Cells

Modelling the steady state operational performance of solid oxide electrolysers/fuel cell systems in order to answer economic questions

by

Andrew Spekreijse

To be publicly defended on: The 30th of May 2023

Supervisor (TU Delft): Ir. Joris Melkert - Faculty of Aerospace Engineering
Supervisors (HyCentA): Di. Julius Rauh
Di. Fabian Radner
Prof. Dr. Alexander Trattner

Cover: Perseverance's Selfie with Ingenuity, Courtesy NASA/JPL-Caltech. Perseverance was sent to Mars in 2020 and onboard the rover there is an experiment called MOXIE. MOXIE, short for Mars Oxygen ISRU Experiment, is a small scale demonstration for creating oxygen gas from Mars's carbon dioxide atmosphere using solid oxide electrolysis, the foundational principal of this thesis

TU Delft

Preface

Kia Ora!

This thesis is the culmination of almost seven years being a student at Delft University of Technology. And what a seven years it has been! It was not seven years I ever expected to undertake when I was 17 years old at high school back in New Zealand; I never expected that I would even move to Europe to study. But I am glad I took the plunge and moved to Delft, because the experiences I have had in Europe have been priceless to my education, both academic and personal. From meeting hundreds of people from dozens of nationalities, to being enabled to explore European cities and countries, to being an active members of the VSV Leonardo da Vinci, Delft Aerospace Rocket Engineering and ALSKV Levitas, I have had a fantastic time living in Delft.

Of course studying and living on the other side of the world from where you grew up is not always fun. There were many personal, professional and academic challenges along the way with COVID-19 probably being the biggest challenge. However, nobody overcomes life's challenges truly alone, and I am ever so thankful to all my whānau and friends, both current and past, who were with me during the times I needed them and the times I didn't. The friends I have spanning around the globe from Europe, to Latin America, Australia and of course New Zealand, have been what has made the success of my student time, and this thesis, possible.

tēnā koutou,

Andrew Spekreijse
Graz, Austria, May 2023

Summary

With climate change is an undeniable reality, hydrogen based energy solutions will become increasingly important for specific aspects of economies. To meet emission targets, Solid Oxide Electrolysers (SOECs) and Solid Oxide Fuel Cells (SOFCs) will become an increasingly useful part of global energy infrastructure. Identifying the economically advantageous areas where SOECs and SOFCs can be deployed inside a complex economic and energy systems requires the creation of numerical models which are capable of analysing economic and energy markets as well as models which replicate the characteristics of SOEC/SOFC operations. This thesis describes the fundamental physical principals used to create numerical models which describe the steady state behaviour of solid oxide cells and SOEC systems and discusses the results for various operation strategies of SOEC systems.

Contents

Nomenclature

Abbreviations

Abbreviation	Definition
BOP	Balance of Plant
Capex	Capital Expenditure
DGM	Dusty Gas Model
GDC	Gadolinium Doped Deria
HHV	Higher Heating Value
ITnA	Institut für Thermodynamik und nachhaltige Antriebssysteme
IWT	Institut für Verbrennungskraftmaschinen und Thermodynamik
LSM	Lanthanum Strontium Manganite
OCV	Open Circuit Voltage
PEM	Proton Exchange Membrane
rSOC	reversible Solid Oxide Cell
ScSZ	Scandium Stabilised Zirconia
SO	Solid Oxide
SOC	Solid Oxide Cell
SOE	Solid Oxide Electrolyzer
SOEC	Solid Oxide Electrolyser Cell
SOFC	Solid Oxide Fuel Cell
TPB	Triple Phase Boundary
YSZ	Yttrium Stabilised Zirconia

1 Introduction

1.1. Why

Climate change is an irrefutable truth [1] and action must be taken immediately to prevent a countless number of human deaths and a sharp and rapid reduction in quality of life for those who remain. Solid oxide electrochemical systems offer an economically viable method to decarbonise national and global economies, helping attain national emission targets cheaply and sustainably. Solid oxide systems allow improved access to hydrogen based energy as a viable and long term solution to long duration energy storage [2]. Hydrogen based energy also allows the possibility of replacing fossil fuel usage in industries where high temperatures are required and where electrical heating is not sufficient, such as steel production.

Hydrogen based energy refers to chemical compounds which store/contain hydrogen within them such as hydrogen gas or ammonia. All hydrogen based energy typically requires hydrogen to be produced first and currently this is done via **steam methane reformation** which uses water and natural gas (methane) to produce hydrogen and carbon dioxide. This is an inherently unsustainable method of hydrogen production and will not help meet emission targets. Electrolysis, however, is the splitting of water into hydrogen and oxygen by applying a voltage across the water. This method of hydrogen production is well established and has been used for decades, although due to current costs is not the favoured method of hydrogen production [3]. Unlike steam methane reformation, electrolysis is a sustainable form of hydrogen production, as water on Earth is effectively a limitless supply of hydrogen for the amount of energy which humanity will be required to store/use. Solid oxide systems, owing to their high efficiencies of around 85% and utilisation of non rare earth elements, offer an economically inciting solution to the current high cost of electrolysis. It is imperative then, that economically viable use cases for solid oxide electrochemical systems are identified so development and deployment of these systems can begin. This is one of the research focus areas of **HyCentA Research GmbH**.

1.2. Thesis at HyCentA

HyCentA GmbH (Hydrogen Centre Austria) is a research institute based in Graz, Austria. It is a private institution co-owned by TU Graz and industry partners with the intent to research and develop hydrogen technologies. As of writing, the current CEO is Prof. Dr. Alexander Trattner. HyCentA undertakes many projects in its capacity as a research institute. This thesis fall under the scope of the **HyTechnomy** project. The HyTechnomy project is focused on researching the technologies required for a hydrogen based economy along with how these technologies can be deployed in the most economic and profitable way. Within the HyTechnomy project, there are various projects related to different hydrogen technologies, such as mobility, storage and production. This thesis topic specifically falls under the production sub-project, known as the **HyGen**[1] project. This project investigates the different forms for hydrogen production and how these technologies can be deployed in an economically sustainable way. As of writing, HyGen has extensively investigated the current state of the art electrolyser systems,

[1] HyGen is short for Hydrogen Generation

Proton Exchange Membrane (PEM) electrolysers. While well established , PEM systems suffer from limited material availability (such as iridium metal) [4] which results in high capital expenditure (capex) costs for the deployment of PEM electrolyser systems, causing higher levelized costs of hydrogen production [2], inhibiting the large scale up of hydrogen production from PEM systems.

Solid Oxide Electrolysers Cells (SOECs), offers a potential solution to some of the challenges of PEM because of the utilisation of cheaper and more abundant materials, lowering the capex and levelized cost of hydrogen production. While many challenges with the implementation of Solid Oxide Cell (SOC) systems exist (see section 2.5), the creation of numerical models describing solid oxide system operation will allow for faster system design along with reducing time required to identify suitable markets for system deployment and commercialisation.

Therefore, the purpose of the thesis is to provide easy to use detailed computer models to HyCentA, which model the steady state operation of (SOCs) and accompanying systems. Because of the potential of SOCs and because the HyTechonomy project investigates all aspects of the hydrogen economy, the models will be created in such a way that they are applicable to both Solid Oxide Electrolyser Cells (SOECs) and Solid Oxide Fuel Cells (SOFCs) for a range of commercially interesting fuel types (see subsection 2.4.1).

HyCentA has limited experience modelling and working with SOCs. This thesis and the model which will be produced, will be a foundational work upon which further research at HyCentA in the area of SOCs will be expanded from. Therefore the thesis report will be explicit in describing SOCs and solid oxide systems to researchers who have limited experience in the field. Additionally, the models created from this thesis must be clearly and sufficiently documented and designed such that future reuse of the models require minimal effort and future upgrades to the models are easy to implement.

[2] That is, the operating costs to produce one unit of hydrogen

2

Literature Review

This chapter will begin with an overview of electrochemistry and electrochemical devices, then it will discuss Solid Oxide Cells (SOCs) in more detail. Afterwards, an overview on the components required for the operation of SOCs, known as the Balance of Plant (BOP) is presented. Finally, an overview of the unique characteristics of SOCs is given.

2.1. Electrochemistry Overview

Electrochemistry is the branch of chemistry which deals with using electricity to perform chemical reactions, typically called **electrochemical** reactions. Electrochemical reactions are a specific type of chemical reaction called **Redox** reactions (Reduction and Oxidation), which occur at the surface of an **electrode**. An electrode is a material which is either negatively or positively charged; electrodes are one of the basic components of an **electrochemical cell**.

An electrolyser or fuel cell, in their most basic form, are **electrochemical cells**. Basically, electrochemical cells are devices in which there are two electrodes present, one negatively charged, one positively charged, at which redox reactions occur at both electrodes. Between the electrodes is an **electrolyte** (in which charged ions pass through) and an external circuit in which electrons travel through. Batteries are another type of electrochemical cell. A graphical view of an electrochemical cell can be seen in Figure 2.1. In an electrochemical cell, the cathode is where the reduction reaction occurs and the anode is where the oxidation reaction occurs.

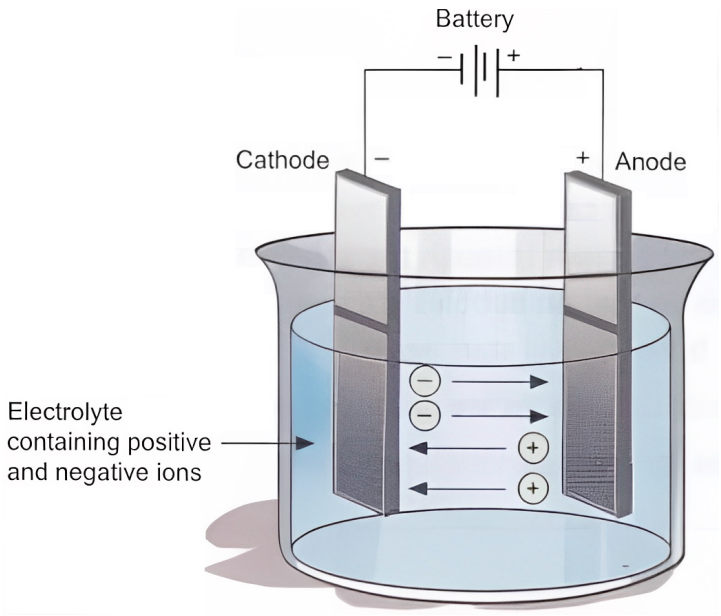

Figure 2.1: Example of a generic electrochemical cell. Image taken adapted from [5]

It should be explicitly noted that there exist different types of electrolyser/fuel cell devices and they follow similar principals to the upcoming explanation of electrochemistry, although the ions which move are different (i.e. OH^- or H^+ ions move through the electrolyte instead of O^{2-} ions) in the case of water electrolysis/fuel cells. The following explanation with accompany chemical equations are **specifically** for SOCs for water electrolysis/fuel cells. An overview of other electrolyser types can be found in subsection 2.1.3. In SOCs, other species such as carbon dioxide, methane and ammonia can also be used in place of water or hydrogen and this is discussed further in subsection 2.4.1. However, the upcoming explanations of electrolysis, which are the foundation of which the models will created upon will be applicable for these different chemical species as well.

2.1.1. Basic Equations

An electrolyser, is a device which can split water into its base elements, hydrogen and oxygen. The basic chemical reaction for this process is as follows:

$$H_2O \longrightarrow H_2 + 0.5\,O_2$$

More specifically, an electrolyser is a device which performs a **redox** reaction on water. That is, it **reduces** and **oxidises** the water to produce hydrogen and oxygen. This process occurs following these **half-equations**:

$$H_2O + 2\,e^- \longrightarrow H_2 + O^{2-} \text{ (reduction)}$$
$$O^{2-} \longrightarrow 0.5\,O_2 + 2\,e^- \text{ (oxidation)}$$

Two mols of electrons reduce the water to hydrogen gas and one mol of oxide ions. This one mol of oxide ions, which have a negative charge, move towards a location which has positive charge. At this location of positive charge, the oxide ions are **oxidised** to 0.5 mols of oxygen gas when the oxide ions loses their electrons to the location with positive charge.

A fuel cell is a device which can combined hydrogen and oxygen together to produce water. The basic chemical reaction for this process is as follows:

$$H_2 + 0.5\,O_2 \longrightarrow H_2O$$

In the above case of producing water from hydrogen and oxygen, half a mol of oxygen gas is **oxidised** to a mol of oxide ions at a location of negative charge, where by this mol of oxide ions move towards a location of positive charge where the oxide ions comes into contact with hydrogen gas, thereby the oxide ions **reduce** in the presence of the one mol of hydrogen gas to form one mol of water. The electrons which the oxygen gas released when it was oxidised, are recombined with the oxygen in the water molecules when the oxide ions are reduced. These electrons are able to do work while travelling from the location of negative charge to the location of positive charge. This process occurs following these half-equations:

$$0.5\,O_2 + 2\,e^- \longrightarrow O^{2-} \text{ (oxidation)}$$
$$H_2 + O^{2-} \longrightarrow H_2O + 2\,e^- \text{ (reduction)}$$

2.1.2. Thermodynamic Principals Of Electrolysis

Electrolysis typically refers to the production of hydrogen and oxygen from water, even though it has been mentioned that other compounds, such as CO_2, can also undergo a similar process to water electrolysis. Therefore, this section, while only talking about water electrolysis, is also applicable to other forms of electrolysis in as far as the mathematical formulations presented are applicable to other forms of electrolysis as well. Furthermore, often the mathematical formulations for electrolysis can be directly reserved and applied to fuel cells.

The fundamental principal of electrolysis is that water splits into hydrogen gas and oxygen gas when a potential (voltage) is applied over the water. To reiterate the balance chemical equation for this process:

$$H_2O \longrightarrow H_2 + 0.5\,O_2$$

The splitting of water is not a spontaneous reaction below water's thermal decomposition temperature of 2200°C, unless energy is provided to the water. In physics terms, the **Gibbs free energy** of this reaction is positive. Gibbs free energy is defined as:

Definition: Gibbs Free Energy

$$\Delta G_m \equiv \Delta H_m - T \cdot \Delta S_m \tag{2.1}$$

Where:
ΔG_m is the Gibbs free energy of a reaction [J/mol]
ΔH_m is the reaction enthalpy of a reaction [J/mol]
T is the temperature [K]
ΔS_m is the change in entropy for a reaction [J/mol K]

The following will describe what each term presented in Equation 2.1 means.

2.1.2.1 Enthalpy

The reaction enthalpy (or enthalpy of reaction) of splitting water is equal to the reaction enthalpy of forming water from its base elements. That is, hydrogen and oxygen gas when they are, for example, burnt together at standard conditions [1]:

$$H_2 + 0.5\,O_2 \longrightarrow H_2O \; \Delta H_m = -286 \text{ kJ/mol}$$

The negative sign in ΔH_m denotes that energy is **released** in this reaction. That is, when hydrogen and oxygen are burned together, energy, in the form of heat and light, is released. In electrolysis, the opposite occurs, energy is **required** for the reaction to occur. That is, ΔH_m is positive.

$$H_2O \longrightarrow H_2 + 0.5\,O_2 \; \Delta H_m = +286 \text{ kJ/mol}$$

[1] 1 atm, 25°C

ΔH_m is equal to the summed enthalpy of the products less the summed enthalpy of the reactants. This is expressed mathematically in Equation 2.2:

Definition: Enthalpy of Reaction

$$\Delta H_m = \sum_i n_i \cdot H_{m,i} - \sum_j n_j \cdot H_{m,j} \tag{2.2}$$

Where:
ΔH_m is the reaction enthalpy for the reaction [J/mol]
n_i is the coefficient of product i in the balanced chemical equation [-]
n_j is the coefficient of reactant j in the balanced chemical equation [-]
$H_{m,i}$ is the enthalpy value for product i [J/mol]
$H_{m,j}$ is the enthalpy value for reactant j [J/mol]

The enthalpy, H_m of a species varies with both pressure and temperature. Therefore, ΔH_m is not constant and the amount of energy released (or required) with a reaction depends on the reactant conditions. For constant pressure (isobaric) conditions, the enthalpy of reaction of water electrolysis can be determined and select cases are shown in Table 2.1. Numerical packages such as **CoolProp** or **RefProp** can be used to determine the enthalpy values for any pressure of temperature conditions. The utilisation of numerical packages for calculation of thermodynamic properties is explained further in chapter 3.

Table 2.1: Reaction enthalpy for splitting of water to hydrogen and oxygen at various temperatures. Pressure is constant at 1 atm. Reference states taken from [6]. Calculated using CoolProp

State of water	Temp [^{o}C]	ΔH_m [kJ/mol]
Liquid	20	286.00
Liquid	25	285.83
Liquid	80	284.10
Gas	100	242.80
Gas	200	243.64
Gas	400	245.43
Gas	800	248.32

2.1.2.2 Entropy

Entropy is a measure of ”randomness” and is a relative measure. The change in entropy, ΔS_m, can be determined using Equation 2.3.

Definition: Change in Entropy

$$\Delta S_m = \sum_i n_i \cdot S_{m,i} - \sum_j n_j \cdot S_{m,j} \tag{2.3}$$

Where:
ΔS_m is the overall change in entropy for the reaction [J/mol K]
n_i is the coefficient of product i in the balanced chemical equation [-]
n_j is the coefficient of reactant j in the balanced chemical equation [-]
$S_{m,i}$ is the entropy value for product i [J/mol K]
$S_{m,j}$ is the entropy value for reactant j [J/mol K]

The values for $S_{m,i}$/$S_{m,j}$ depend on the phase of i/j and the temperature of i/j. For the case of water electrolysis, the initial phase of the water therefore is relevant. That is, is the water being

electrolysed gaseous (steam), or liquid and what temperature the water is at. Similar to enthalpy, the value of entropy can be determined by CoolProp or RefProp.

2.1.2.3 Gibbs Free Energy

Combining this all together, for various temperatures and phases of water, the Gibbs free energy required for splitting water can be determined and is shown in Table 2.2. This process can be replicated for other species (such as carbon dioxide) but will not be done here.

Table 2.2: Gibbs free energy for splitting of water to hydrogen and oxygen at various temperatures. Pressure is constant at 1 atm. Reference state taken from [6]. Calculated using CoolProp

State of water	Temp [°C]	ΔG_m [kJ/mol]
Liquid	20	237.95
Liquid	25	237.13
Liquid	80	228.30
Gas	100	225.16
Gas	200	220.33
Gas	400	210.14
Gas	800	188.38

The equation which relates potential (voltage) to Gibbs free energy for a redox reaction is shown in Equation 2.4.

Definition: Potential and Gibbs free energy

$$E_{reaction} = -\frac{\Delta G_m}{z \cdot F} \tag{2.4}$$

Where:
$E_{reaction}$ is the voltage equivalent for the reaction [V]
ΔG_m is the change in Gibbs free energy [J/mol]
z is the number of electrons involved in the reaction [-]
F is Faraday's constant [C/mol]

To explain Table 2.2 and how it relates to Equation 2.4 and its impact on electrolysis; the smaller the change in Gibbs free energy is, the less energy required to electrolyse water. Through the relation between Gibbs free energy and potential in Equation 2.4, the smaller ΔG_m is, the less potential (voltage), $E_{reaction}$, required to electrolyse water.

However, the change in Gibbs free energy for the reaction assumes the reaction, $H_2O \longrightarrow H_2 + 0.5\,O_2$, occurs at stochiometric conditions. In practice, this rarely occurs. Therefore, the concentration/partial pressures of the products/reactants also impact the voltage. Specifically, the concentrations impact the **reaction quotient**.

Definition: Reaction Quotient

For a generic chemical reaction:

$$aA + bB \longrightarrow cC + dD$$

Then the Reaction Quotient is defined by:

$$K_C = \frac{[C]^c \cdot [D]^d}{[A]^a \cdot [B]^b} \tag{2.5}$$

Where:
K_C is the reaction quotient [-]
$[X]$ is the concentration of species X [mol/L]
x is the coefficient in the chemical equation of species X [-]

All the above, that is, Gibbs free energy, (Equation 2.1) and the Reaction Quotient, (Equation 2.5), can be combined and summarised in the **Nernst Equation**, Equation 2.6.

Definition: Nernst Equation

$$E_{cell} = E_0 - \frac{RT}{zF} \cdot \ln(K_C) \tag{2.6}$$

Where:
E_{cell} is the overall cell voltage [V]
F is Faraday's constant [C/mol]
z is the number of electrons involved in the reaction [-]
E_0 is the standard potential of the cell [V]
R is the universal gas constant [J/mol K]
T is the temperature of the cell [K]
K_C is the reaction quotient [-]

If the reaction species are in the gas phase, the Nernst Equation can be modified using the ideal gas law to work with partial pressures. Specifically for water electrolysis:

Definition: Nernst Equation - Water

$$E_{cell} = E_0 - \frac{RT}{zF} \cdot \ln\left(\frac{p_{H2} \cdot p_{O2}^{0.5}}{p_{H2O}}\right) \tag{2.7}$$

Where:
F is Faraday's constant [C/mol]
z is the number of electrons involved in the reaction [-]
E_0 is the standard potential of the cell [V]
R is the universal gas constant [J/ mol K]
T is the temperature of the cell [K]
p_{O2} is the partial pressure of the produced oxygen gas [Pa]
p_{H2} is the partial pressure of the produced hydrogen gas [Pa]
p_{H2O} is the partial pressure of the reactant water stream [Pa]

If the water is gaseous, then the partial pressure of the steam is used. If the water is liquid, a numerical value of 1 is used (i.e. $p_{H2O} = 1$.

The Nernst Equation determines the *minimum* voltage to electrolyse water dependant on the phase, temperature and concentration. The minimum voltage required to electrolyse is known as the **Open Cell Voltage** (OCV) or the Nernst voltage. In fuel cells, the OCV determines the *maximum* voltage which can be obtained by a fuel cell dependant on the phase, temperature and concentration. In reality, the voltage applied to water (in electrolysers) will be higher than the OCV due to overpotentials. In fuel cells, the obtainable voltage will be lower than the OCV because of overpotentials. Overpotentials are discussed further in subsection 3.1.2.

For the electrolysis of water, the required cell potential, E_0, will change depending on the phase and temperature of the input water as the Gibbs free energy changes. For liquid water as the input, at standard conditions [2], the voltage required to split water is calculated as follows:

$$
\begin{aligned}
E_{cell} &= E_0 - \frac{RT}{zF} \cdot \ln\left(\frac{p_{H2} \cdot p_{O2}^{0.5}}{p_{H2O}}\right) \\
E_{cell} &= -\frac{\Delta G_{std}}{2 \cdot 96485} - \frac{RT}{zF} \cdot \ln\left(\frac{1 \cdot 1^{0.5}}{1}\right) \\
E_{cell} &= -\frac{237130}{2 \cdot 96485} - \frac{RT}{zF} \cdot 0 \\
E_{cell} &= -1.23 \ \text{V}
\end{aligned}
$$

For gaseous water, this becomes more complicated as the partial pressures of H_2 and H_2O will change on average in the cell and locally near the surface of the electrodes/Triple Phase Boundary (TPB). This is because in a SOEC, H_2 and H_2O exist as a mixture one one side of the cell in the gaseous phase, and not all H_2O is used in the redox reaction because of gas transport limitations along with local variations in the number of molecules near the negatively charged electrode. This and the impacts of it are discussed further in subsubsection 3.1.2.1. However, for the purposes of demonstration; water at 100°C in the gas phase, with full and complete usage of all H_2O entering the cell, resulting in the partial pressures of H_2O and H_2 both being equal to 1 atm, the voltage required to electrolyse is:

$$
\begin{aligned}
E_{cell} &= E_0 - \frac{RT}{zF} \cdot \ln\left(\frac{p_{H2} \cdot p_{O2}^{0.5}}{p_{H2O}}\right) \\
E_{cell} &= -\frac{\Delta G_{100,g}}{2 \cdot 96485} - \frac{RT}{zF} \cdot \ln\left(\frac{1 \cdot 1^{0.5}}{1}\right) \\
E_{cell} &= -\frac{225160}{2 \cdot 96485} - \frac{RT}{zF} \cdot 0 \\
E_{cell} &= -1.16 \ \text{V}
\end{aligned}
$$

Under the same assumptions for the 100°C case at 800°C instead, the OCV would be:

$$
\begin{aligned}
E_{cell} &= E_0 - \frac{RT}{zF} \cdot \ln\left(\frac{p_{H2} \cdot p_{O2}^{0.5}}{p_{H2O}}\right) \\
E_{cell} &= -\frac{\Delta G_{800,g}}{2 \cdot 96485} - \frac{RT}{zF} \cdot \ln\left(\frac{1 \cdot 1^{0.5}}{1}\right) \\
E_{cell} &= -\frac{188380}{2 \cdot 96485} - \frac{RT}{zF} \cdot 0 \\
E_{cell} &= -0.977 \ \text{V}
\end{aligned}
$$

This shows that at higher temperatures, the voltage required for electrolysis decreases for gas phase water and that gas phase water requires a lower applied potential to electrolyse than liquid phase water. These reductions in voltage might not seem significant but they can have large impacts in the reduction of power required for electrolysis and obtainable electrical efficiency.

[2] 25°C, 1 atm

2.1.2.4 Thermoneutral Potential

Comparing the Gibbs free energy and reaction enthalpy values, as presented in Table 2.1 and Table 2.2 respectively, for various temperatures, it can be seen that there is an energy difference between the electrical energy required to electrolyse (Gibbs free energy) and the total energy required for the reaction (reaction enthalpy) to occur. This can be seen for a range of temperatures in Table 2.3.

Table 2.3: Difference between Gibbs free energy and reaction enthalpy for various temperatures of water

State of water	Temperature [°C]	ΔG_m [kJ/mol]	ΔH_m [kJ/mol]	Difference (ΔH_m - ΔG_m) [kJ/mol]
Liquid	20	237.95	286.00	48.04
Liquid	25	237.13	285.83	48.70
Liquid	80	228.30	284.10	55.80
Gas	100	225.16	242.80	17.65
Gas	200	220.33	243.64	23.32
Gas	400	210.14	245.43	35.29
Gas	800	188.38	248.32	59.93

The presented results from Table 2.3 indicates that less energy is required to electrolyse water than the theoretical maximum energy which can be obtained from the utilisation of the produced hydrogen and oxygen gasses. The reason this difference can occur is that when electrolysing water, there is an increase in entropy by going from a single mol of a liquid/gas to one and a half mols of gasses, which is thermodynamically favourable. However, requiring less energy to begin electrolysis than the amount of energy being obtained is a violation of the law of conservation of energy and therefore, additional energy is required during electrolysis. As a result, the electrolysis of water is an **endothermic reaction**.

Typically, the additional energy required for water to electrolyse comes from thermal energy. This thermal energy can come from the surrounding environment, a dedicated heat source (such as waste heat from industrial processes) or by applying a higher voltage for the electrolysis of water. For physical reasons which are discussed in subsection 3.1.2, higher voltages than what the Gibbs free energy would indicate, are already required to electrolyse water; therefore it is practical in many cases to only apply a higher voltage to ensure the temperature of environment does not decrease, which if unaccounted for, would decrease the temperature of the reactants sufficiently that the Gibbs free energy, and therefore voltage required for electrolysis to occur, to increase. The voltage, which if applied to an electrolyser, results in zero temperature change, is called the **thermoneutral potential**.

Definition: Thermoneutral Potential

$$E_{\text{thermo neutral}} = -\frac{\Delta H}{z \cdot F} \tag{2.8}$$

Where:
$E_{\text{thermo neutral}}$ is the thermoneutral voltage [V]
ΔH is the enthalpy required to split water in a given phase [J/mol]
z is the number of electrons involved [-]
F is Faraday's constant [C/mol]

The extra energy required by electrolysing at a voltage higher than the theoretical voltage, (the voltage required just from the Gibbs free energy value), is an **irreversible** loss. That is, energy which can not be reclaimed back when utilising the produced hydrogen and oxygen.

2.1.3. Electrolyser Types

As mentioned in section 2.1, electrolysers are devices which split water into hydrogen and oxygen gas via the process discussed in subsection 2.1.2. The type of electrolysis described in section 2.1 is what occurs for solid oxide electrolysers. However as also mentioned, different ions can be transported inside an electrochemical cell to acheive the same result. The end product is the same; producing hydrogen and oxygen gas, only the method is different. However this difference in method can lead to

large variations in technical performance, capabilities and cost for the electrolysers themselves. This section will briefly outline the different types of electrolysers which exist.

2.1.3.1 Alkaline Electrolysers

Alkaline electrolysers are the oldest type of electrolysers. Alkaline electrolysers are devices which perform electrolysis where hydroxide, OH^-, ions move from the cathode towards the anode. Like the name suggests, this electrolysis occurs in an alkaline environment. That is, a basic environment, so the PH of the water is higher than 7. This is achieved by potassium hydroxide (KOH) being added to the water during electrolysis to maintain a higher than 7 PH [7]. Alkaline electrolysis occurs at low temperatures (80°C max) and can produce hydrogen on a large scale. Alkaline electrolysers are usually cost effective capex wise as the electrode are often made from nickle which is a cheap material to purchase compared to other electrolyser types [7]. In alkaline electrolysers, there is no membrane, meaning that alkaline electrolysers generally have poor on-off capabilities due to the diffusion of gas particles between cathode and anode [8].

2.1.3.2 PEM Electrolysers

Proton Exchange Membrane (PEM) electrolysers work by hydrogen/hydronium (H^+/H_3O^+) ions travelling through a hydrogen/hydronium ion conducting membrane going from the anode to the cathode. The membrane used in PEM electrolysers prevents diffusion of charged particles between the two electrodes, which allows PEM to have excellent on/off characteristics which makes it ideal for many applications. Additionally, PEM electrolysers are also able to have high pressure gradients between their electrodes, allowing them to produce high pressure hydrogen or perform electrochemical compression on hydrogen. The drawback of PEM is its high cost [7]. The electrodes are typically made from noble metals such as platinum and iridium which are expensive to produce, due to the rarity of these materials in the Earth's crust and other competing commercial uses (such as catalytic converters in cars) for these materials. The membrane used in PEM, Nafion, is also expensive, despite being developed in the 20th century.

2.1.3.3 AEM Electrolysers

Alkaline Electrolyte Membrane (AEM) electrolysis is a mix between alkaline electrolysis and PEM electrolysis. Considering nickle can be used as the electrode material in alkaline electrolysers, the biggest drawback of alkaline electrolysers is the on/off capabilities of the system; without a membrane preventing charged particles diffusion, on/off characteristics are poor. PEM electrolysers are more expensive but have great on/off capabilities because of the membrane present. Therefore the intent of AEM is to introduce a membrane to combined the low cost of alkaline electrolysers and the practical usefulness of PEM electrolysers. This technology is still in early stages of development [8].

2.1.3.4 Solid Oxide Electrolysers

Solid Oxide Electrolyser Cells, SOECs, are the main focus of this thesis. SOECs are unique amongst electrolyser technologies as no hydrogen atoms/ions/compounds are moved between the cathode and anode during operation, instead only oxide ions are transported. This means reductions of other compounds, such as CO_2 is possible with the same technology. This is beneficial as, for example, CO_2 reduced to CO (carbon monoxide) is a useful reaction in the development of life support systems for space exploration [9] and for synfuel production. The downsides to SOECs are the high temperature at which they have to operate and the inability to have large pressure gradients between electrodes. These challenges will be elaborated further in section 2.5.

2.2. Solid Oxide Cells

This section explains in more details the functioning of Solid Oxide Electrolyser Cells (SOECs) and Solid Oxide Fuel Cells (SOFCs) and the different component inside both of these devices, commonly referred together as Solid Oxide Cells (SOCs).

There two "types" of temperature operations of SOCs. "High" temperature (700-1000°C) and "low" temperature (600-700°C). In general, lower temperature operations of SOCs are preferred as material compatibility and degradation of materials are better and lower respectively [10]. However, at "low" temperatures, the ionic conductivity of the electrolyte membrane is also significantly lower along with

the catalytic activity of the electrodes [11], and therefore ”high” temperature SOCs are in use today and ”low” temperature SOCs are an area of active research.

2.2.1. Physical Design

There are two physical designs for a single SOC; tubular or planar cell designs. The differences between these two types are shown in Figure 2.2.

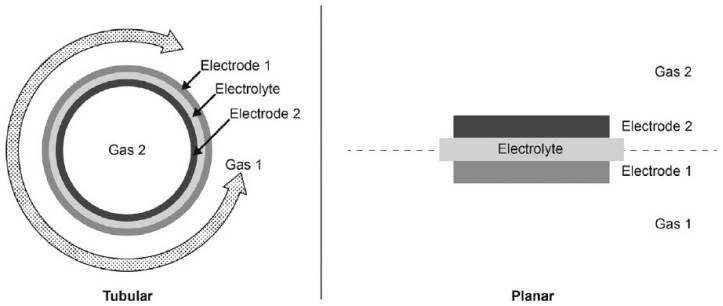

Figure 2.2: Figure showing planar and tubular SOC designs in a basic form. Image taken from [10]

There are advantages and disadvantages to using both tubular and planar designs. These are summarised in Table 2.4. Additionally, these different design options have an impact on the formation of **stacks**, which is discussed further in subsection 2.2.4. Currently, planner SOC systems make up the majority of the existing market for SOFC systems [12].

Table 2.4: Summarised pros and cons of tubular and planar solid oxide cell designs [10]

	Advantages	Disadvantages
Tubular	High mechanical strength No high temperature seals required	Lower power density Higher manufacturing costs
Planar	Higher power densities Easier to manufacture	Limited mechanical strength High temperature seals required

Beyond this, planar SOCs can come in various forms. Specifically, the part of the cell which provides the mechanical strength to the cell as it operates can be different. The reason for requiring mechanical strength for the cell in the first place is to ensure that the cell will not mechanically fail once fluids are moving through the cell, which will apply mechanical force on the cell components (i.e. electrodes and electrolyte). There are three main types of cells, graphically shown in Figure 2.3 and discussed in the following sections.

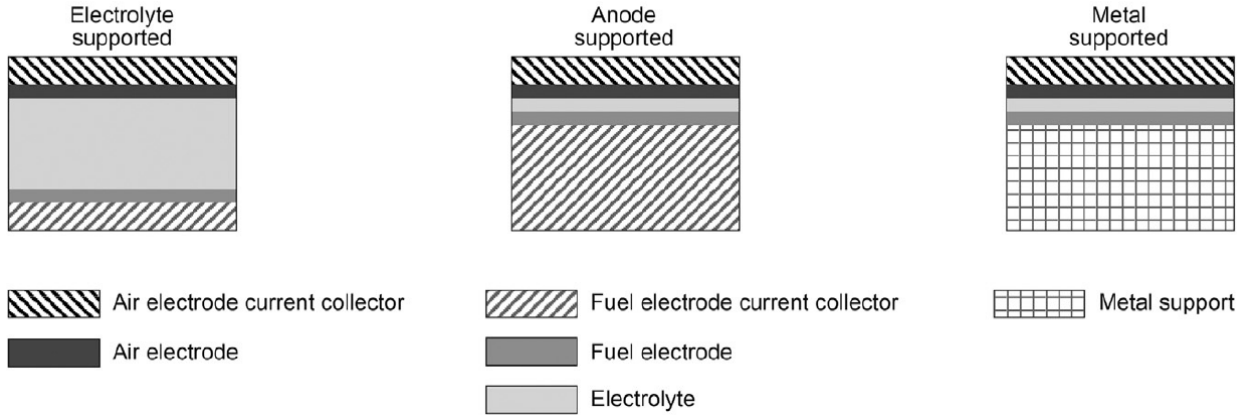

Figure 2.3: Types of planar SOCs. Image adapted from [10]

2.2.1.1 Anode Supported SOCs

Anode Supported Cells (ASCs) are SOCs which have the mechanical stiffness of the cell provided by the anode material. As a result, the anode is the thickest part of the cell, meaning a thin electrolyte and cathode layers are possible. As diffusion of reactants occurs on the cathode side, a thicker anode layer does little to impaire performance , therefore anode supported cells are beneficial for SOEC.

2.2.1.2 Electrolyte Supported SOCs

Electrolyte Supported Cells (ESCs) are SOCs in which the electrolyte provides mechanical stiffness to the cell. ESC are the oldest cell type and have been proven to operate for time periods of 40 000 hours [13]. The drawbacks of this design are are the higher ohmic losses originating from thicker electrolytes. However because of both electrodes being thin, the dynamics of gas permeation into electrodes is better and therefore these designs are better for reversible Solid Oxide Cells (rSOCs), that is, systems which can function as both electrolysers and fuel cells. Additionally, thicker electrolyte layer improves the gas sealing between the anode and cathode layers.

2.2.1.3 Metal Supported SOCs

Metal Supported Cells (MSC) are a newer type of SOC design. In this design, the electrode and electrolyte layers are as thin as possible and the mechanical support for the cell comes from an additional metal layer upon which the cell is manufactured. The advantages of this design is that metal supported SOCs allow for more dynamic operations resulting from faster start-up time and tolerance for larger thermal gradients (100 K/cm) [13] [14].

2.2.1.4 Comparison of SOC types

Each type of SOCs have their relative advantages and disadvantages compared to each other, is presented in Table 2.5

Table 2.5: Relative comparison of different planar SOC designs. [15] [13]

	ESC	ASC	MSC
Production of H_2	Low	High	Medium
Durability	High	Low	High
On-off cycling performance	Low	Medium-High	High
Cost	Low	Medium	Medium-Low
Operating temperature [$^\circ C$]	850-1000	700-800	500-800

2.2.2. Electrolytes

The electrolyte is a large limitation in the design and development of SOCs. There are few materials which support oxide ions conduction and the ones which do exist, only support conduction at elevated temperatures (+600°C), which is the fundamental reason why SOCs operate at high temperatures. The following section covers the requirements for solid oxide electrolytes along with the currently used electrolyte materials in SOCs.

2.2.2.1 Electrolyte Requirements

According to [11], the following are the requirements for electrolytes in SOCs:

- The electrolyte should be chemically stable in its environment
- The electrolyte must have good ionic conductivity of oxide ions
- The electrolyte must have very low electrical conductivity
- The electrolyte must be gas tight to prevent mixing of gasses from the cathode to the anode and vice versa
- The electrolyte must be thin as possible to minimise ohmic overpotentials (discussed further in subsubsection 3.1.2.3)
- The thermal expansion coefficient of the electrolyte should be similar to the adjoining cell layers (cathode and anode)
- The cost of the raw materials and manufacturing costs should be as low as possible

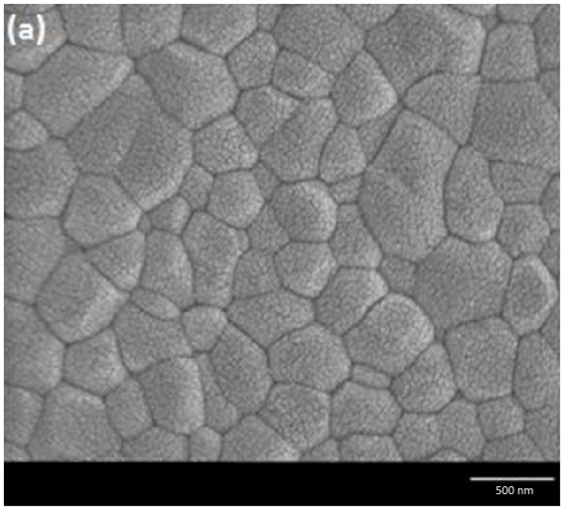

Figure 2.4: Grain boundaries of Yttrium Stabilised Zirconia (YSZ). The polygons are grains with the black lines between the grains being grain boundaries. Image adapted from [16]

The requirements for electrolytes are somewhat conflicting. The requirements of high ionic conductivity but also high gas tightness happen to be inversely related to each other [10]. This comes from the reality that the internal grain structure of an electrolyte is more inducive to gas tightness when there are many grain boundaries perpendicular to the travel direction from the cathode to the anode. Conversely, fewer grain boundaries in an electrolyte results in higher conductivity, but resulting in bigger grains [10]. As a result, manufacturing differences have a large impact on the resulting conductivity of a given electrolyte ceteris paribus. An image showing grains and grain boundaries can be seen in Figure 2.4. In Figure 2.4, the grains are the polygons, which are surrounded by ”black lines” which are the grain boundaries.

2.2.2.2 Stabilised Zirconia

Zirconia is short for zirconium dioxide, which has the chemical formula: ZnO_2. Stabilised zirconia refers to **doping** the zirconia lattice with other atoms or ions in order to change the properties of the material, specifically relating to molecular structure and conductivity. Like many ceramic materials, the micro structure of the zirconia lattice changes with temperature. Different micro structures are known as **phases**. Doping ”stabilises” the phase of zirconia at lower temperatures. Zirconia has three different phases, shown in Figure 2.5 which occur at different temperatures. The different phases require different volumes to exist in. For zirconia to be most effective as an electrolyte, the phases which only naturally occur at higher temperatures (cubic+tetragonal) are desired as these phases have the highest conductivity [11]. Via doping, the higher temperature phases can be made ”stable” at lower temperatures. It should be noted that the materials used for doping can be elements or ions. The most common dopents for zirconia are Y^{3+} and Sc^{3+} [10] [11].

In state of the art SOC electrolytes, oxide ions move through the electrolyte lattice by ”hopping” through the lattice to and from electron vacancies [10]. Besides stabilising zirconia to a more ion conductive phase, doping can enhance this ”hopping” effect. Both Y^{3+} and Sc^{3+} have lower oxidation states than the zriconium ion, Zn^{4+} in the lattice. Because the dopent has a low concentration relative to the other cation (Zn^{4+}), the ratio of oxide ions to Zn ion is ”good”, while the ratio of Y or Sc ions is ”not good”. Therefore oxide ions don’t want to be ”settled” around these 3+ cations, promoting further movement of the oxide ions, improving conductivity.

Yittrium Stabalized Zirconia (YSZ) is a well developed and researched electrolyte and is currently the state of the art electrolyte due to its stability, conductivity and mechanical stiffness. YSZ is formed by doping ZnO_2 with Y_2O_3 [11] as Y_2O_3 contains the conductivity improving Y^{3+} ion. The conductivity of YSZ changes with doping level of Y^{3+} with the maximum value being obtained at 8 mol% [11]. This

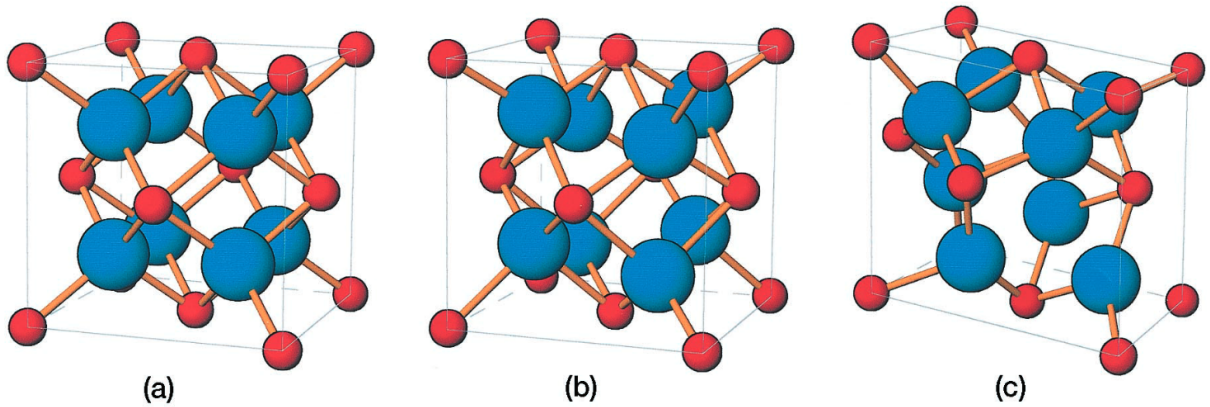

Figure 2.5: The three different phases of zirconia: a) Cubic (2370 °C ->) b) Tetragonal (1170-2370°C) c) Monoclinic (-> 1170°C). Images taken from [17]

Table 2.6: Conductivity of x-YSZ at select temperatures. Data taken from [11]. These data do not share a common manufacturing method or manufacturing quality. Differences in manufacturing method and quality can significantly impact conductivity [11]

Electrolyte	Conductivity [S/cm]	Temperature [K]
8YSZ	0.13	1273
8YSZ	0.083	1173
10YSZ	4.52e-6	673
10YSZ	0.034	1073

particular ratio of YSZ is known as **8YSZ**. Another common dope percentage value seen in literature is 10 mol%, known as 10YSZ, suffers less degradation from long term use, when compared to 8YSZ [11]. However there is already significant conductivity loss at this higher percentage as can be seen in Table 2.6

YSZ, while overall has good characteristics, is only ionically conductive at high temperatures. Because of other materials in an SOC and their requirements, the challenges of which are presented in section 2.5, electrolyte materials with higher conductivities at lower temperatures are desirable.

Scandium Stabilised Zirconia (ScSZ) is another form of stabilised zirconia which has good ionic conductivity. Sc^{3+} ions are added by doping zirconia with Sc_2O_3 [11]. At similar temperatures as 8YSZ, ScSZ, at certain doping ratios, has an even higher ionic conductivity as shown in Table 2.7. These higher conductivities are the result of the Sc^{3+} cation having a closer ionic radius to Zr^{4+} compared to Y^{3+}

ScSZ is less used as an electrolyte due to the higher cost of Sc compared to Y. Similar to YSZ, there is an optimum doping level for ScSZ. This doping level has been reported to be 8 mol% Sc_2O_3 [18]. Again similar to YSZ, additionally doping impacts the stabilisation of zirconia into its other phases/phase combinations at different temperatures. Unlike YSZ, ScSZ is prone to phase changes away from the cubic phase due to less stability around its operating points in terms of phase transitions [10]. However this is commonly resolved with co-doping. Co-doping is the process of adding multiple impurities (for an

Table 2.7: Ionic conductivity of x-ScSZ at select temperatures. Data taken from [11] and [18]. These data do not share a common manufacturing method or ensure comparable manufacturing quality which can have a large impact on ionic conductivity

Electrolyte	Conductivity [S/cm]	Temperature [K]
9-11ScSZ	0.28-0.34	1273
6ScSZ	0.18	1273
8ScSZ	0.31	1273

Table 2.8: Conductivity values for doped ceria. Data from [11]. These data do not share a common manufacturing method or ensure comparable manufacturing quality which has a large impact on conductivity

Electrolyte	Conductivity [S/cm]	Temperature [K]
15GDC	4.04e-2	973
20GDC	9e-2	1073
25GDC	1.01e-2	873
17SDC	5.7e-3	873
20SDC	8.8e-2	1073

Table 2.9: Conductivity values for LSGM compounds. Data from [11]. These data do not share a common manufacturing method or ensure comparable manufacturing quality which has a large impact on conductivity

Electrolyte	Conductivity [S/cm]	Temperature [K]
$La_{0.8}Sr_{0.2}Ga_{0.8}Mg_{0.2}O_3$	0.17	1073
$La_{0.8}Sr_{0.2}Ga_{0.8}Mg_{0.2}O_3$	0.025	873
$La_{0.8}Sr_{0.2}Ga_{0.83}Mg_{0.17}O_{2.815}$	0.17	1073
$La_{0.8}Sr_{0.2}Ga_{0.83}Mg_{0.17}O_{2.815}$	0.03	873
$La_{0.85}Sr_{0.15}Ga_{0.85}Mg_{0.15}O_{2.85}$	0.051	973
$La_{0.85}Sr_{0.15}Ga_{0.85}Mg_{0.15}O_{2.85}$	0.015	873

indicative example; both Y^{3+} and Sc^{3+} doped together in zirconia) to further improve material properties and stability. Because co-doping is an extensive topic with its foundation in material science, it is outside the scope of this thesis. Co-doping will not be discussed further besides saying that co-doping is typically not done with YSZ as it is already stable and additional dopends besides Sc are added to ScSZ to improve the stability of the electrolyte material with little impact on performance [18]. Furthermore, co-doping is not exclusive to zirconia, as co-doping is also utilised with other electrolyte materials.

2.2.2.3 Ceria

Cerium dioxide, also known as ceria, is another type of electrolyte material used in SOCs. Ceria has high ionic conductivity at lower temperatures than zirconia, as can be seen by comparing data in Table 2.6 and Table 2.8. Similar to other electrolyte materials such as zirconia, ceria is stabilised at more conductive phases by doping other ions into its lattice. Typical doping ions are Gd^{3+} and Sm^{3+} as these ions are similar in ionic radius to Ce^{4+}. The notations for these compounds are as follows:

- GDC - Gadolinium Doped Ceria
- SDC - Samarium Doped Ceria

As mentioned in the opening section on electrolytes, large variations in conductivity can be observed based of difference in manufacturing methods impacting grain boundary sizes and structure. The biggest drawback with ceria as an electrolyte is the reduction of Ce^{4+} to Ce^{3+} in reducing environments, allowing some electric conductivity through the electrolyte, although co-doping has been introduced to help solve this issue [19] as well as using an electrolyte blocking layer; i.e. a layered electrolyte, discussed further in subsubsection 2.2.2.5.

2.2.2.4 LSGM

LSGM is short for electrolytes which are **strontium doped lanthanum gallates**. In short, strontium, Sr, doped in a lattice of $LaGaO_3$. LSGM has higher conductivity to other materials, such as YSZ at lower temperatures, which is advantageous as high temperatures pose issue for SOC operation, which is discussed further in section 2.5. This is a similar motivation for ceria based electrolytes [11]. Often magnesium, Mg, is co-doped into the lattice to improve overall performance [11]. Various conductivity values of LSGM at different temperatures are presented in Table 2.9. Similar to YSZ, conductivity of LSGM depends on the concentration of Sr and Mg dopends.

LSGM reacts with nickle particles present in electrodes, degrading both electrode and electrolyte [11], making it less useful as an electrolyte as the utilisation of nickle in the electrodes is a big advantage of SOCs. However, similar to ceria, an electrolyte blocking layer can prevent this material compatibility problem [20].

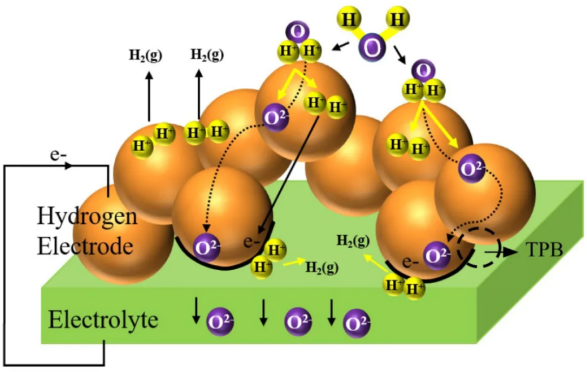

Figure 2.6: Illustration of what the triple phase boundary is. Image taken from [21]

2.2.2.5 Layered Electrolytes

Layered electrolytes refers to the concept of using multiple electrolyte layers in a cell to prevent undesirable interactions between different materials and fluids. For example, ceria is not stable in areas of higher oxygen partial pressure or other reducing conditions, as it will in the aforementioned conditions, reduce from Ce^{4+} to Ce^{3+}. However, ceria is compatible with Sr (Strontium) containing cathode materials where as an electrolyte material like zirconia is not. Therefore ceria is commonly used between the fuel electrode and electrolyte (which is often zirconia based) as an additional layer [10]. Choosing which electrolytes to have in layered configuration is a detailed design choice and outside the scope of this thesis. Layered electrolytes will not be discussed further nor will they be implemented in the models presented in chapter 3.

2.2.3. Electrodes

Electrodes are the surfaces at which redox reactions occur inside an electrochemical cell. Electrodes when it comes to fuel cells and electrolysers are often fully or partly made up on **catalytic material**. The electrodes are made up of catalytic material as it reduces the activation energy required for the redox reactions to occur, reducing the **overpotential** of the cell. The concept of reducing overpotentials at electrodes is discussed more in subsubsection 3.1.2.2.

Additionally, because of the nature of SOCs, the gas species, ions, electrons (and catalyst particles) are all required to meet together at one location for redox reactions to occur. This location is known as the **Triple Phase Boundary**, TPB. To achieve this, solid oxide cell electrodes are mixtures of catalyst particles and electrolyte materials, know as a **cermet**. This cermet allows large areas of TPB to occur, improving hydrogen production at the electrodes. A graphical illustration of what and where the TPB is can be seen in Figure 2.6.

2.2.3.1 Electrode Requirements

As already mentioned, electrodes are where the redox reaction occurs inside the SOC. It should be remembered that *different* redox reactions occur at the electrodes and therefore the requirements of each electrode are different in some aspect, although in general they also share many similar requirements.

Requirements for fuel electrodes:

- Low cost
- High ionic conductivity
- High electric conductivity
- Porous material for gas transport
- Stable in material, thermal and chemical environment
- Comparable thermal expansion with adjacent materials
- Large TPB area

Additional requirements for oxygen/air electrode

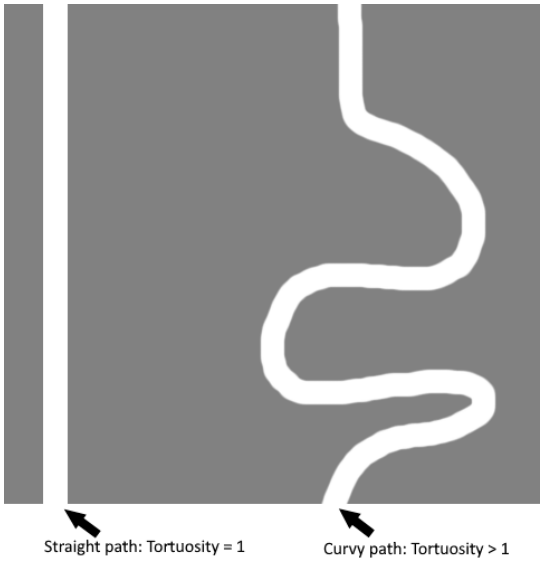

Figure 2.7: Tortuosity. The greater the ration between distance travelled between two points and the displacement between two points, the greater the tortuosity. The smallest value possible is one

- Stable in oxygen rich environment

As a result of the requirements for electrodes being porous for gas transport as well as large TPB area, SOC electrodes have unique microscopic geometries which tend to not have ”straight lines” from the TPB to the other side of the electrode. This is known as ”tortuosity”, which is graphically explained in Figure 2.7

2.2.3.2 Fuel Electrodes

Fuel electrodes need to support water splitting into hydrogen gas and oxide ions in electrolyser mode and water formation in fuel cell mode. Nickle is common catalyst material to use in fuel electrodes as it is catalytically active for the aforementioned reactions at elevated temperatures as well as being a relatively inexpensive material. Other catalytic materials include platinum and ruthenium [22]. The state of the art fuel electrode for SOCs is **Ni-YSZ** [23].

There are numerous challenges with nickle based electrodes [14]. Specifically, at SOC operational temperatures, nickle is prone to oxidise to NiO (nickle oxide) and also reduce from NiO back to Ni when oxygen is present. There is a large volumetric change when this redox reaction of Ni/NiO occurs, however usage of both materials, nickle oxide and nickle in a cermet in a controlled ratio can result in minimised volume changes during operation [23]. Additionally, nickle has a high surface mobility between 800 and 1000°C, meaning at operational temperatures, nickle particles agglomerate inside the electrode, reducing the TPB length and reducing overall electrode performance [23].

Nickle based electrodes also have the issue of coking when used with carbon based fuels (CO_2 in SOEC mode or CH_4 in SOFC mode) [24]. Ceramic electrodes have been introduced to address this problem, such as ceria based electrodes [23]. However, this thesis is focused on water based systems, not carbon based systems therefore a more in-depth discussed of these electrode types is omitted.

2.2.3.3 Air Electrodes

Air electrodes support oxygen formation from oxide ions in SOEC mode and oxygen gas to oxide ion formation in SOFC mode. As nickle readily oxidises to NiO, nickle is an undesirable catalytic material to use at the air electrode. Platinum use to be used as the catalyst material however it is less commonly used now due to its high cost [10]. The current state of the art air electrode material is LSM-YSZ, strontium doped lanthanum mangnite YSZ [25]. The biggest challenge with these electrode types is the delamination of the air electrode from the electrolyte along with crack formation at the electrode-electrolyte interface [25].

2.2.4. Stacks

In practice, a single planar solid oxide cell is never used by itself. This is for a variety of reasons:

- Other components are required to support the operation of a solid oxide system, which are discussed in section 2.3
- A single cell typically produces very little hydrogen gas. Therefore to get practically useful quantities, more cells are required

As a result, single cells are operated together as a **stack**. The purpose of this thesis is not to explain electrical circuits, therefore it is sufficient to say that SOCs are placed in **series** in order to reduce power loss from high currents in the circuit when they are formed as a stack. However this means the the voltages applied over the stacks can be high, depending on the number of cells in the stack. There is an inherent trade off between stack size and cost/space/efficiency. A stack is by design, very compact and one stack of 50 cells would cost less and be more efficient than 50 one cell stacks as less end plates, stack connectors etc would be needed. However with higher numbers of cells in a stack, the probability of stack failure increases, assuming the probability of a single cell failure is constant. This is because as the cells are in series, if one cell fails, the electrical conductivity of the entire stack is compromised. Given these design considerations, in SOCs, stack sizes are typically between 30 and 100 cells [26].

The advantages which stacks offer also have drawbacks. Namely, the usage of cells in series requires each cell to be electrically connected but isolated from ionic and gas transfer. This requires the use of **sealing materials** if the cell type is planar. Tubular designs are effectively ”big cells” and the tubular design allows for the electrodes to be used as seals.

2.2.4.1 Seal Materials

Sealing is a layer whose need comes from the requirement to create stacks. Sealing is one of the biggest challenges with solid oxide systems, as suitable materials, also stable at high temperature and oxidation conditions, are not common. In low temperature electrolysis/fuel cells like PEM, plastic based seals like teflon can be used. These technologies are well established and operate well in the oxidising and reducing environments present in electrolysers, however as they are all polymer based, none of them are compatible with 600°C+ operation.

Requirements for seals in SOCs are [10]:

- Gas tight
- High electrical resistivity
- Comparable thermal expansion coefficient with adjacent layers
- Strong resistance to thermal cycling
- Compatible with both ceramic electrodes and metallic inter connectors

Glass-ceramic are the preferred material for seals in SOCs [10]. While glass seals are solid at high temperatures and can be engineered such that their coefficient of thermal expansion is compatible with adjacent layers, glass-ceramic seals have technical challenges [27] [10], specifically:

- Degradation from thermal cycling
- Cracking from temperature gradients
- Poisoning from adjacent layers

Typically, tubular designs avoid the requirement for seals as the anodes and cathodes are completely self contained and the connection to other cells is not done via stacking. A single cell view of tubular and planar cells in a ”stacking” configuration can be seen in Figure 2.8.

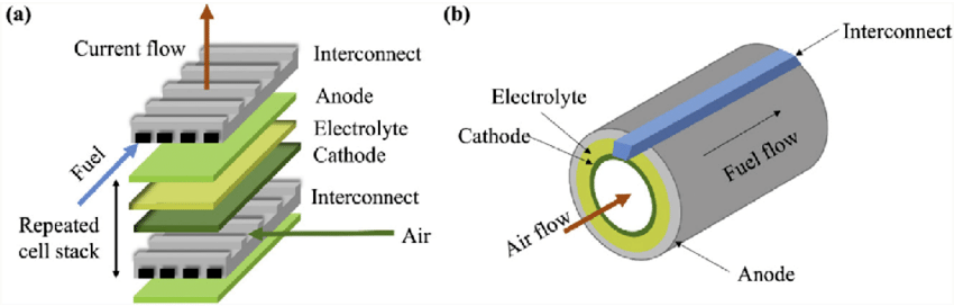

Figure 2.8: 3D visualisation of planar and tubular SOFCs. Image taken from [28]

2.3. Balance of Plant for SOCs

Solid oxide systems require high temperatures to operate. Heating up fluids to the required temperature for SOC operation is energy intensive. To minimise energy usage, ensure correct input fluid and to enable movement of fluids around the system, various auxiliary components are utilised next to the electrolyser/fuel cell stacks. Specifically, designs for SOC systems also included heat exchangers, trim heaters and pumps. Collectively, these components are called the **Balance of Plant**, BOP. BOP is the collective term for non stack/cell components which are required for the operation of an electrolyser/fuel cell system.

2.3.1. System Designs

Various system designs for SOCs exist. For commercial systems, this information is typically confidential [29], however some papers do exist and present different design options [30] [31] [32] [33], some of which are shown in Figure 2.9. Design choice is a result of system requirements, component availability and operation conditions. It should be noted that Figure 2.9 just shows one potential design option, different design options are possible.

2.3.2. Trim Heaters

Trim heaters are heaters used right before flow input into the SO stack. These heaters are required to ensure the input temperature of the inflow fluids (in the case of SOECs, namely water, hydrogen and air inputs) are at the correct temperature when entering the cell. Failure to do this can cause thermal shock and faster degradation of the electrolyte as well as premature failure of the cell/stack [34]. Trim heaters can be either electrical or combustion powered. Modelling of trim heaters is shown in subsection 3.2.4.

2.3.3. Heat Exchangers

Heat exchangers are used in SOC systems to recover the heat from the products leaving the stack and to heat up the incoming flow into the stack. This is done to improve overall efficiency by minimising additional heating of the flows. Both the anode and cathode sides of the stack use heat exchangers. Modelling of heat exchangers is further disused in subsection 3.2.3

2.3.4. Pumps

Pumps are required to move the fluid around the system. Pumps achieve this by either increasing the kinetic energy of the fluid flow or increasing the total pressure of the fluid, inducing it to move then it experiences a pressure gradient. This thesis will focus on the second approach as it is typically the more energy intensive method and therefore the ”worst case” scenario. Typically, low pressure differences are utilised in SOC to prevent damage to the electrolytes of the cell, which as ceramic materials, are easy to fracture under mechanical force. The modelling of pumps is elaborated in subsection 3.2.5.

2.3.5. Vaporisers

Vaporisers are devices which turn compounds which are liquid into gasses. The physical changes which can be applied to a species to obtain this result; raising temperature and lowering pressure. For most species utilised in SOCs, outlined in subsection 2.4.1, the only species which at standard

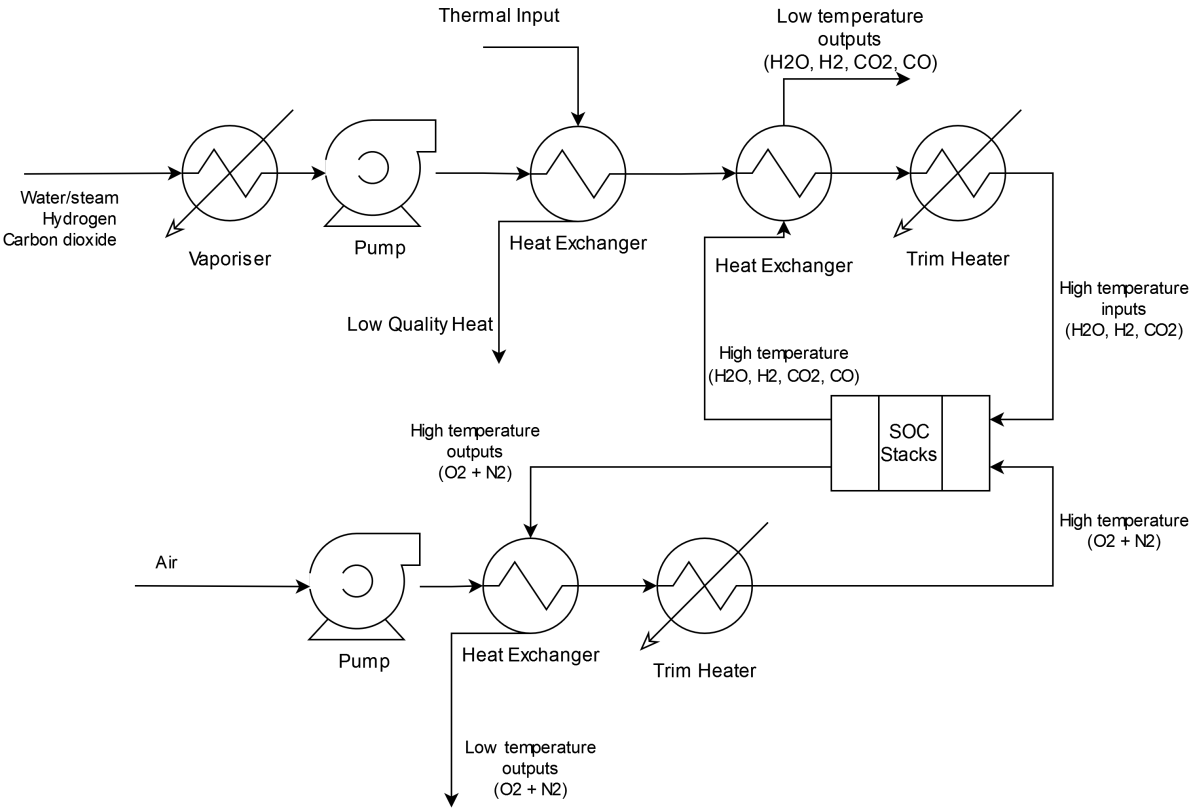

Figure 2.9: SOEC/SOFC system design inspired from from [32], [31]

conditions [3] is in a liquid phase is water. For practical reasons, it is common to simply heat the water to vaporise it. This in practice is very similar to how trim heaters operate. The modelling of vaporisers is discussed further in subsection 3.2.6.

2.4. Uses For Solid Oxide Cells

Solid oxide cells have many beneficial uses owing to their unique method of operation. These benefits are explained in the following section.

2.4.1. Input Flexibility

SOCs are unique when compared to AEM, alkaline or PEM electrolysers as SOCs are able to electrolyse compounds besides water, specifically carbon dioxide. This is possible because of the high temperatures at which SOCs operate. SOCs have already been used on Mars for this exact purpose [9]. The applicability of this to Mars is that it enables local oxygen production on Mars for both human life support and oxidiser production for rockets.

The chemical equations for carbon dioxide electrolysis are as follows:

$$CO_2 \longrightarrow CO + 0.5\,O_2 \text{ (overall)}$$
$$CO_2 + 2\,e^- \longrightarrow CO + O^{2-} \text{ (reduction)}$$
$$O^{2-} \longrightarrow 0.5\,O_2 + 2\,e^- \text{ (oxidation)}$$

Furthermore, in fuel cell mode, the high temperatures of SOC allow for fuels which are not hydrogen, such as ammonia and methane, in contrast to PEM fuel cells which do not allow this. The advantages of this is that SOFCs are compatible with more volumetric dense fuel sources which allows for more productive utilisation of chemically stored energy.

[3] 1 atm, 25°C

Ammonia, when used as a fuel in SOFCs, first undergoes a decomposition reaction and then the resulting hydrogen is able to react similar to a hydrogen-oxygen SOFC. The decomposition reaction is endothermic while fuel cell operations are exothermic, therefore correct design of such systems is required to ensure thermal stability in the system [35]. The reactions steps which occur are [35]:

Overall reaction:
$$2\,NH_3 + 1.5\,O_2 \longrightarrow N_2 + 3\,H_2O \text{ (overall)}$$
Component reactions:
$$2\,NH_3 \longrightarrow N_2 + 3\,H_2 \text{ (decomposition)}$$
$$3\,H_2 + 3\,O^{2-} \longrightarrow 3\,H_2O + 6\,e^- \text{ (oxidation)}$$
$$1.5\,O_2 + 6\,e^- \longrightarrow 3\,O^{2-} \text{ (reduction)}$$

The reaction steps for methane usage in SOFCs is more complex with more reaction pathways being possible, they are summarised in [36].

2.4.1.1 Co-Electrolysis

Co-electrolysis is when multiple species are fed into the cathode side of a SOEC where both input species are able to be reduced. An example combination researched before is water and carbon dioxide co-electrolysis. There are benefits to this approach over single species electrolysis. If carbon dioxide and water are inputs to an SOEC system, the outputs would be a mix of hydrogen, water, carbon monoxide and carbon dioxide. From this mixture, water is easily able to be separated out, leaving hydrogen, carbon monoxide and carbon dioxide. This mixture is commonly called **syngas** [37] and is able to be turned into synthetic fuels by already established and commercialised processes [38]. Alternatively, additional water can be reacted with the syngas via the water gas shift to convert more carbon monoxide to hydrogen and carbon dioxide, providing more hydrogen output then otherwise would be obtained [39].

2.4.2. Waste Heat Usability

Looking again at Table 2.3; plotting the relationship between enthalpy, Gibbs free energy, the difference between enthalpy and Gibbs free energy versus temperature, Figure 2.10 can be produced. What can be seen in Figure 2.10 is that the Gibbs free energy decreases while enthalpy remains mostly constant for increasing temperature. As the difference between represents the extra energy required for electrolysis to occur, at higher temperatures, a greater percentage of energy requires for electrolysis to occur can come from not electrical sources (as Gibbs free energy represents the energy required from electricity). What this means is that for high temperature electrolysis, if the thermal energy required is provided from other sources, such as waste heat from industrial sources, higher electrical efficiencies can be obtained. This is not inherent to SOCs, however other electrolyser types operate at much lower temperatures therefore only SOCs are currently able to utilise this reality.

2.5. Challenges With Solid Oxide Cells

There exist numerous challenges with SOCs, preventing rapid large scale adoption, although they are a technology already available commercially from companies such as Sunfire GmbH and Bloom Energy. An in-depth review of the technical challenges is not the purpose of this thesis, but a brief overview will be given instead:

Besides the challenge of sealing materials, as discussed in subsubsection 2.2.4.1, the main issue with SOCs is **degradation**. Degradation can be defined in multiple ways and is caused by a combination of different processes [10]:

Degradation in the context of SOCs is defined as:

- Increase in area specific resistance of the system during operation
- Increase (if SOEC) or decrease (if SOEC) in voltage at a set current density
- Loss of performance over time

The mechanisms which causes degradation can include [10] [27]:

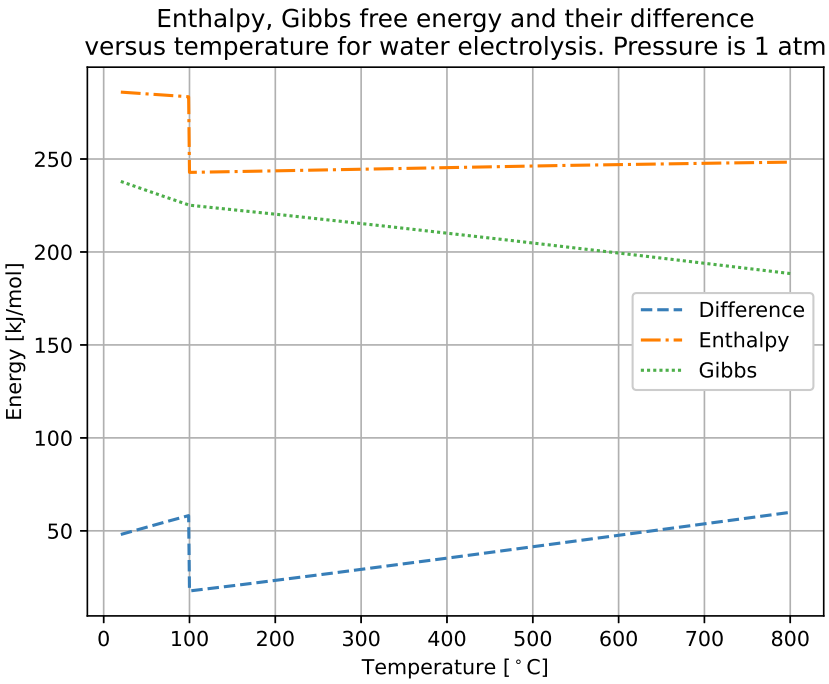

Figure 2.10: Relation of enthalpy, Gibbs free energy and the difference between the two as a function of temperature. At higher temperatures, the Gibbs free energy decreases, while enthalpy remains relatively constant. The difference increases as a result

- Catalytic particle agglomeration
- Inter cell layer particle diffusion
- Reduction in ionic conductivity of electrolyte
- Nickle reduction
- Changes in electrolyte micro-structure
- Sulphur and carbon deposition
- Nickle depletion
- Temperature fluctuations
- Fuel flow impurities
- Voltage/current density fluctuations

The modelling of these processes, their interdependence, temporal dependence, material dependence and temperature dependence is a still not fully understood at a fundamental level [40]. As modelling of degradation is a research area which could fill many PhD theses, it should be considered outside the scope of this master thesis. However, the models produced by this thesis will be written such that future researches can upgrades the existing models to account for degradation processes.

3

Modelling

This chapter discusses the modelling approach to the SOC models which have been created. The ultimate purpose is to create a model which is usable by HyCentA's **Hydra model**. The Hydra model is a MATLAB/Simulink model developed by HyCentA to investigate the economic feasibility of operating electrolyser systems in various techno-economic environments. To create a model which is usable by Hydra, three models have been constructed and each has a specific purpose, summarised below.

- **Detailed Cell Model** (Written in Python)
  - Models the relationship between voltage and current density for a single SOEC/SOFC
  - Determines the production and consumption levels for relevant fluids in electrolysis mode for a single SOEC given either voltage or current density as an input
- **SOEC System Model** (Written in Python)
  - For a given range of utilisable thermal energy and electrical power inputs, determine the overall system electrical efficiency and save these results
  - For a given range of utilisable thermal energy and electrical power inputs, determine the usable output thermal energy of the system of the system and save these results
- **Simulink Model** (Written in Simulink)
  - Fast utilisation of results from SOEC system model for all feasible ranges of specified available electrical power and thermal energy inputs
  - Callable by the Hydra model

The different models and how they relate to each other is visualised in Figure 3.1.

Both the detailed model and the SOEC system model require information about thermodynamic properties, as discussed in subsection 2.1.2. For all models which require it, the thermodynamic properties of pure fluids and mixtures are determined via **CoolProp** [41]. CoolProp determines thermodynamic properties of compounds using cubic equations of state, specifically Soave-Redlich-Kwong and Peng-Robinson. Cubic equations of state are able to determine fluid properties such as enthalpy and entropy [42]. For thermodynamic properties which are only relative, e.g. enthalpy, a reference point at standard conditions[1] is used with reference values taken from [6].

[1] 1 atm, 25°C

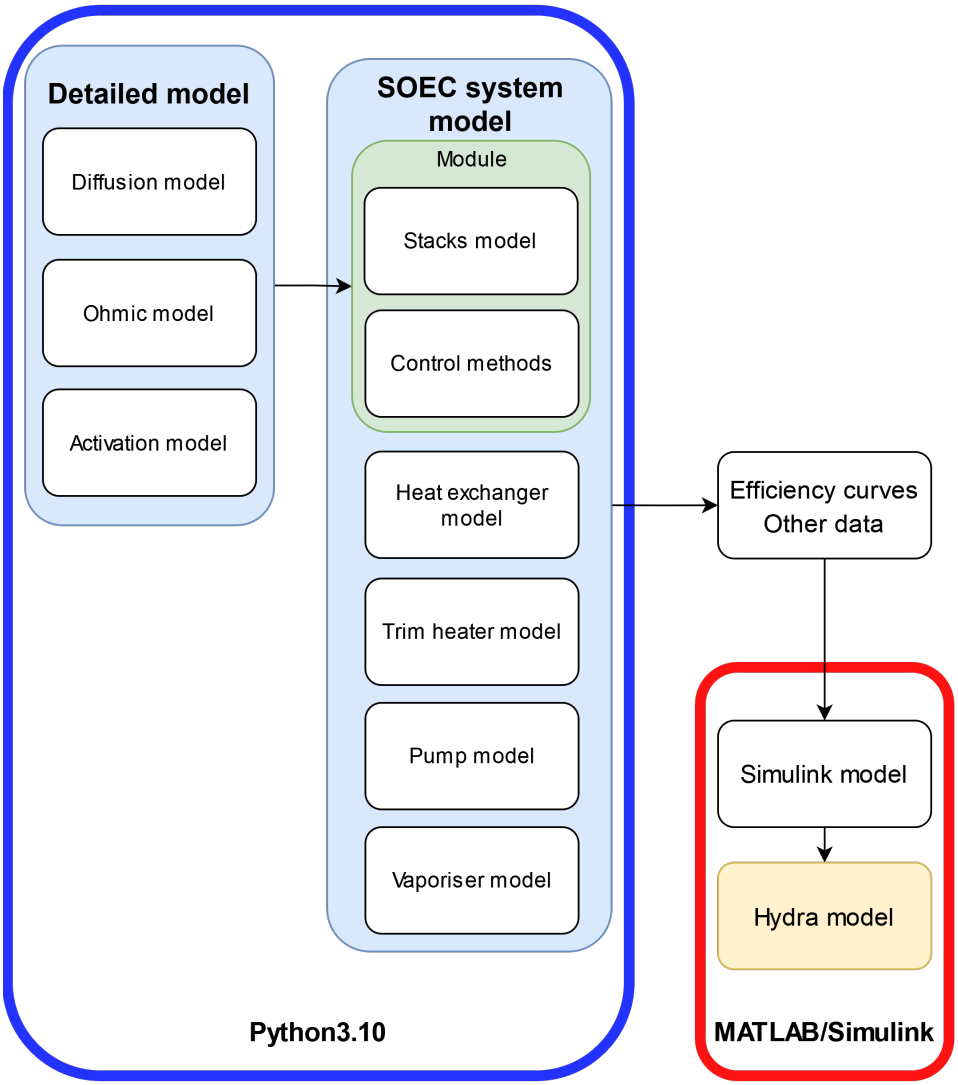

Figure 3.1: Flow diagram of how different models relate to each other

3.1. Detailed SOC Model

3.1.1. Assumptions

All models are built with some assumptions made. The following assumptions are made in the detailed model presented along with justifications of why these assumptions are valid. The assumptions made are:

- All gasses behave as ideal gasses
- Nitrogen is a spectator/inert species when air is used in a cell (i.e. nitrogen does not participate in the reaction)
- Air only consist of oxygen and nitrogen
- Gas mixtures are well mixed
- 1D model is sufficient to describe a solid oxide cell
- No side reactions occur

3.1.1.1 Ideal Gas Law Assumption

When the inter molecular forces between gas particles in a gas are negligible, the compressability factor of this gas will be equal to 1. When a compressibility factor is equal to 1, then the ideal gas law may be used. The compressibility factor is defined as:

Species	Temperature [K]	Pressure [MPa]	Compressibility [-]
Water	1000	0.1	0.99975
Hydrogen	1000	0.1	1.0002
Nitrogen	1000	0.1	1.0003
Oxygen	1000	0.1	1.0003
Carbon dioxide	1000	0.1	1.0002
Carbon monoxide	750	0.1	1.0004
Ammonia	1000	0.1	0.99998
Methane	750	0.1	1.0003

Table 3.1: Compressibility factors of select ”Pure Fluids” calculated by RefProp: Version 9.0, NIST Standard Reference Database 23

Definition: Compressibility Factor

$$Z = \frac{n \cdot R \cdot T}{P \cdot V} \tag{3.1}$$

Where:
Z is the compressibility factor [-]
n is the number of mols of the gas in question [mols]
R is the universal gas constant [J/mol K]
T is the temperature of the gas in question [K]
P is the pressure of the gas in question [Pa]
V is the volume the gas in question exists in [m3]

RefProp is a common tool to determine the properties of fluids at various conditions and is utilised in this instance of proving the validity of the ideal gas law assumption because RefProp is standard commercial software for thermodynamic properties. The compressibility factors for the species utilised in the detailed model around the operating point of SOCs are shown in Table 3.1. For the species evaluated at 750 K rather than 1000 K, this is the result of RefProp not being able to compute thermodynamic properties of those species at higher temperatures. However, they will still behave as ideal gasses because as a species’s temperature increases while keeping its pressure constant; if the species was already in the gaseous phase (as can be indicated by its phase diagram), then it will remain a gas and become more ”ideal”, as higher temperatures mean faster movement of gas particles and a lower chance of gas particles acting upon each other through inter molecular forces.

3.1.1.2 Nitrogen Spectator

Nitrogen does not have the ability to become an ion and transport itself though an oxide ion conducting membrane. Therefore all nitrogen gas input through a cell will remain a gas and not be involved in the electrochemical reaction occurring.

3.1.1.3 Contents of Air

Air is a mixture of gasses. In the detailed model, air is treated to only contain nitrogen and oxygen gas. In reality, dry air contains the following gasses [43]:

- Nitrogen(78.084%)
- Oxygen (20.946%)
- Argon (0.9340%)
- Carbon dioxide (0.0417%)
- Neon (0.001818%)
- Helium (0.000524%)
- Methane (0.000187%)
- Krypton (0.000114%)

It is important to note that the faction of gasses in the atmosphere is not constant. For instance, the amount of carbon dioxide and methane are increasing [1]. However for the purposes of this explanation, they do not change significantly *compared* to the amount of nitrogen and oxygen in the atmosphere.

The detailed model, when using air as an input, considers air to be only a mixture of oxygen and nitrogen gas. This is a valid assumption because the percentage of air which is just these compounds is over 99%. When including Argon, this percentage is approximately 100%. As argon is a noble gas and therefore nonreactive, it exists as a monatomic gas and does not, under the conditions which the detailed SOC model operates, become an ion. Therefore a similar logic which was applied to nitrogen in subsubsection 3.1.1.2 can be made with argon and therefore argon can be ignored.

3.1.1.4 Well Mixed Gas Mixtures

The detailed model treats all gasses in a mixture as having the same temperature by virtue of the second law of thermodynamics [2] occurring over a sufficiently long period of time. Combined with the assumption of ideal gas, all gases inside a mixture fully exist within a volume together without any interaction; thereby being well mixed.

3.1.1.5 1D Model Sufficient

In reality, a single side of an electrochemical cell exists in three dimensions, therefore the gasses present in the electrode can move and therefore change in concentration in three dimensions. For simplification purposes, it is assumed that going between gas inflow and gas outflow, (i.e. y direction), each ”slice” of the cell, i.e. going from ”bulk” concentration towards the membrane, (x direction), is constant. Moreover, depth (z direction) for a given x slide is also constant along it’s length.

3.1.1.6 No Side Reactions

In the detailed model, it is assumed that the gas species at the same electrode do not interact together. For the case of water electrolysis, hydrogen and water simply do not react together. For oxygen and nitrogen together, these species do react together, but only above 1300°C [44].

3.1.2. Potentials and Overpotentials

An electrical potential is required to applied over a cell or stack in order to split water. This potential, called the **cell potential** can be split into two types. The **Nernst Potential** and **overpotentials**. In essence, the Nernst Potential is the minimum voltage which has to be applied to electrolyse the water and an overpotential is an ”extra” voltage required to overcome physical impedance to electrolysis, which increase with increasing current densities. The total overpotential is the result of smaller overpotentials due to inefficiencies and physical limitations inside the electrolyser cell. The governing equations for the Nernst Potential and the various overpotentials are discussed below.

3.1.2.1 Nernst Potential

The Nernst potential/voltage is the reversible potential of the cell. That is, if you produce hydrogen and oxygen gas via electrolysis, when you want to later use the produced hydrogen and oxygen gas in say a fuel cell, the maximum voltage which can be achieved is the Nernst voltage. The Nernst potential is calculated from the Nernst Equation, as described in subsection 2.1.2. The equation is repeated here for convenience:

$$E_{cell} = E_0 - \frac{RT}{zF} \cdot \ln\left(\frac{p_{H2} \cdot p_{O_2}^{0.5}}{p_{H_2O}}\right)$$

The above is specific for the electrolysis of water. The Nernst Equation can therefore be generalised to the following for both electrolyser and fuel cell operation for any input

[2] heat moves from hot object to cold objects

Definition: Generalised Nernst Equation

$$E_{cell} = \frac{-\Delta G_0}{z \cdot F} - \frac{R \cdot T}{z \cdot F} \cdot \ln\left(\frac{\Pi p_{products,cathode}^{\upsilon_{products,cathode}} \cdot \Pi p_{products,anode}^{\upsilon_{products,anode}}}{\Pi p_{reactants,cathode}^{\upsilon_{reactants,cathode}} \cdot \Pi p_{reactants,anode}^{\upsilon_{reactants,anode}}}\right) \tag{3.2}$$

Where:
E_{cell} is the potential the cell requires/delivers [V]
ΔG_0 is the Gibbs free energy of the reaction [J/mol]
z is the number of electrons involved in the electrochemical reaction [-]
F is Faraday's constant [C/mol]
R is the universal gas constant [J/mol K]
T is the reaction temperature [K]
$p_{products,cathode}$ is the partial pressure of the products at the Cathode [Pa]
$p_{reactants,cathode}$ is the partial pressure of the reactants at the Cathode [Pa]
$p_{products,anode}$ is the partial pressure of the products at the Anode [Pa]
$p_{reactants,anode}$ is the partial pressure of the reactants at the Anode [Pa]
$\upsilon_{products,cathode}$ is the stochiometric coefficient of the products at the cathode in the reaction [-]
$\upsilon_{reactants,cathode}$ is the stochiometric coefficient of the reactants at the cathode in the reaction [-]
$\upsilon_{products,anode}$ is the stochiometric coefficient of the products at the anode in the reaction [-]
$\upsilon_{reactants,anode}$ is the stochiometric coefficient of the reactants at the anode in the reaction [-]

In subsection 2.1.2 it was mentioned that because steam and hydrogen were both in existence around the same electrode (the cathode), that the partial pressure of each would impact the other and therefore impact the Nernst Potential. Here it is important to note that there is always a difference between local and average partial pressures in a cell. That is, the partial pressure close to the electrodes and therefore the Triple Phase Boundaries (TPBs) will often be different than the average partial pressure far away from the electrode in the channels. This phenomena is not limited to H_2O and H_2, however H_2O and H_2 will be used as an example to demonstrate the modelling challenges this causes.

Furthermore, many SOECs also run, through the anode, heated air, in which oxygen has a partial pressure of about 0.2 bar. This is done for heating reasons and to reduce the partial pressure of oxygen to minimise electrode degradation. Therefore there is an impact at both electrodes of the partial pressure of species changing locally and on average. Figure 3.2 shows the impacts of partial pressure change.

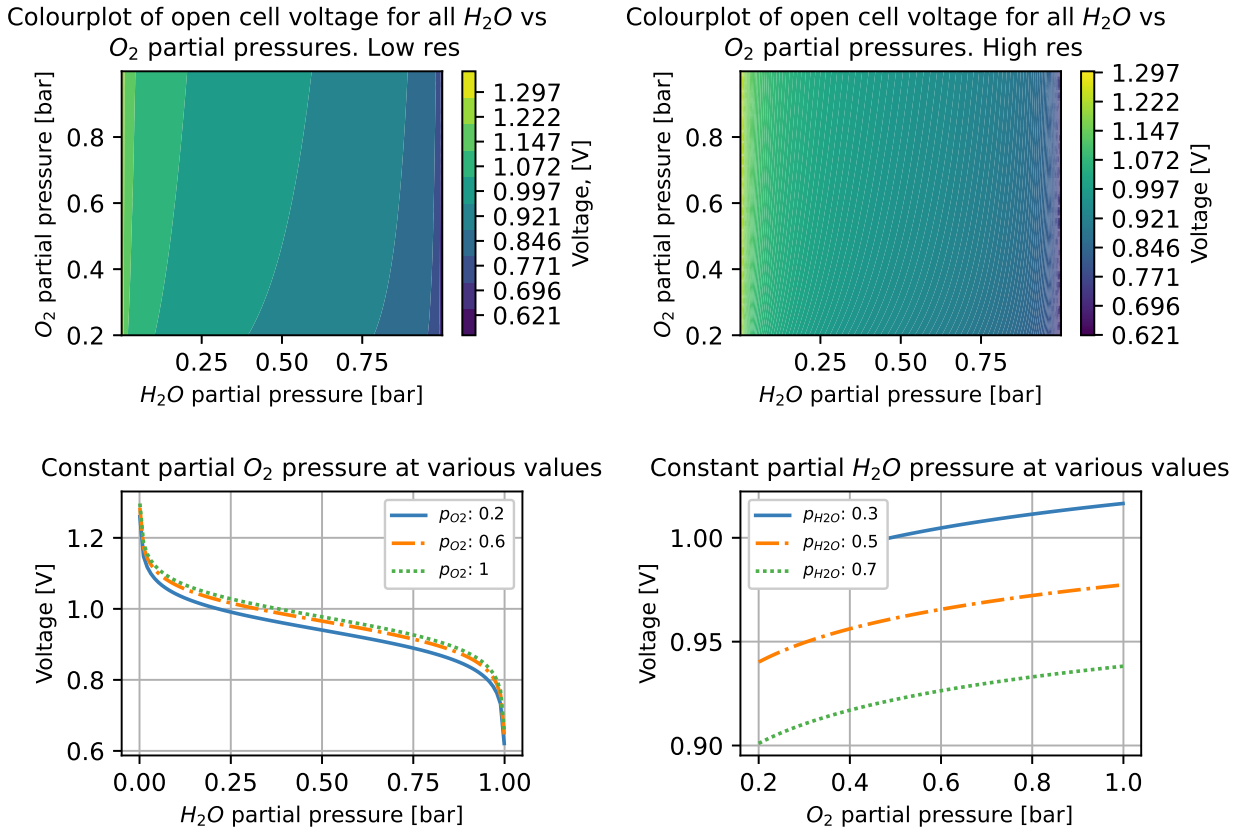

Figure 3.2: Plots of the impacts of various partial pressures of O_2 and H_2O. The partial pressure of H_2, p_{H_2} is always $1 - p_{H_2O}$

As can be seen in the top left plot in Figure 3.2, as expected from the Nernst Equation, higher partial pressure of H_2O decreases the Nernst Potential of the system. This impact is easier to see in the left top plot rather than the top right plot which is the same data but a higher resolution to better visualise the transition in potential.

The bottom left plot of Figure 3.2 shows for a given partial pressure of O_2, the Nernst Potential decreases with increasing H_2O partial pressure, meaning decreasing H_2 partial pressure. As H_2O concentration increases, the potential required for electrolysis decreases. The difference between the opposite ends of H_2O partial pressure (between 0.9 and 0.1 bar) in required potential is about 23% for all values of fixed O_2 partial pressures.

When observing the bottom right plot in Figure 3.2, it can be seen that for a given H_2O partial pressure, for varying O_2 partial pressures, the Nernst Voltage increases. For all fixed H_2O partial pressures, the variation between low and high O_2 partial pressures, a change in potential of around 4% is observed.

In general, Figure 3.2 shows that for a numerical model, accounting for the diffusion effects of H_2 in H_2O is a relevant feature to model. In steady state conditions of operation, the partial pressure of the H_2O and H_2 in various parts of the cathode side of the cell will be assumed constant along the length of the electrode (see subsection 3.1.1), therefore the average local values in one part of the electrode for H_2O partial pressure would be sufficient. While the impact of O_2 partial pressure is less significant compared to H_2O and H_2, it is nevertheless large enough to be included in a detailed numerical model.

3.1.2.2 Activation Overpotential

Activation overpotential refers to extra potential required for the redox reaction to initially take place in the cell progressively in the forward direction. At each electrode, the activation overpotential can be determined from the **Butler-Volmer Equation**, Equation 3.3. At each electrode, there are both oxidation and reduction reactions occurring as to some small degree [45], the overall half equation at one electrode exists in some form of equilibrium. This is represented by the charge transfer coefficients. To determine the total activation overpotential, the activation overpotential at the cathode and anode are summed together.

Definition: Butler Volmer Equation

Bulter-Volmer Equation [a]

$$i = i_0 \left(\exp\left(\frac{\alpha_c \cdot z \cdot F \cdot \eta_{act,el}}{R \cdot T} \right) - \exp\left(-\frac{\alpha_a \cdot z \cdot F \cdot \eta_{act,el}}{R \cdot T} \right) \right) \tag{3.3}$$

[a] equation taken from [46]

Where:
i is the current density [A/cm^2]
i_0 is the exchange current density [A/cm^2]
α_c and α_a are the charge transfer coefficients of the cathodic reaction and anodic reaction at the electrode respectively [-]
z is the number of electrons involved in the reaction [-]
F is Faraday's constant [C/mol]
$\eta_{act,el}$ is the activation overpotential at the electrode [V]
R is the universal gas constant [J/mol K]
T is the temperature [K]

For a given electrode, if the charge transfer coefficients are both taken to be equal, that is $\alpha_c = \alpha_a = \alpha$, then Equation 3.3 for a single electrode can be simplified:

$$i = i_0 \left(\exp\left(\frac{\alpha_c \cdot z \cdot F \cdot \eta_{act,el}}{R \cdot T} \right) - \exp\left(-\frac{\alpha_a \cdot z \cdot F \cdot \eta_{act,el}}{R \cdot T} \right) \right) \tag{3.4}$$

$$\frac{i}{i_0} = \exp\left(\frac{\alpha \cdot z \cdot F \cdot \eta_{act,el}}{R \cdot T} \right) - \exp\left(-\frac{\alpha \cdot z \cdot F \cdot \eta_{act,el}}{R \cdot T} \right) \tag{3.5}$$

$$\text{let}: x = \frac{\alpha \cdot z \cdot F \cdot \eta_{act,el}}{R \cdot T}$$

Then:

$$\frac{i}{i_0} = \exp(x) - \exp(-x) \tag{3.6}$$

Using:

$$2 \cdot sinh(x) = \exp(x) - \exp(-x) \tag{3.7}$$

Then

$$\frac{i}{i_0} = 2 \cdot sinh(x) \tag{3.8}$$

$$x = sinh^{-1} \frac{i}{2 \cdot i_0} \tag{3.9}$$

$$\frac{\alpha \cdot z \cdot F \cdot \eta_{act,el}}{R \cdot T} = sinh^{-1}\left(\frac{i}{2 \cdot i_0} \right) \tag{3.10}$$

$$\eta_{act,el} = \frac{R \cdot T}{\alpha \cdot z \cdot F} \cdot sinh^{-1}\left(\frac{i}{2 \cdot i_0} \right) \tag{3.11}$$

In reality, the charge transfer coefficients are usually different and vary with electrode material [47]

[45], although in SOC modelling, they are commonly taken to be 0.5 for all cases [48] [49]. A calculation of the error magnitude of this assumption is given in Appendix C.

As the previous derivation only gives the overpotential at one electrode, the activation overpotential for both electrodes needs to be summed to give the total activation overpotential. The exchange current density, i_0, is not the same at both electrodes as different reactions occur at different electrodes.

Definition: Activation overpotential

Activation overpotential at the cathode:

$$\eta_{act,cat} = \frac{R \cdot T}{\alpha \cdot z \cdot F} \cdot sinh^{-1}\left(\frac{i}{2 \cdot i_{0,cat}}\right) \tag{3.12}$$

Activation overpotential at the anode:

$$\eta_{act,an} = \frac{R \cdot T}{\alpha \cdot z \cdot F} \cdot sinh^{-1}\left(\frac{i}{2 \cdot i_{0,an}}\right) \tag{3.13}$$

Where:

i is the current density [A/cm^2]
$i_{0,cat}$ and $i_{0,an}$ is the exchange current density at the cathode and anode respectively [A/cm^2]
z is the number of electrons involved in the reaction [-]
F is Faraday's constant [C/mol]
α is the charge transfer coefficient of the electrode [-]
$\eta_{act,cat}$, $\eta_{act,an}$ is the activation overpotential at the cathode and anode respectively [V]
R is the universal gas constant [J/mol K]
T is the temperature [K]

For cases where the charge transfer coefficients are not equal, Equation 3.3 can be solved numerically via root finding such that for a given current density, the corresponding activation overpotential can be found. The methods employed in the detailed model are Newton's Method and bisection if Newton's Method does not converge successfully.

Definition: Total activation overpotential

Total activation overpotential:

$$\eta_{act} = \eta_{act,cat} + \eta_{act,an} \tag{3.14}$$

Where:
η_{act} is the overall activation overpotential [V]
ηcat and ηan is the overpotential at the cathode and anode respectively [V]

3.1.2.2.1 Exchange Current Density

Exchange current density, i_0, is the measure of how catalytically active an electrode is. That is, with no applied voltage, in the presence of reactants, a higher i_0 indicates that the redox reaction of the electrode will occur with the electrons present in the electrode at a faster rate, although this reaction will be balanced in the forward and reverse directions (i.e. no net production of any products). A higher exchange current density is indicative of higher catalytic activity at the electrodes owning to favourable reaction kinetics. The exchange current density therefore depends on material type as different materials are better supported for the redox reaction than others. Additionally, reaction rates are dependant on temperature governed by a relation known as **Arrenius's Equation**. Furthermore, reaction rates also depend on concentration levels; the higher the local concentration of a reactant, the higher the reaction rate.

Typically, the exchange current density is a parameter specific to an electrode with all its individual manufacturing and material characteristics. Therefore it is normally experimentally calculated by curve fitting variables to an equation which describes the exchange current density. However, there is no standard equation used and values found in literature are often printed without details on the material, surface area or clear indication of where these values come from [46] [48] [49].

Reference [49], comprises of research on different exchange current densities for different electrode types for both SOEC and SOFC configurations. While in practice the exchange current density will change based upon:

- Temperature
- Species concentration/partial pressure
- Electrode area
- Catalyst particle distribution

Only some of these are practical to measure/calculate while in operation (temperature, species concentration/partial pressure, catalyst particle distribution, electrode surface area change during operation). Therefore, in [49], the following is adopted:

Definition: Exchange Current Density Relations

$$i_{0,O_2} = r_{O_2} \cdot \left(\frac{y_{O_2}}{y_{O_2,ref}}\right)^{A} \cdot \exp\left(-\frac{E_{a,O_2}}{RT}\right) \tag{3.15}$$

$$i_{0,fuel} = r_{fuel} \cdot \left(\frac{y_{H2}}{y_{H2,ref}}\right)^{B} \cdot \left(\frac{y_{H_2O}}{p_{H_2O,ref}}\right)^{C} \cdot \exp\left(-\frac{E_{a,fuel}}{RT}\right) \tag{3.16}$$

[a]

[a] Equations taken from [49]

Where:
i_{0,O_2} is the exchange current density for O_2 electrode [A/cm^2]
r_{O_2} is the reaction rate constant for the O_2 electrode [-]
y_{O_2} is the molar fraction of O_2 [-]
$y_{O_2,ref}$ is the molar fraction of O_2 in the preference conditions [-]
A is a gas concentration exponent which is determined by fitting the equation to data [-]
E_{a,O_2} is the activation energy of the species reacting at the O_2 electrode [J/mol]

$i_{0,fuel}$ is the exchange current density for $fuel$ electrode [A/cm^2]
r_{fuel} is the reaction rate constant for the $fuel$ electrode [-]
y_{H2} is the molar fraction of H_2 [-]
$y_{H2,ref}$ is the molar fraction of H_2 in the preference conditions [-]
B is a gas concentration exponent which is determined by fitting the equation to data [-]
y_{H_2O} is the molar fraction of H_2O [-]
$y_{H_2O,ref}$ is the molar fraction of H_2O in the preference conditions [-]
C is a gas concentration exponent which is determined by fitting the equation to data [-]
$E_{a,fuel}$ is the activation energy of the species reacting at the $fuel$ electrode [J/mol]

R is the universal gas constant [J/mol K]
T is the temperature [K]

Expanding the equations given in [49], a general form can be derived:

Definition: Exchange Current Density Relations - General

$$i_{0,w} = r_w \cdot \Pi_{k=1} \left(\frac{y_{q_k}}{y_{q_k,ref}} \right)^{A_k} \cdot \exp\left(-\frac{E_{a,w}}{RT} \right) \tag{3.17}$$

[a]

[a] Equation adapted from [49]

Where:
$i_{0,w}$ is the exchange current density at the w electrode [A/cm^2]
w is the electrode. Can either be fuel or oxygen electrode
r_w is the reaction rate constant for the w electrode [-]
y_{q_k} is the molar fraction of species q_k [-]
k is a numerical indication of a species at an electrode [-]
$y_{q_k,ref}$ is the molar fraction of q_k in the reference conditions [-]
A_k is a gas concentration exponent which is determined by fitting the equation to data [-]
$E_{a,w}$ is the activation energy of the species reacting at the w electrode [J/mol]
R is the universal gas constant [J/mol K]
T is the temperature [K]
k is a reference to a species which exists at electrode w

From the results presented in [49], the required numerical values for the correct usage of Equation 3.15 and Equation 3.16, can be seen in Table 3.2. The values presented in Table 3.2 will be used to model i_0 in Equation 3.17.

Table 3.2: Data used for fitting Equation 3.15 and Equation 3.16 as presented in [49]. The error range on the A, B, C values comes from the different results obtained for the curve fitting at different temperatures. See Equation 3.15 for explanation of symbols.

Electrode Material	SOEC Mode			SOFC Mode		
Oxygen Electrode	E_a [kJ/mol]	r [-]	A [-]	E_a [kJ/mol]	r	A [-]
LSM	187	7.5e7	0.33 ± 0.03	174	2.1e7	0.35 ± 0.06
LSCF/GDC	83	4200	0.26 ± 0.09	105	40000	0.31 ± 0.11
Fuel Electrode	E_a [kJ/mol]	r [-]	B [-] C [-]	E_a [kJ/mol]	r [-]	B C
Ni-ScSZ cermet	180	2.7e7	0.27 ± 0.01 0.17 ± 0.09	149	1.7e6	0.52 ± 0.04 0.37 ± 0.11
Ni-GDC cerment	159	2.7e6	0.49 ± 0.06 0.56 ± 0.02	132	2.2e5	0.51 ± 0.03 0.54 ± 0.05
Ni-GDC co impregnated on LST-GDC	97	8400	0.75 ± 0.06 0.54 ± 0.07	101	14700	0.77 ± 0.14 0.49 ± 0.06
Rh-GDC co-impregnated on LST-GDC	101	14900	0.61 ± 0.11 0.50 ± 0.06	106	26000	0.69 ± 0.08 0.52 ± 0.03

3.1.2.3 Ohmic Overpotential

In electrochemical cells, the movement of charged particles (i.e. ions and electrons) results in energy losses. The reason for this is the materials in which charged particles move through have a natural resistance to this movement. This resistance leads to an over potential which the cell experiences is called the **ohmic overpotential**.

In SOCs, the charged particles which move are **electrons** (through the electrodes and bi-polar plates) and **oxide ions** (through the electrolyte). As the cell can be electrically modelled as ”resistors in series”, the total resistance of charged particles to movement through the cell can be expressed by Equation 3.18 [50].

$$R_{tot} = R_{mem} + R_{cat} + R_{an} + R_{con} \tag{3.18}$$

Where:
R_{tot} is the total resistance [Ωcm^2]
R_{mem} is the resistance from ions moving through the membrane (electrolyte) [Ωcm^2]
R_{cat} is the resistance from electrons moving through the cathode [Ωcm^2]
R_{an} is the resistance from electrons moving through the anode [Ωcm^2]
R_{con} is the resistance from electrons moving between solid-solid interfaces (i.e. electrode to bipolar plate) [Ωcm^2]

This total resistance can then be used to determine the ohmic overpotential using an area dependant version of Ohm's Law:

Definition: Ohmic Overpotential - Ohm's law

$$\eta_{ohmic} = R_{tot} \cdot i \tag{3.19}$$

[50]

Where:
η_{ohmic} is the ohmic overpotential [V]
R_{tot} is the summed resistance of the electrical and electrolyte components in the cell [Ωcm^2]
i is the current density going through the cell [A/cm^2]

Most papers neglect the impact of the electrical resistance in the cell as it is negligible compared to the resistance from the electrolyte[50] [51]. In other words, the resistance from the oxide ion travelling through the membrane is the dominate ohmic overpotential in the cell. This is demonstrated in Appendix A.

The ohmic resistance for the membrane can be described by the following:

Definition: Membrane Resistance

$$R_{mem} = \frac{l_{mem}}{\sigma_{mem}} \tag{3.20}$$

Where:
R_{mem} is the ohmic resistance of membrane [Ωcm^2]
l_{mem} is the thickness of the membrane [cm]
σ_{mem} is the membrane conductivity [S/cm] [a]

[a] S is the unit Siemens. It is equivalent to one over ohms. That is

$$4\ S = \frac{1}{4}\ \Omega$$

The conductivity of an oxide ion transport capable membrane is highly dependant on temperature [50], shown by Equation 3.21.

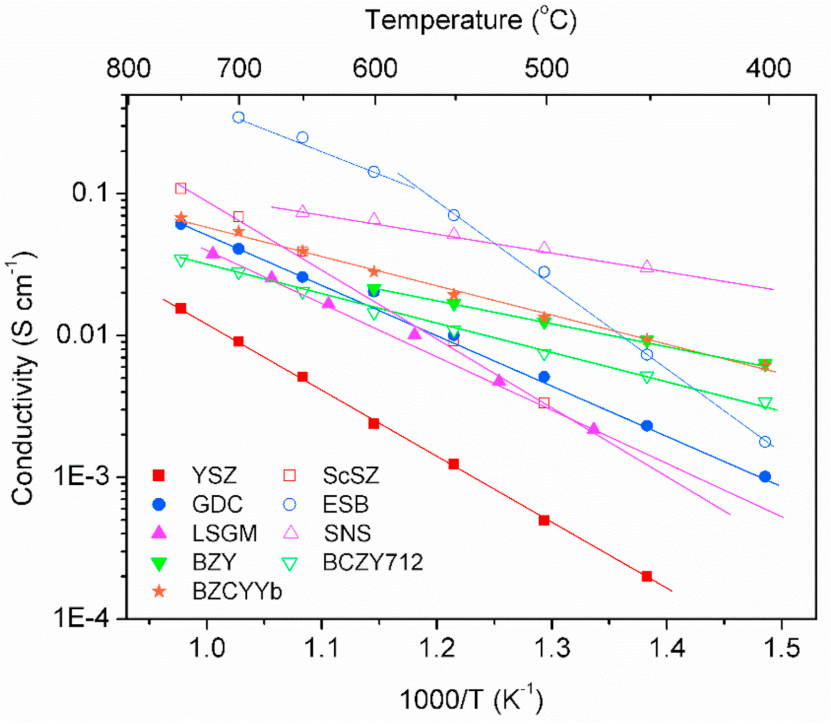

Figure 3.3: Oxygen ion conductivity vs temperature for selected electrolyte materials. Image taken from [52]

Definition: Electrolyte Conductivity

$$\sigma_{mem} = \frac{\sigma_0}{T} \cdot \exp\left(\frac{-E_{el}}{R \cdot T}\right) \tag{3.21}$$

a

[a] Taken from [50]

Where:
σ_{mem} is the conductivity of the membrane [S/m]
σ_0 is the pre-exponential factor of the conductivity [S/m]
T is the temperate of the membrane [K]
E_{el} is the activation energy for ion transport [J/mol]
R is the universal gas constant [J/mol K]

As mentioned in subsection 2.2.2, different electrolytes exist with different ionic conductivities. Therefore σ_0 and E_{el} in Equation 3.21 are **not** constant between materials. Data for σ_0 and E_{el} can be found using data presented in other papers. Specifically, data from Figure 3.3 which comes from [52], can be taken and curve fitted to Equation 3.21 for various commonly used electrolyte materials. The data was taken from the plot using **Plot Digitizer** [53]. For select materials, the results of the curve fit are presented in Table 3.3.

3.1.2.4 Concentration Overpotential

Electrolysers produce as much H_2/O_2 from H_2O as directly proportional to the number of electrons supplied to the water in the reaction; this comes from the conservation of charge law. For every two moles of electrons, one more of hydrogen and half a mol of oxygen will be produced (assuming sufficient H_2O supply). This is irrespective of potential applied (assuming the potential is above the Nernst Potential). At some point, the transport of H_2O towards the location of the electrons in the electrode will be limited by diffusion ”speed limits”. This phenomena increases the required potential which must be applied to the cell to produce the same current density. The increased potential for this is called

Material	σ_0 [S/m]	E_{el} [J/mol]	R^2
8YSZ	133 117 255.5	96 611.97	0.99999
8ScSZ	1 678 024 660.99	101 049.61	0.99999
GDC	44 369 254.18	75 433.20	0.99999
LSGM	58 121 151.64	79 730.44	0.99998

Table 3.3: Curve fit values for select electrolyte materials. data comes from selecting point of a line of the relevant curve in Figure 3.3 and then curve fitting the data using the equation Equation 3.21. The R^2 values from the curve fits are shown in the last column. The function ”curve_fit” from scipy's optimization package was used to determine the curve fit values

the **concentration overpotential** or the **diffusion overpotential** [46]. The effects of this phenomena have already been described in subsubsection 3.1.2.1 with the changes in partial pressure near the electrodes. While other literature considered these effects separately, a diffusion model will be incorporated to determine the partial pressure near the electrodes for the Nernst Potential, therefore including the effects of concentration overpotential. As a result, concentration overpotential is not separately modelled.

3.1.3. Diffusion Models

As mentioned in subsubsection 3.1.2.1 and subsubsection 3.1.2.4, the partial pressure of the reactants/products at the electrodes impacts the potential required to electrolyse water. The phenomena around transport limitations was discussed in subsubsection 3.1.2.4 and this will be expanded upon in this section.

There are three main methods in literature to model transport phenomena around electrodes in SOCs [54]. These methods are diffusion models which describe the mass transport behaviour of gasses around porous materials (i.e. the electrodes). The models used are:

- Fick's Diffusion Model
- Stefan-Maxwell Model
- The Dusty Gas Model (DGM)

Only two models will be discussed. These models will be Fick's diffusion and DGM. Stefan-Maxwell is not discussed as DGM is already an extended version of the Stefan-Maxwell model [55]. The main differences between Fick's and DGM is that DGM accounts for Knudsen diffusion phenomena over a wider range of porous media structures [3] and does not assume equal-molar counter diffusion which Fick's law assumes as this is an invalid assumption if the difference in compound molar mass is significantly different [55].

It should be noted that the literature regarding diffusion modelling/mass transport phenomena modelling is typically semi-empirical in formulation. Additionally, the field is an active area of research and treated with caution as inconsistencies with model usage occur regularly [56].

3.1.3.1 Fick's Diffusion

Fick's diffusion is the simplest diffusion model used in SOC modelling and also the least computationally expensive. The generic form of Fick's diffusion is shown in Equation 3.22.

[3] Knudsen diffusion is explained later in this section

Definition: Fick's law of Diffusion

$$N_q = -\frac{D_q^{eff}}{RT} \cdot \nabla(X_q P) \tag{3.22}$$

Where:
N_q is the molar flux of species q [mol/m^2]
D_q^{eff} is the effective diffusion coefficient of species q [m^2/s]
X_q is the molar fraction of species q [-]
P is the operating pressure [Pa]
R is the universal gas constant [J/mol K]
T is the temperature [K]

[a]

[a] Equation adapted from [57] to be n-dimensional

The effective diffusion coefficient, D_q^{eff} can be expressed using the **Bosanquet Formula** for a binary gas mixture. For gas mixtures with more than two species, the dusty gas model is required due to the formulation of Fick's diffusion model. In general, the Bosanquet Formula has a limited range of validity, but it is regularly used in SOC modelling to include the effects of Knudsen diffusion without requiring the computational expense of the dusty gas diffusion model. The main limiting factor of the Bosanquet Formula is only valid when the molecular weights of the bi-molecular system are comparable is the formula valid [56]. A study of the Bosanquet Formula on single species systems shows that the Bosanquet formula is increasingly more valid as the pore radius of the porous material increases [58], the applicability of this study to non unitary systems is unclear but is worth keeping in mind when using the formula.

Definition: Bosanquet Formula

$$\frac{1}{D_q^{eff}} = \frac{1}{D_{q,Kn}^{eff}} + \frac{1}{D_{w-q}^{eff}} = \frac{\xi}{\phi} \cdot \left(\frac{1}{D_{w-q}} + \frac{1}{D_{q,kn}} \right) \tag{3.23}$$

[a]

[a] Equation taken from [59] although it is not called this in the reference

Where:
D_q^{eff} is the effective diffusion coefficient [m^2/s]
ξ is the tortuosity of the porous material [-]
ϕ is the porosity of the porous material [-]
D_{w-q} is the **Molecular Binary Diffusion Coefficient** [m^2/s]
$D_{q,K}$ is the **Knudsen Diffusion Coefficient** [m^2/s]

The molecular binary diffusion coefficient and the Knudsen diffusion coefficient can be calculated using the equations shown in subsubsection 3.1.3.3.

For the 1D case of gas diffusion through a porous material, Fick's diffusion model can be solved into closed form equations for the electrolysis of a species, a. Using the method for finding a closed form solution for Fick's diffusion from [57].

Using the relation of conservation of charge:

$$N_q = \frac{i}{zF} \tag{3.24}$$

Where:
N_a is the molar flux of species a [mol/m^2]

z is the number of electrons involved in the reaction [-]
F is Faraday's constant [C/mol]
i is current density [A/m^2]

With the boundary conditions:

$$\frac{\partial X_q}{\partial x}|_{x=d} = -\frac{i}{zF} \cdot \frac{RT}{D_q^{eff} P}$$
$$X_q|_{x=0} = X_q^{bulk}$$

Where:
X_a is the molar ratio of species a [-]
X_a^{bulk} is the molar ratio of species a far away from the electrode [-]
x is the 1D length of the electrode [m]
d is the total thickness of the electrode [m]
R is the universal gas constant [J/mol k]
T is the temperature [K]
z is the number of electrons involved in the reaction [-]
F is Faraday's constant [C/mol]
D_a^{eff} is the effective diffusion coefficient of species a [m^2/s]
P is the operating pressure [Pa]
i is the current density [A/m^2]

With $x = d$ being the location of the electrode-electrolyte interface, the following results:

Definition: Closed form 1D Fick's Diffusion generic: Molar fractions

$$X_a = X_a^{bulk} - \frac{RT}{D_a^{eff} \cdot P} \cdot \frac{i}{zF} \cdot x \tag{3.25}$$

Where:
X_a is the molar ratio of species a [-]
X_a^{bulk} is the molar ratio of species a far away from the electrode [-]
x is the 1D length of the relevant electrode [m]
R is the universal gas constant [J/mol K]
T is the temperature [K]
F is Faraday's constant [C/mol]
D_a^{eff} is the effective diffusion coefficient of species a [m^2/s]
P is the operating pressure at the electrode [Pa]
i is the current density [A/m^2]

For steam electrolysis, this becomes:

Definition: Closed form 1D Fick's Diffusion: Molar fractions - H_2O Electrolysis

$$X_{H_2O} = X_{H_2O}^{bulk} - \frac{RT}{D_{H_2O}^{eff} \cdot P} \cdot \frac{i}{2F} \cdot x \tag{3.26}$$

$$X_{H_2} = 1 - X_{H_2O} = 1 - \left(X_{H_2O}^{bulk} - \frac{RT}{D_{H_2O}^{eff} \cdot P} \cdot \frac{i}{2F} \cdot x \right) \tag{3.27}$$

$$X_{O_2} = X_{O_2}^{bulk} - \frac{RT}{D_{O_2}^{eff} \cdot P} \cdot \frac{i}{2F} \cdot x \tag{3.28}$$

Where:
X_{H_2O} is the molar ratio of H_2O [-]
X_{H_2} is the molar ratio of H_2 [-]
X_{O_2} is the molar ratio of O_2 [-]
$X_{H_2O}^{bulk}$ is the molar ratio of species H_2O far away from the electrode [-]
$X_{O_2}^{bulk}$ is the molar ratio of species O_2 far away from the electrode [-]
x is the 1D length of the relevant electrode [m]
R is the universal gas constant [J/mol K]
T is the temperature [K]
F is Faraday's constant [C/mol]
$D_{H_2O}^{eff}$ is the effective diffusion coefficient of species H_2O [m^2/s]
$D_{O_2}^{eff}$ is the effective diffusion coefficient of species O_2 [m^2/s]
P is the operating pressure at the electrode [Pa]
i is the current density [A/m^2]

Utilising the relationship for partial pressure of a gas:

$$p_q = \frac{n_q \cdot \frac{R \cdot T}{V}}{\sum_i^T n_i \cdot \frac{R \cdot T}{V}} \cdot P = X_q \cdot P$$

Then the following relations can be used to determine the partial pressure of the species near the surface of the electrode-electrolyte interface

Definition: Closed form 1D Fick's Diffusion: Partial Pressures

$$p_{H_2O} = p^{bulk}_{H_2O} - \frac{RT}{D^{eff}_{H_2O}} \cdot \frac{i}{2F} \cdot x \tag{3.29}$$

$$p_{H2} = P - p_{H_2O} = P - \left(p^{bulk}_{H_2O} - \frac{RT}{D^{eff}_{H_2O}} \cdot \frac{i}{2F} \cdot x \right) \tag{3.30}$$

$$p_{O_2} = p^{bulk}_{O_2} - \frac{RT}{D^{eff}_{O_2}} \cdot \frac{i}{2F} \cdot x \tag{3.31}$$

Where:
p_q is the partial pressure of species q [Pa]
p^{bulk}_q is the partial pressure of species q far away from the electrode [Pa]
x is the 1D length of the relevant electrode [m]
R is the universal gas constant [J/mol K]
T is the temperature [K]
F is Faraday's constant [C/mol]
D^{eff}_q is the effective diffusion coefficient of species a [m^2/s]
P is the operating pressure at the electrode [Pa]
i is the current density [A/m^2]

3.1.3.2 DGM

The Dusty Gas Model (DGM) is a more computational expensive diffusion model which is superior to Fick's diffusion model in that DGM is not limited to modelling only binary gas systems and it accurately incorporates Knusden diffusion where Fick's diffusion typically relies on the not-always-valid Bosanquet Fomula.

Definition: Dusty Gas Model - Generic

$$J_k = -\left(\Sigma_{l=1}^{N} \frac{P}{R \cdot T} \cdot D_{k,l}^{DGM} \nabla y_l + \left(\Sigma_{l=1}^{N} \frac{P}{R \cdot T} \cdot \frac{D_{k,l}^{DGM} \cdot y_l}{D_{l,Kn}^{e}}\right) \cdot \frac{B_g}{\mu} \nabla P\right) \tag{3.32}$$

Where: $D_{k,l}^{DGM}$ = H^{-1} with the entries of H being expressed by:

$$h_{k,l} = \left(\frac{1}{D_{k,Kn}^{eff}} + \Sigma_{j=1,j\neq k} N \frac{y_j}{D_{k,j}^{e}}\right) \delta_{k,l} + (\delta_{k,l} - 1) \frac{y_k}{D_{k,l}^{e}} \tag{3.33}$$

[a]

[a] Equation adapted from [56] and [50]

Where:
N is the total number of gas species in exist around the porous electrode [-]
y_k is the mol fraction of species k [-]
J_k is the molar flux of species k inside the porous electrode [mol/m^{2}s]
$D_{k,Kn}^{eff}$ is the effective Knudsen coefficient of species k inside the porous electrode [m^2/s]
$D_{k,l}^{eff}$ is the effective binary diffusion coefficient of species k in species l [m^2/s]
B_g is the permeability constant [m^2]
δ_{kl} is Kronecker delta [-]
μ is the mixture viscosity
P is the total pressure in the electrode [Pa]
R is the universal gas constant [J/mol K]
T is the temperature [K]

When assuming diffusion only occurs in one dimension, Equation 3.32 reduces to the following:

Definition: Dusty Gas Model - 1D

$$J_k = -\left(\Sigma_{l=1}^{N} \frac{P}{R \cdot T} \cdot D_{k,l}^{DGM} \frac{\partial y_l}{\partial z} + \left(\Sigma_{l=1}^{N} \frac{P}{R \cdot T} \cdot \frac{D_{k,l}^{DGM} \cdot y_l}{D_{l,Kn}^{e}}\right) \cdot \frac{B_g}{\mu} \frac{\partial P}{\partial z}\right) \tag{3.34}$$

Where: $D_{k,l}^{DGM} = H^{-1}$ with the entries of H being expressed by:

$$h_{k,l} = \left(\frac{1}{D_{k,Kn}^{eff}} + \Sigma_{j=1,j\neq k} N \frac{y_j}{D_{k,j}^{e}}\right) \delta_{k,l} + (\delta_{k,l} - 1) \frac{y_k}{D_{k,l}^{e}} \tag{3.35}$$

[a]

[a] Equation adapted from [56] and [50]

Where:
N is the total number of gas species in exist around the porous electrode [-]
y_k is the mol fraction of species k [-]
J_k is the molar flux of species k inside the porous electrode [mol/m^{2}s]
$D_{k,Kn}^{eff}$ is the effective Knudsen coefficient of species k inside the porous electrode [m^2/s]
$D_{k,l}^{eff}$ is the effective binary diffusion coefficient of species k in species l [m^2/s]
B_g is the permeability constant [m^2]
δ_{qw} is Kronecker delta [-]
∂z is refers to the direction into the electrode, towards the electrode-electrolyte interface
μ is the mixture viscosity
P is the total pressure in the electrode [Pa]
R is the universal gas constant [J/mol K]
T is the temperature [K]

While in reality the total pressure inside the electrode changes as a function of electrode thickness (given a fixed species flux) [56], if the thickness of the electrode does not exceed 500 μm, then the numerical difference between assuming fixed total pressure (isobaric diffusion) and variable total pressure inside the electrode is negligible [60]. Therefore, Equation 3.34 can be simplified further:

Definition: Dusty Gas Model isobaric - 1D

$$J_k = -\Sigma_{l=1}^{N} \frac{P}{R \cdot T} \cdot D_{k,l}^{DGM} \frac{\partial y_l}{\partial z} \tag{3.36}$$

Where: $D_{k,l}^{DGM} = H^{-1}$ with the entries of H being expressed by:

$$h_{k,l} = \left(\frac{1}{D_{k,Kn}^{eff}} + \Sigma_{j=1,j\neq k} N \frac{y_j}{D_{k,j}^{e}} \right) \delta_{k,l} + (\delta_{k,l} - 1) \frac{y_k}{D_{k,l}^{e}} \tag{3.37}$$

[a]

[a] Equation adapted from [56] and [50]

Where:
N is the total number of gas species in exist around the porous electrode [-]
y_k is the mol fraction of species k [-]
J_k is the molar flux of species k inside the porous electrode [mol/m^{2}s]
$D_{k,Kn}^{eff}$ is the effective Knudsen coefficient of species k inside the porous electrode [m^2/s]
$D_{k,l}^{eff}$ is the effective binary diffusion coefficient of species k in species l [m^2/s]
δ_{qw} is Kronecker delta [-]
∂z is refers to the direction into the electrode, towards the electrode-electrolyte interface
P is the total pressure in the electrode [Pa]
R is the universal gas constant [J/mol K]
T is the temperature [K]

The following need to be determine to solve the DGM diffusion equation:

- J_k - molar flux of the species k being investigated
- $D_{k,Kn}^{eff}$ - effective Knudsen coefficient of species k
- $D_{k,l}^{eff}$ - effective binary diffusion coefficient of species k and l

Similar to Fick's diffusion, the driving force for diffusion is the chemical reaction at the electrode-electrolyte interface, therefore the molar flux species experience is directly proportional to the experienced current density based of the relation from conservation of charge. i.e.

$$N_q = \frac{i}{zF} \tag{3.38}$$

Where:
N_a is the molar flux of species a [mol/m^2]
z is the number of electrons involved in the reaction [-]
F is Faraday's constant [C/mol]
i is current density [A/m^2]

Additionally, effective diffusion coefficients are a function of porous material porosity and tourorosity, specifically:

Definition: Effective Diffusion Coefficients

$$D^{eff} = \frac{\phi}{\xi} D \tag{3.39}$$

Where:
D^{eff} is an effective diffusion coefficient [m^2/s]
ϕ is the porosity of the material [-]
ξ is the tourtorosity of the material [-]
D is a diffusion coefficient [m^2/s]

The formulae required to calculated Knudsen and binary diffusion coefficients can be found in sub-subsection 3.1.3.3.

3.1.3.3 Diffusion Coefficients

Definition: Molecular Binary Diffusion Coefficient

Molecular Binary Diffusion Coefficient obtained by the Chapman-Enskog theory of ideal gas

$$D_{w-q} = 0.00266 \cdot \left(\frac{1}{M_w} + \frac{1}{M_q} \right)^{0.5} \cdot \frac{T^{3/2}}{P \cdot \sigma_{q-w}^2 \cdot \Omega_D} \tag{3.40}$$

[a]

[a] Equation modified from [61]. This equation is empirical and simplified from a more detailed equation

Where:
M_q and M_w are the molar mass of species q and w respectively [g/mol]
T is the temperature [K]
P is the operating pressure [bar]
Ω_D is a dimensionless diffusion collision integral [-]
σ_{q-w} is the average mean characteristics length of species q and w [Å]

The average mean characteristic length of species q and w, σ_{q-w} can be found from:

$$\sigma_{q-w} = \frac{\sigma_q + \sigma_w}{2} \tag{3.41}$$

Where:
σ_{q-w} is the average mean characteristics length of species q and w [Å]
σ_q is the mean characteristic length of species q [Å]
σ_w is the mean characteristic length of species w [Å]

The dimensionless diffusion collision integral can be found analytically with the following [55] [48] [61]:

$$\Omega_D = \frac{1.06036}{\tau^{0.1561}} + \frac{0.193}{exp(0.47635 \cdot \tau)} + \frac{1.03587}{exp(1.52996 \cdot \tau)} \frac{1.76474}{3.89411 \cdot \tau} \tag{3.42}$$

Where:

$$\tau = \frac{k \cdot T}{\varepsilon_{q,w}} \tag{3.43}$$

Where the Lennard-Jones energy, $\varepsilon_{q,w}$ is equivalent to: [55] [48]

$$\varepsilon_{q,w} = \sqrt{\varepsilon_q \cdot \varepsilon_w} \tag{3.44}$$

Where ε_q and ε_w are the **Lennard-Jones** potentials for species q and w respectively [K] [61].

Knudsen diffusion describes additional diffusion of molecules inside porous materials where collisions with the surface of the material can occur.

Definition: Knudsen Diffusion

$$D_{q,Kn} = 9700 \cdot r\sqrt{\frac{T}{M_q}} \tag{3.45}$$

[a]

[a] Equation adapted from [59]

Where:
$D_{q,Kn}$ is the Knudsen Diffusion Coefficient [cm^2/s]
r is the mean pore radius of the electrode [cm]
M_q is the molar mass of species q [g/mol]
R is the universal gas constant [J/mol K]
T is the temperature [K]

3.1.3.4 Partial Pressure Modelling

The Fick's diffusion model calculate the partial pressure of a single species, however the partial pressure of each species is important as it is the partial pressure of a species at the surface of an electrode which determines the Nernst Potential of a cell as described in subsubsection 3.1.2.1. It should be noted that the following is specifically only relevant for Fick's diffusion as DGM already accounts for all species partial pressures. However as Fick's diffusion is *only* valid for binary systems, the equations which follow, while generic and are compatible with non binary systems, should only be used with binary gas systems when applied to Fick's diffusion.

The overall pressure of a system is equal to the sum of the pressures exerted by the gasses inside the system. The pressure of a single gas inside a mixture of gasses is known as its **partial pressure**. For a single species gas, the partial pressure is equal to the system pressure. For a multi species gas mixture, assuming ideal gas law holds, the partial pressure of a single species is equal to the molar ratio of the gas in the mixture, multiplied by the total pressure, that is:

Definition: Partial Pressure

$$p_x = \frac{n_x}{\Sigma_{i=1}^{T} n_i} \cdot P_{total} \tag{3.46}$$

Where:
p_x is the partial pressure of species x [Pa]
n_x is the number of moles of species x in the mixture [mols]
T is the total number of gasses in the mixture [-]
n_i is the number of mols of species i [mols]
P_{total} is the total pressure of system [Pa]

For a multi species, balanced reaction, namely,

$$\upsilon_A\text{A} + \upsilon_B\text{B} \longrightarrow \upsilon_C\text{C} + \upsilon_D\text{D} + \upsilon_E\text{E} + ...$$

Where species A, B, C, D, E are all at the same electrode, then the partial pressures in the system at the electrode can be expressed as (where P_T is the total pressure):

$$P_T = p_A + p_C + p_D + p_E + ...$$
$$P_T - p_A - p_B = p_C + p_D + p_E + ...$$

When no side reactions occur, then the chemical reaction which occurs is balanced in its stochiometric ratio, then the products at the electrode are proportional to each other based of their stochiometric coefficient in the balanced electrochemical equation. i.e.

$$P_T - p_A - p_B = p_C + p_D + p_E + ...$$
$$P_T - p_A - p_B = z \cdot p_C$$

With:

$$z = \frac{1}{\upsilon_C} \Sigma_{i=C} \upsilon_i$$

Where:
z is a ratio between the products at the electrode [-]
υ_i is stochiometric ratio of product species i [-]
υ_C is stochiometric ratio of species C [-]
P_T is the total pressure of the system [Pa]
p_A, p_B... are the partial pressures of species A, B... [Pa]

The partial pressure of the reactants at the electrode, A and B, are found via the diffusion models. Therefore, once the reactant partial pressure at the electrode have been calculated, the partial pressure of the product species can be determined via the following:

$$p_C = \frac{P_T - \Sigma_{j=1} p_j}{z}$$
$$p_i = p_C \cdot \frac{\upsilon_i}{\upsilon_C}$$

Where:
p_j is the partial pressure of reactant species j [Pa]
p_i is the partial pressure of product species i [Pa]
υ_i is the stochiometric ratio of product species i [-]
υ_C is the stochiometric ratio of product species C [-]
p_C is the partial pressure of product species C [Pa]
P_T is the total pressure [Pa]

3.1.4. Detailed Model Results

The output of the detailed model is known as a **voltage-current curve**, or a **V-I curve**. Examples of V-I curves for both SOEC and SOFC modes can be seen in Figure 3.4 and Figure 3.5 respectively. The V-I curve is the relationship between the applied/obtained voltage from the cell (depending if it is in SOEC or SOFC mode) and the current density the cell experiences. At current densities close to 0 A/cm^2, the Nernst Voltage is what both SOEC and SOFC cells experience. As the current density increases, the activation overpotential dominates and the voltage rises quickly in SOEC mode and decreases quickly in SOFC mode. The voltage approaches vertical as the current density approaches the **limiting current density**. This is the current density at which gas particles in the electrodes are not able to move to the triple phase boundary fast enough to maintain the current density, and therefore the voltage required in SOEC mode approaches infinity and the voltage obtained in SOFC mode approaches 0 V.

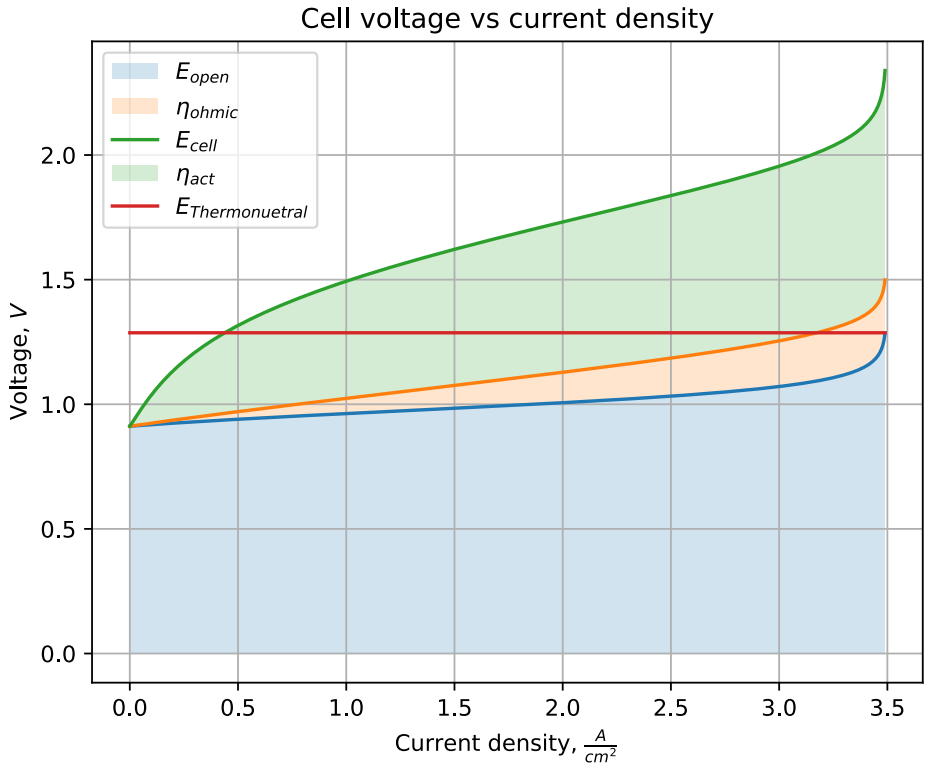

Figure 3.4: Example voltage-current density curve for a SOC in electrolysis mode

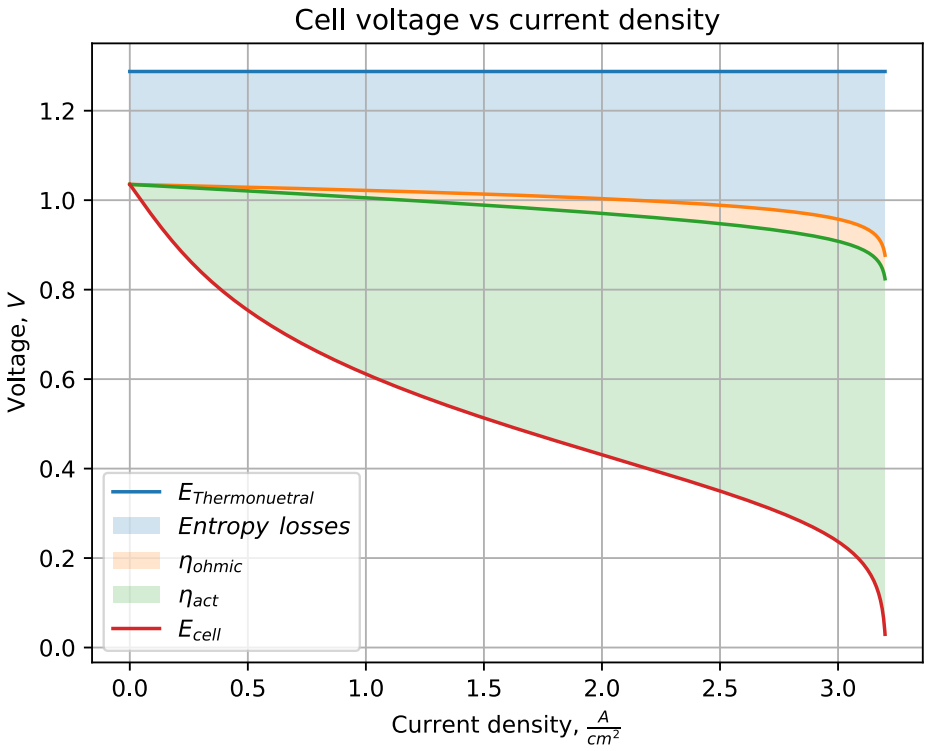

Figure 3.5: Example voltage-current density curve for a SOC in fuel cell mode

3.2. SOEC System Model

The SOEC system model takes the detailed model, combines it with models for the Balance of Plant (BOP) components of a SOEC system, and produces efficiency curves which are utilised by the Simulink model (discussed in section 3.3) for a range of electrical and thermal power values. This section first presented the SOEC system layout, then goes onto discuss the BOP models along with the models for cell operation in stacks. Finally, the method for producing the efficiency curves is presented.

3.2.1. Assumptions

This section outlines the assumptions made specifically in the SOEC system model. As the detailed model feeds directly into the SOEC system model, all assumptions discussed in subsection 3.1.1 are valid here as well. The assumptions explicitly made in the SOEC system model are:

- Isobaric flow
- Single phase flow

3.2.1.1 Isobaric flow over BOP components

Isobaric means the pressure of a system stays constant while a thermodynamic process occurs. In the context of the SOEC system model, this means that over the stack component and all BOP components, **except for the pumps**, it is assumed that there is no pressure change occurring. This is a realistic assumption if the flow of the system is small and there are no flow constricting orifices. A detailed design of all system components is beyond the scope of this thesis and therefore for simplicity, it is assumed that the pressure change in non pump components is negligible.

3.2.1.2 Single phase flow

Single phase refers to each species inside a flow stream existing only in one phase. For example, if water and hydrogen are in a flow, then assuming the hydrogen is its gaseous phase, the water is either fully in its liquid phase or fully in its gaseous phase. It is assumed that no species exits on it's saturation curve where both liquid and gaseous phases both exist (i.e. two phase flow). This assumption is valid as the only feasible location inside the designed system model where two phase flow can occur is in a heat exchanger. To prevent two-phase flow occur, water coming into the heat exchanger will first go through the vaporiser which ensures the water is away from its saturation curve. No other species which can be utilised in the SOEC system model exist near its saturation curve.

3.2.2. SOC System Layout

Figure 3.6 shows a flow system diagram of the SOEC system implemented in the SOEC system model. This system diagram shows that both the anode and cathode side of the system have heat exchangers which exchange high temperature output flow from the stacks with the incoming flows used for electrolysis. Each side also has a trim heat to ensure each flow has the correct temperature going into the stack system. Each side has a pump to create the pressure difference required for the flows to move through the system. The cathode side also has another heat exchanger from which thermal energy from waste industrial process (such as steel production, paper production etc) is able to be used to improve the overall system electrical efficiency by providing a part of energy required for the heating of the incoming flows.

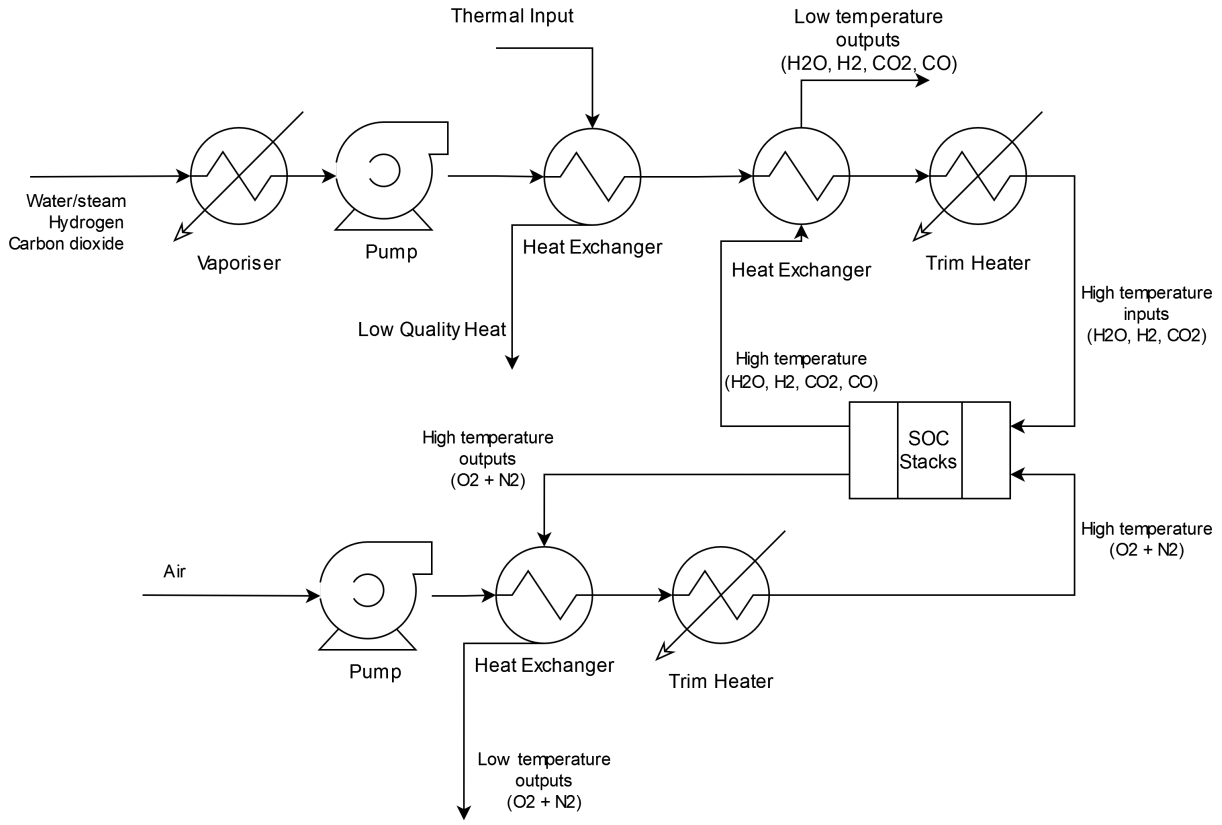

Figure 3.6: System layout design for the SOEC system model. Inspired by other system designs available in the public domain. See subsection 2.3.1

3.2.3. Heat Exchanger Modelling

Heat exchangers are used in SOC systems to recover the high levels of thermal energy leaving the SOEC (the ”hot” flow) and transfer it to the incoming flow into the SOEC (the ”cold” flow) in order to improve the energy efficiency of the system. The heat exchanger was modelled as a **counter flow heat exchanger**. A counter flow heat exchanger has the hot and cold flows coming in from different ends of the heat exchanger, allowing for higher temperature changes between the hot and cold fluids when compared to other heat exchanger types (namely parallel/co-current flow heat exchangers. The workings of a counter flow and co-current flow heat exchangers can be seen in Figure 3.7.

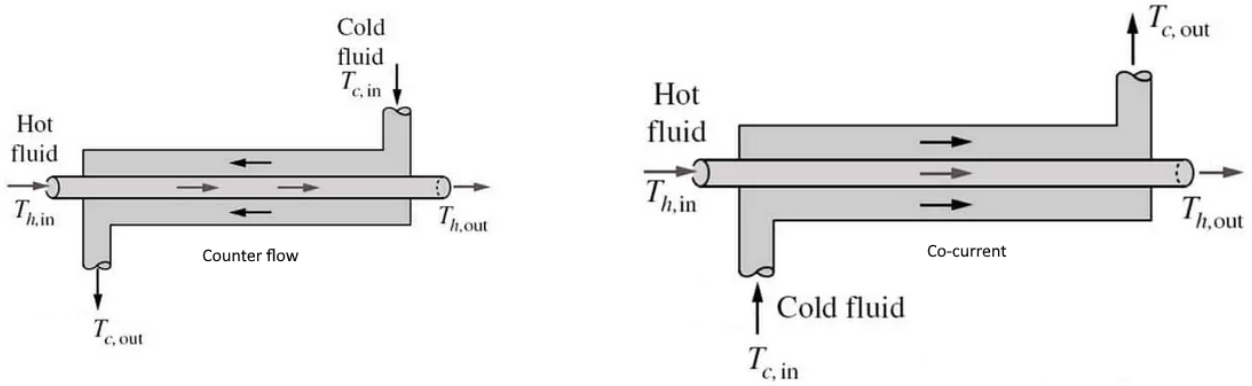

Figure 3.7: Graphical view of the workings of a counter flow and co-current heat exchanger. Image adapted from [62]

A heat exchanger can be modelled as a device which transfers enthalpy from the hot flow to the cold flow. The maximum theoretical enthalpy change for the hot flow occurs when the temperature of the hot flow at the inlet will have its temperature at the outlet equal to the temperature of the cold flow at the inlet. Similar logic applies for the maximum enthalpy change of the cold flow, albeit the temperature roles reversed. Mathematically this is:

$$\Delta H_{cold,\,,max,\,theory} = H_{cold,\,fcn}(T_{hot,\,in}) - H_{cold,\,fcn}(T_{cold,\,in}) \tag{3.47}$$
$$\Delta H_{hot,\,,max,\,theory} = H_{hot,\,fcn}(T_{hot,\,in}) - H_{hot,\,fcn}(T_{cold,\,in}) \tag{3.48}$$
$$\tag{3.49}$$

Where:
$\Delta H_{cold,\,,max,\,theory}$ is the theoretical maximum enthalpy change of the hot flow [J]
$\Delta H_{hot,\,,max,\,theory}$ is the theoretical maximum enthalpy change of the cold flow [J]
$H_{cold,\,fcn}()$ is the enthalpy of the cold flow at the conditions specified inside the parenthesis [J]
$H_{hot,\,fcn}()$ is the enthalpy of the hot flow at the conditions specified inside the parenthesis [J]
$T_{hot,\,in}$ is the temperature of the hot flow entering the heat exchanger [K]
$T_{cold,\,in}$ is the temperature of the cold flow entering the heat exchanger [K]
Note that units of joules, J, will become units of watts, W, when dealing with flows.

The maximum enthalpy change is equal to the **lowest** of the aforementioned maximum theoretical enthalpy changes, multiplied by the efficiency of the heat exchanger. That is:

$$\Delta H_{actual} = \eta_{exchange} \cdot MIN(\Delta H_{cold,\,,max,\,theory}, \Delta H_{hot,\,,max,\,theory}) \tag{3.50}$$

Where:
ΔH_{actual} is the enthalpy transfer the hot and cold flows [J]
$\eta_{exchange}$ is the efficiency of the heat exchanger [-]
$\Delta H_{cold,\,,max,\,theory}$ is the theoretical maximum enthalpy change of the hot flow [J]
$\Delta H_{hot,\,,max,\,theory}$ is the theoretical maximum enthalpy change of the cold flow [J]
$MIN()$ is a function which finds the minimum numerical value of the values inside its parenthesis separated by a comma
Note that units of joules, J, will become units of watts, W, when dealing with flows.

Therefore, the enthalpy of the hot and cold flow at the exit of the heat exchanger can be determined from the following:

$$H_{cold,\,out} = H_{cold,\,fcn}(T_{cold,\,in}) + \Delta H_{actual} \tag{3.51}$$
$$H_{hot,\,out} = H_{hot,\,fcn}(T_{hot,\,in}) - \Delta H_{actual} \tag{3.52}$$

Where:
$H_{cold,\,out}$ is the enthalpy of the cold flow at the exit of the heat exchanger [J]
$H_{hot,\,out}$ is the enthalpy of the hot flow at the exit of the heat exchanger [J]
$H_{cold,\,fcn}()$ is the enthalpy of the cold flow at the conditions specified inside the parenthesis [J]
$H_{hot,\,fcn}()$ is the enthalpy of the hot flow at the conditions specified inside the parenthesis [J]
$T_{hot,\,in}$ is the temperature of the hot flow entering the heat exchanger [K]
$T_{cold,\,in}$ is the temperature of the cold flow entering the heat exchanger [K]
ΔH_{actual} is the enthalpy transfer the hot and cold flows [J]
Note that units of joules, J, will become units of watts, W, when dealing with flows.

For the enthalpy values $H_{cold,\,out}$ and $H_{hot,\,out}$, there exists a single temperature at which they occur at, given a known mixture composition and pressure, assuming single phase flow. Therefore via root finding, the temperature value can be determined for the flows as they leave the heat exchanger.

3.2.4. Trim Heater Modelling

The trim heater is a device used to ensure the temperature of the fluid going into the electrolyser is at the required temperature. The trim heater is modelled as a joule heater. The amount of energy required to heat some mass up by a given temperature can be determined by taking the difference in enthalpy values between the different temperatures, assuming the heating process is isobaric and knowing the mass composition in terms of species in existence.

Definition: Trim Heater Model

$$P_{trim} = \frac{\dot{m} \cdot (h_2 - h_1)}{\eta_{trim}} \tag{3.53}$$

Where:
P_{trim} is the power required by the trim heater [W]
h_1 and h_2 are the specific enthalpy of the fluid flow at state 1 (the "cold" state) and state 2 (the "hot" state) respectively [J/kg]
$\dot{m}$ is the mass flow of the fluid flow [kg/s]
η_{trim} is the efficiency of the trim heater [-]

3.2.5. Pump Modelling

The movement of the fluids around the system is provided by pumps; devices which increase the total pressure of the fluid such that a pressure difference exists over the SOC stack and BOP, enabling fluid movement. The pressure differences used to move fluids around SOC systems is about 60 mbar [29]. Assuming the gas fluids behave as ideal gasses and the compression is adiabatic, then the temperature after adiabatic compression can be determined and the difference in enthalpy at the start and end points will give the energy for compression.

Definition: Pump Model

With:

$$T_2 = T_1 \cdot \frac{P_1 + \Delta P^{\left(\frac{\gamma-1}{\gamma}\right)}}{P_1} \tag{3.54}$$

The power required for Adiabatic Compression is:

$$P_{pump} = \frac{H(T_2, P_1 + \Delta P) - H(T_1, P_1)}{\eta} \tag{3.55}$$

[a]

[a] Adapted from [63] page 10-41

Where:
P_1 is pressure of the fluid at state 1 [Pa]
ΔP is the change in pressure f the fluid [Pa]
T_1 is the temperature of the fluid at state 1 [K]
T_2 is the temperature of the fluid at state 2 [K]
γ is the ratio of specific heats for the fluid [-]
P_{pump} is the energy required for compression of the fluid [J] [a]
$H(T_x, P_x)$ is the enthalpy of the fluid at state T_x, P_x [J]
η is the efficiency of the compressor [-]

[a] Note that units of joules, J, will become units of watts, W, when dealing with flows

3.2.6. Vaporiser Modelling

The vaporiser is a device which converts all liquid phase species into gaseous phase species. In this instance, water is the only species which might be liquid given the initial conditions. The vaporiser is modelled in a similar method to the trim heater, with the only caveat being that for numerical reasons, the vaporiser has to heat up the fluid higher than the temperature at the saturation curve (given a constant pressure). In essence, the vaporiser is modelled as a trim heater, as described in subsection 3.2.4.

Definition: Vaporiser Model

$$P_{vap} = \frac{\dot{m} \cdot (h_{fcn}(T_{sat} + y, P_1) - h_{fcn}(T_1, P_{1)})}{\eta_{trim}} \tag{3.56}$$

Where:
P_{vap} is the power required by the vaporiser [W]
$h_{fcn}()$ is the specific enthalpy of the flow at the conditions specified inside the parenthesis [J/kg]
T_{sat} is the temperature at which the species exists as both a gas and liquid [K]
y is the temperature to additionally heat the fluid by [K]
P_1 is the partial pressure of the species to vaporise [Pa]
$\dot{m}$ is the mass flow of the fluid flow [kg/s]
η_{trim} is the efficiency of the trim heater [-]

3.2.7. Stack Modelling

As mentioned in subsection 2.2.4, two different designs for cells are possible; tubular and planar with the majority of SOFC systems in use today being planner systems. As the manufacturing process for SOFC and SOEC planar systems are similar, and considering the fact that existing European companies are already commercialising planar SOC systems [29], the planar cell design will be used in the system modelling. Also mentioned in subsection 2.2.4, a stack is a collection of single cells connected electrically in series. In effect, it is one cell repeated as many times as there are cells in the stack. Therefore, a single cell can be modelled and the inputs/outputs for this cell can be multiplied by the number of cells present in the stack. As there is a practical limit to the number of cells in a single stack as discussed in subsection 2.2.4, multiple stacks are used in SOEC systems. With multiple stacks in a module [4], different control methods can be employed to operate the stacks at different current density levels, impacting stack life and overall system efficiency. Different control strategies are described in subsection 3.2.8.

As mentioned in section 3.1, it is possible for SOC to above or below the thermoneutral voltage, resulting in thermal energy being required for or produced during operation. In terms of modelling, it is assumed that the output temperature from the stacks is **constant** at the temperature the cells operate at. Therefore, when the system operates in endothermic conditions, the input temperature (controlled by the trim heaters) will be raised such that the thermal energy requirement for continued electrolysis is made up for by the increase in enthalpy of the incoming flow (above the cell operating temperature). When the system is running exothermic, the input temperature is kept constant at the required input temperature of the cells and all the excess thermal energy produced is considered to radiate/convect away from the system.

When stacks are not in operation (known as standby mode), they need to remain heated (explained further in section 3.3). The power for this ”heating” is calculated from a set percentage of the stacks design power, and this power amount is required to be given to the stack when it in standby mode.

3.2.8. Control Methods

A single stack can only be operated one way, in that all cells inside a stack operate with the same current density/power level. A module, which is a collection of stacks, can be operated in different ways. That

[4] a module is a collection of stacks

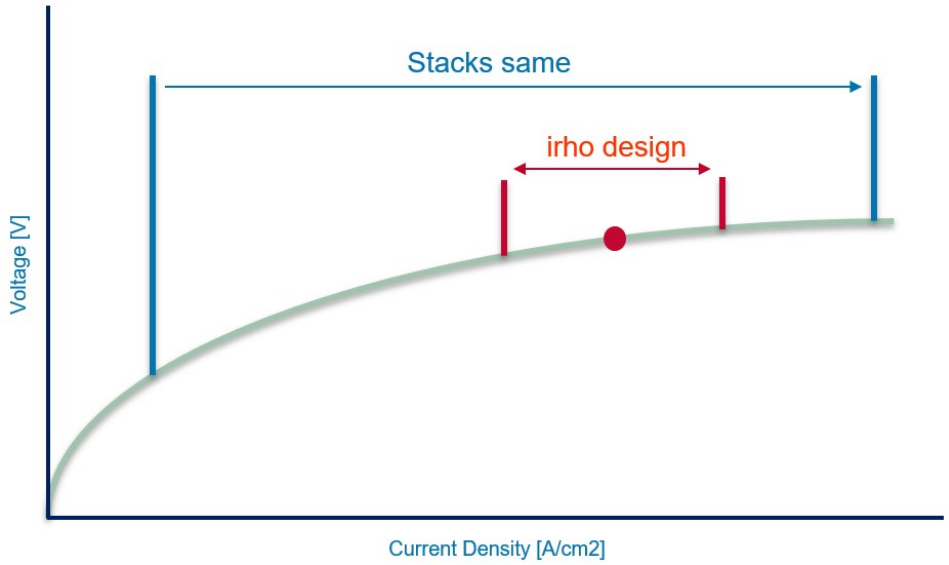

Figure 3.8: The two different control strategies which have been implemented. This figure shows how stacks are operated on a cell level for the different control methods. "stacks same" operates all stacks (and therefore cells) at the **same** current density, with the overall system going from a low current density to a high current density together. "irho design" operates a limited number of stacks as close to their design current density as possible. The stacks which are on, are allowed to operate within a limited current density range. The stacks which are not on, have a current density of 0 A/cm^2. More stacks are turned on as the system power increases

is, some stacks could be off entirely while others are at maximum power, or all stacks could be on at the same power level. Other research has focused on single stack operation, with consideration to efficient BOP control [64]. The SOEC system model is written to focus on module/stack leading operation, with the BOP operating as required to support the desired operation of the stacks.

Two different control methods are implemented

- stacks same
- irho design

In essence, these control methods just operate the stacks, on a cell level, differently as known in Figure 3.8. Figure 3.8 shows how the current density (on a cell level) in different control system designs.

3.2.8.1 irho design

This operation strategy is intended to operate the system on the principal that SOECs degrade less when they are operated at their design current density, with minimal fluctuations between the maximum and minimum operating current densities. In reality, stacks will vary their operating current density as the power over a stack will change as power available to a system/desired output changes. Therefore, there is a minimum power level a stack requires to operate and a maximum power level it can withstand. For smooth transition between changes in power to a module, more stacks can be turned on. For the module to have a smooth power transition between stack levels, the maximum power level of n many stacks should be greater than or equal to the minimum power level of $n + 1$ stacks. This can be graphically demonstrated in Figure 3.9.

3.2.8.2 Stacks same

This operation strategy operates all stacks in a system at the same current density. The advantages of this system is there is no sudden change in current density of cells as all stacks are operated with the same current density. However given certain current density ranges, the minimum power at which a system can operate at increases significantly. The advantage is that a higher efficiency at the same system power level (compared to irho design control method) is possible, as typically the lower the current density if a cell, the higher the electrical efficiency.

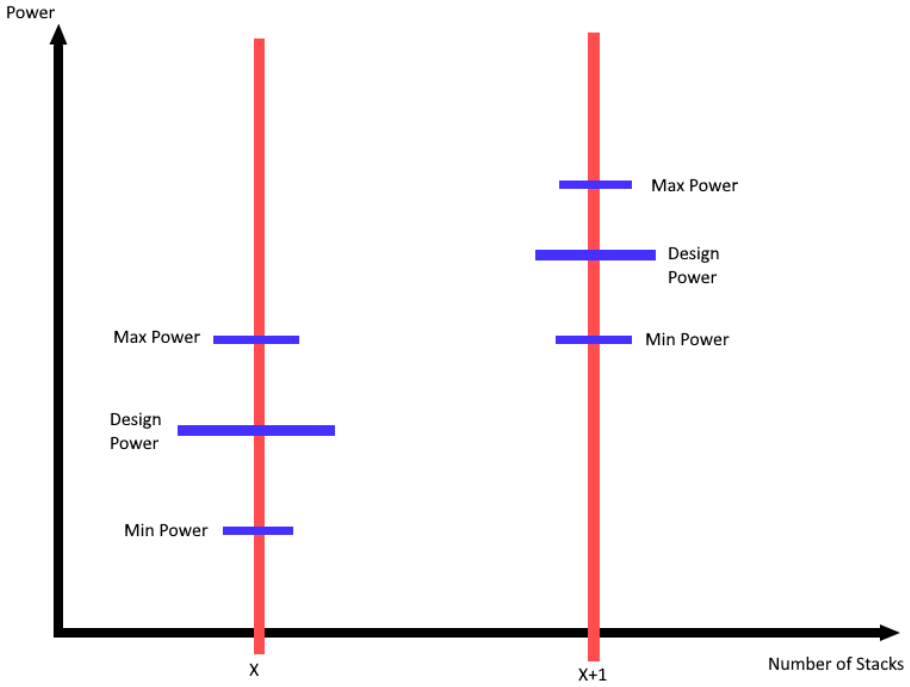

Figure 3.9: Graphical explanation of how the control logic works for stack power control. The maximum power level for x cells is either greater than or less than the minimum power level for $x+1$ stacks. As more stacks are added, the range between min power and max power for $x+1$ stacks becomes smaller.

3.2.9. Energy Balance

The energy balance is required to ensure conservation of energy in the simulations. There are three aspects to the energy balance which are considered:

- Flow enthalpy
- Electrical power
- Losses

Gravitational potential energy can be neglected because of low density gradients and kinetic energy can be neglected because systems can be designed such that velocities can be low. Flow enthalpy refers to the change in enthalpy of the fluid flows going into and leaving the system of both the flows which go to/from the cathode anode as well as the thermal energy coming from industry. Electrical power refers to the electricity going to power the system. Losses refers to all energy losses from operation of the BOP components and the stacks. Graphically this can be visually seen in Figure 3.10. In mathematical notation, this is described by Equation 3.57.

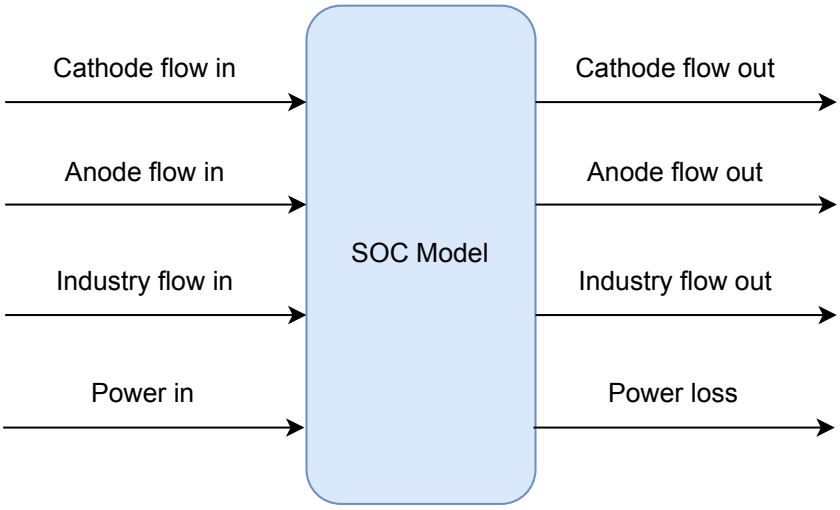

Figure 3.10: Graphic illustrating the energy inflows and outflows from the SOEC system used by the energy balance

Definition: Energy Balance

$$P_{elec} + H_{Cathode,1} + H_{Anode,1} + H_{Industry,1} = P_{loss} + H_{Cathode,2} + H_{Anode,2} + H_{Industry,2} \quad (3.57)$$

Where:
P_{elec} is the electrical power input [W]
$H_{Cathode,1}$ is the enthalpy of the cathode flow going into the system [W]
$H_{Anode,1}$ is the enthalpy of the anode flow going into the system [W]
$H_{Industry,1}$ is the enthalpy of the industry flow going into the system [W]
P_{loss} is the irreversible heat loss from the balance of plant components and the stack [W]
$H_{Cathode,2}$ is the enthalpy of the cathode flow going out of the system [W]
$H_{Anode,2}$ is the enthalpy of the anode flow going out of the system [W]
$H_{Industry,2}$ is the enthalpy of the industry flow going out of the system [W]

3.2.10. Mass Balance

The mass balance is required to ensure continuity of mass flow in the simulations. This is done by ensuring the mass entering the system is equal to the mass leaving the system. This is graphical illustrated in Figure 3.11. In maths notation, this is described by Equation 3.58.

Definition: Mass Balance

$$\dot{m}_{Cathode,1} + \dot{m}_{Anode,1} = \dot{m}_{Cathode,2} + \dot{m}_{Anode,2} \quad (3.58)$$

Where:
$\dot{m}_{Cathode,1}$ is the mass flow of the cathode flow entering the system [kg/s]
$\dot{m}_{Anode,1}$ is the mass flow of the anode flow entering the system [kg/s]
$\dot{m}_{Cathode,2}$ is the mass flow of the cathode flow leaving the system [kg/s]
$\dot{m}_{Anode,2}$ is the mass flow of the anode flow leaving the system [kg/s]

3.2.11. Efficiency Curves

The purpose of the SOEC system model is to take the detailed model and balance of plant models and for a range of electrical power and thermal power values, determine the system electrical efficiency of the produced hydrogen (or carbon monoxide). For a given electrical and thermal power case, the

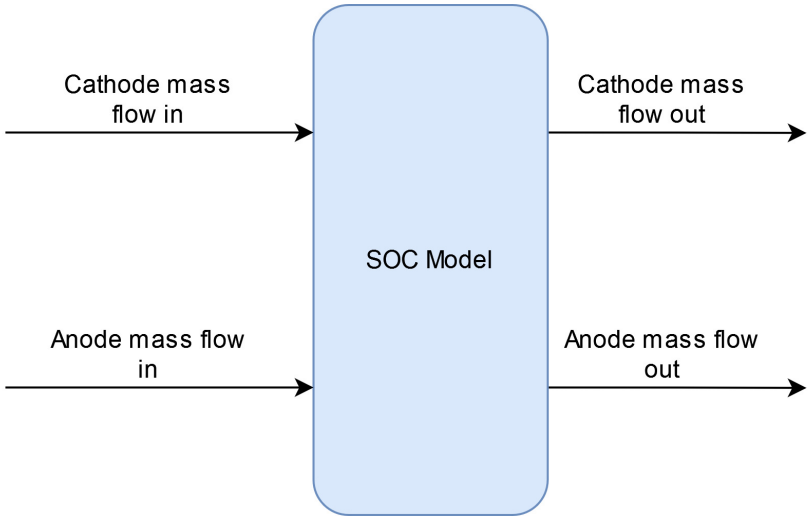

Figure 3.11: Graphic illustrating the mass inflows and outflows from the SOEC system used by the mass balance

SOEC model ensures the produced results pass the mass and energy balance checks and then the overall electrical efficiency of the system is determined using Equation 3.59.

Definition: Electrical Efficiency

$$\eta_{elec} = \frac{\dot{n}_{H2} \cdot HHV_{H2}}{P_{electrical,in}} \tag{3.59}$$

Where:
η_{elec} is the electrical efficiency of the system [-]
$\dot{n}_{H2}$ is the molar flow rate of produced hydrogen [mol/s]
HHV_{H2} is the higher heating value of hydrogen gas [J/mol]
$P_{electrical,in}$ is the electrical power put into the system [W]

The Higher Heating Value (HHV) is the maximum energy obtainable when reacting species together via complete combustion. In reality, it is not a fixed value but changes with pressure and temperature. For the purpose of consistent evaluation, HHV is often taken to be constant and is calculated at standard conditions [5]. HHV can be calculated with the following:

With the reaction: aA + bB $\longrightarrow$ cC + dD
Then:

$$HHV = c \cdot h_C + d \cdot h_D - (a \cdot h_A + b \cdot h_B) \tag{3.60}$$

Where:
HHV is the higher heating value [J/kg]
a is the stochiometric coefficient for reactant A [-]
b is the stochiometric coefficient for reactant B [-]
c is the stochiometric coefficient for reactant C [-]
d is the stochiometric coefficient for reactant D [-]
h_A is the enthalpy of species A at standard conditions [J/kg]
h_B is the enthalpy of species B at standard conditions [J/kg]
h_C is the enthalpy of species C at standard conditions [J/kg]
h_D is the enthalpy of species D at standard conditions [J/kg]

[5] 1 atm, 25°C

In other literature, the lower heating value is used to evaluate efficiency [65]. Using the lower heating value effectively assumes that the water produced by utilising hydrogen fuel will remain gaseous. While this is true for combustion engines, it is not the case for fuel cells as, for example, when hydrogen and oxygen are fed into a PEM fuel cell, the produced water is in liquid form, meaning the energy required for the gaseous water to condense to liquid water is utilised by the fuel cell, meaning the HHV is a more appropriate value.

3.3. Simulink Model

As mentioned previously, the Hydra model is a MATLAB/Simulink model developed by HyCentA to answer various economic questions about the production and utilisation of hydrogen and hydrogen fuel, specifically for the energy system in Austria. The model described in section 3.2 is used as the basis for the creation of the Simulink model through the efficiency curves produced by the former. The efficiency curves are implemented in the Simulink by creating a **lookup table** object in MATLAB and importing this object into a data dictionary utilised by the Simulink model. This lookup table can be thought of as a ”virtual SOEC system model” and the entire Simulink model as an interface for this virtual SOEC system model.

3.3.1. Control Logic

The virtual SOEC system has a minimum and maximum power at which it is able to operate at. Any power provided to the system below the minimum power level which the efficiency curves were generated on, will mean not all stacks can operate, meaning all the power to the system will be treated as ”overflow” power and passed through the Simulink model. Additionally, any power supplied to the model above the maximum power the efficiency curves were generated on is more power than the system is able to handle safely. Therefore all power above the maximum power of the model will be treated as ”overflow” power and be passed through the Simulink model.

Turning an SOC system ”on” from ambient temperature (known as a cold start) can take more than one hour [66]. This is a result of a slow heating process of the stack components being required to prevent large thermal gradients inside the system and thermal shock of the ceramic materials used in the stack. The number of thermal cycles also contributes to cell degradation [10] . As a result of these large ”turn on” times and the damage to the materials over many thermal cycles, it is more practical to keep the SOC system ”heated” when it is not being used to produce hydrogen or electrical energy. This therefore necessitates energy for ”standby mode” such that the system can be ”turned on” quickly when required. In the Simulink model, whenever there is insufficient energy input to operate the system, power is required to maintain the system’s temperature.

4

Model Verification

This chapter discusses the verification of the models presented in chapter 3. Ultimately the Simulink model must be verified. As the Simulink model is effectively a Simulink interpreter for the SOEC system model, the SOEC system model will be verified instead. Verification of the SOEC system model will necessitate verification of the detailed model as the detailed model is used as an input into the SOEC system model. This chapter will first describe the logic for the verification process undertaken, then the remainder of the chapter will go through the outlined verification process.

4.1. Why verification

When determining if a numerical models of a system is describing the system accurately, the model is ideally compared to the actual system through measurements of the system. This process is known as **validation**.

Often it is not possible or practical to obtain measurement data for the system being modelled. In these cases, a method known as **verification** is used as an alternative to validation. In verification, the constructed model is compared to other models, describing the entire system (or a part of the system) created by others. Unfortunately, due to data acquisition limitations, verifying the SOEC system model against an actual SOEC system is not possible. Consequently, verification of the SOEC system model will be performed instead of validation of the SOEC system model.

4.2. Verification Process

The verification of the hydra model will be done by comparing the sub-models of the overall SOEC system model to either other models or data which exist in the public domain. In this way, the entire SOEC system model can easier be verified as finding data for sub-models of the SOEC system model will be easier when compared to the challenge of finding an SOEC system which has the same Balance of Plant (BOP) layout and cell design while also providing detailed data.

Verification of the SOEC system model compromises of the following tasks:

- Verify the detailed model
  - Verify diffusion model
  - Verify activation model
  - Verify ohmic model
- Verify the BOP Models
  - Verify heat exchanger model
  - Verify vaporiser model
  - Verify trim heater model
  - Verify pump model

4.3. Verification Detailed Model

4.3.1. Verification Diffusion Model

The model used to describe diffusion was discussed in subsection 3.1.3. Only Fick's diffusion model is implemented because of time constraints. The diffusion model is compared to the data presented in [67]. This paper is somewhat unclear about some specific values it uses to produce various plots it presents. This section will attempt to clarify these uncertainties for future researches.

[67] only shows relationships between **current density** and **concentration overpotential**. As mentioned in subsubsection 3.1.2.4, concentration overpotential is incorporated into the Nernst Potential. To evaluate the diffusion models and verify them against [67], a relationship between current density and concentration overpotential needs to be defined. The relationship from [67] is presented below; note that it is only valid for water consuming SOFC:

Definition: Concentration Overpotential

$$\eta_{concentration} = -\frac{RT}{2 \cdot F} \cdot \ln\left(\frac{y_{H2} \cdot y^I_{H2O}}{y_{H2O} \cdot y_{H2O} \cdot y^I_{H2}}\right) \tag{4.1}$$

[a]

[a] Equation taken from [67]

Where:
$\eta_{concentration}$ is the concentration overpotential [V]
R is the universal gas constant [J/mol K]
T is the temperature [K]
F is Faraday's constant [C/mol]
y_{H2} and y_{H2O} are the concentration of H_2 and H_2O at the electrode respectively [mol/m^3]
y^I_{H2} and y^I_{H2O} are the concentration of H_2 and H_2O at the inlet respectively [mol/m^3]

The diffusion models relate current density to concentration at the electrodes. Using this relationship, verification of the diffusion model can be undertaken. As indicated earlier, [67] does not clearly specify specific values for the following:

- Porosity
- Tortuosity
- Pore radius

The paper does cite three references which it says it gets values from. Specifically, one of these references, [68], indicates that the porosity and tortuosity values can vary between:

- 0.3 and 0.4 for porosity
- 3 and 6 for tortuosity

No value for pore radius was given. However, using the sample code present at the end of [67] for the DGM model, the pore radius is 0.5 μm. In the same place tortuosity and porosity are also specified. Fixing tortuosity at the value specified here (6) as it has the widest range, guess-and-check testing for various values of porosity, it can be found that a porosity value of 0.325 gives a reasonably good fit to the data points, as shown in Figure 4.1

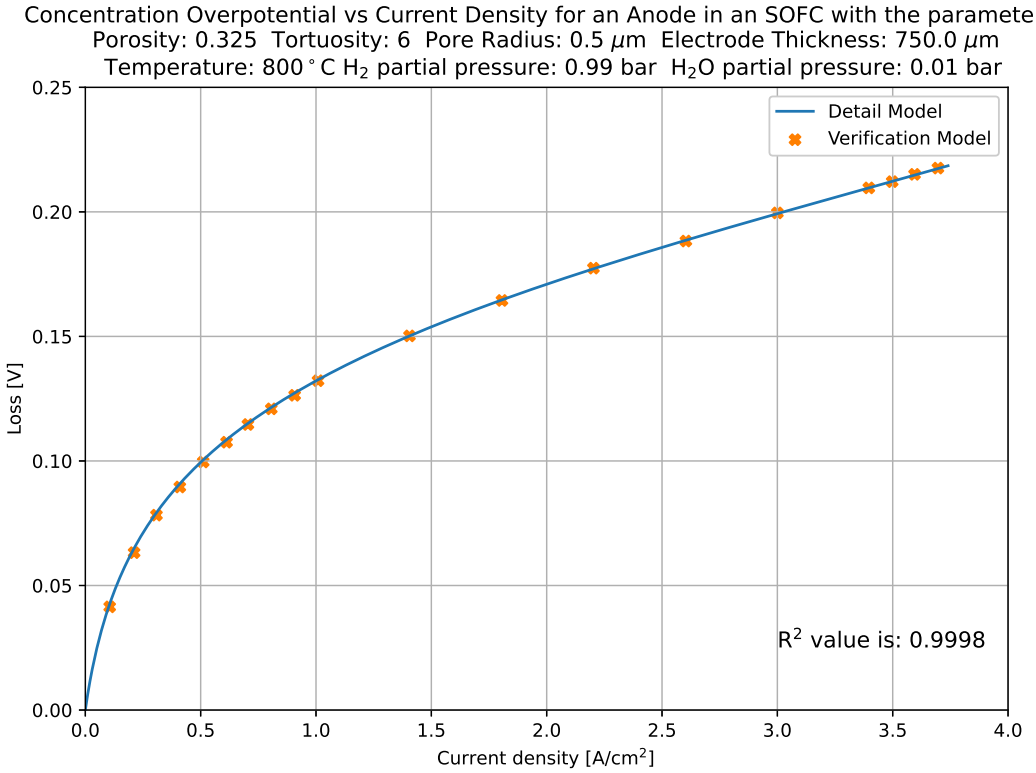

Figure 4.1: Plot showing relation between current density and concentration overpotential. The solid line shows results from diffusion model inside the detailed model and the orange marks show select data points from the Fick's diffusion model from [67] running with the settings shown in the figure's title

Using the same values for porosity, tortuosity and pore radius but changing the incoming partial pressure values and plotting for the other case which is shown in [67] can give an indication if the pore radius, tortuosity and porosity values are correct. This is assuming that authors of [67] only changed the partial pressure inflow settings between producing their plots which the diffusion model is being verified against. The results of the different partial run case can be seen in Figure 4.2

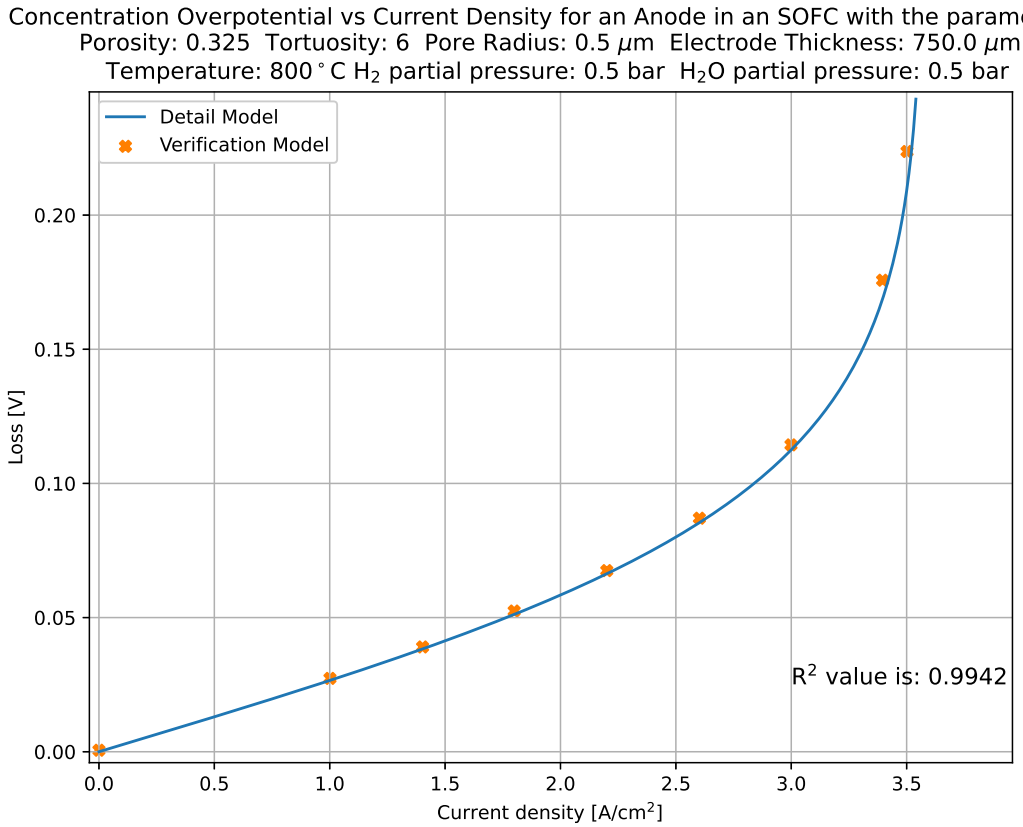

Figure 4.2: Plot showing relation between current density and concentration overpotential. The solid line shows results from diffusion model inside the detailed model and the orange marks show select data points from the Fick's diffusion model from [67] running with the settings shown in the figure's title

As can be seen in Figure 4.2, using the same settings for porosity, tortuosity and pore radius as determined from Figure 4.1, the fit is acceptable visually. It also has a calculated R^2 value of 0.9942 for this fit. This shows that the values selected for Figure 4.1 are valid and shows that Fick's diffusion is verified, assuming the authors did not change the porosity, tortuosity and pore radius values between runs. It was considered asking the authors of [67] what settings they used, but considering the paper was published 19 years ago, it was considered unlikely the authors would remember.

4.3.2. Verification Activation Model

The model used to described for activation overpotential is described in section 3.1.2.2. The main equation used to model this overpotential was the the Butler-Volmer Equation, Equation 3.3, which is repeated here for convenience:

$$i = i_0 \left(\exp\left(\frac{\alpha_c \cdot z \cdot F \cdot \eta_{act,el}}{R \cdot T} \right) - \exp\left(-\frac{\alpha_a \cdot z \cdot F \cdot \eta_{act,el}}{R \cdot T} \right) \right) \tag{4.2}$$

Where:
i is the current density [A/cm^2]
i_0 is the exchange current density [A/cm^2]
α_c and α_a are the charge transfer coefficients of the cathodic reaction and anodic reaction at the electrode respectively [-]
z is the number of electrons involved in the reaction [-]
F is Faraday's constant [C/mol]
$\eta_{act,el}$ is the activation over-potential at the electrode [V]
R is the universal gas constant [J/mol K]
T is the temperature [K]

The main variables which change in this equation impacting the activation overpotential (when assuming the charge transfer coefficients are both equal to 0.5, the derivation and justification for given in subsubsection 3.1.2.2) are the **exchange current density,** i_0 for both the anode and cathode. The equation which is used to describe the exchange current density is given in subsubsection 3.1.2.2 and is repeated here for convenience.

$$i_{0,w} = r_w \cdot \Pi_{k=1} \left(\frac{y_{q_k}}{y_{q_k,ref}} \right)^{A_k} \cdot \exp\left(-\frac{E_{a,w}}{RT} \right) \tag{4.3}$$

Where:
$i_{0,w}$ is the exchange current density at the w electrode [A/cm^2]
w is the electrode. Can either be fuel or oxygen electrode
r_w is the reaction rate constant for the w electrode [-]
y_{q_k} is the molar fraction of species q_k [-]
k is a numerical indication of a species at an electrode [-]
$y_{q_k,ref}$ is the molar fraction of q_k in the reference conditions [-]
A_k is a gas concentration exponent which is determined by fitting the equation to data [-]
$E_{a,w}$ is the activation energy of the species reacting at the w electrode [J/mol]
R is the universal gas constant [J/mol K]
T is the temperature [K]
k is a reference to a species which exists at electrode w

As mentioned in subsubsection 3.1.2.2, typically, numerical models of SOC determine the exchange current density by curve fitting experimental data. Therefore, without access to an experimental set-up, data from other papers was instead used. Specifically, exchange current density data was used from [49]. Therefore, the verification process is determining if the models and data the detailed model produces, match the same results as presented in [49].

The resolution of the curve fit plots presenting the relation between species molar fraction and exchange current density, in Figure 2 and Figure 3 from [49] are not sufficiently high enough to accurately compare the detailed model's replication of the curve fits presented in [49]. To preform verification, the data points utilised in [49] from which the curve fits are created are determined, are instead taken and plotted next to the exchange current density values the detailed model predicts. To determine the coordinates of the data points presented in [49], the plot in question from [49] is loaded into **Plot Digitizer** [53] and the relevant coordinates are extracted and plotted. [49] presents its data with error bars, but the data points taken for verification are from the specified experimental data points. If the detailed model's curve and the data points from [49] look like a valid curve fit, it is likely that the detailed model successfully replicates the curve fit from [49] and therefore can be considered verified.

Only two cases of verification using the previously described method will be presented here. The remaining curves will be shown in Appendix B. The cases which will be shown here are:

- Ni-GDC for an SOEC at 1223 K. Results presented in Figure 4.3
- LSM for an SOEC at 1223 K. Results presented in Figure 4.4

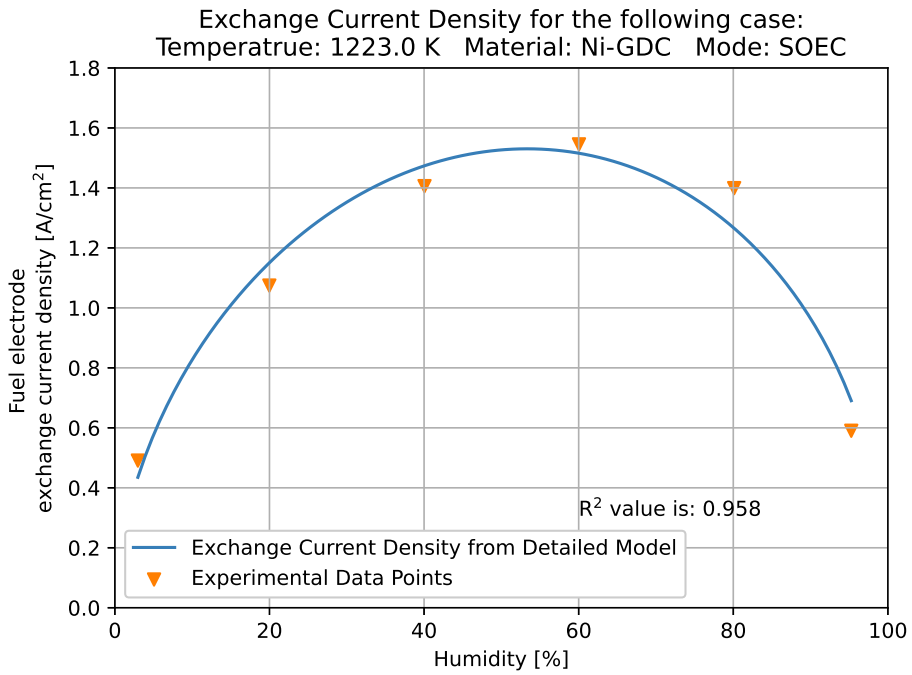

Figure 4.3: Plot showing the relation between humidity and electrode exchange current density. The solid line is the exchange current density the detailed model produces. The exchange current density model used by the activation model are the same as the curve fit model from [49]. The individual data points are taken from [49], Figure 3, for the fuel electrode of an SOEC at 1223 K for the electrode cermet Ni-GDC

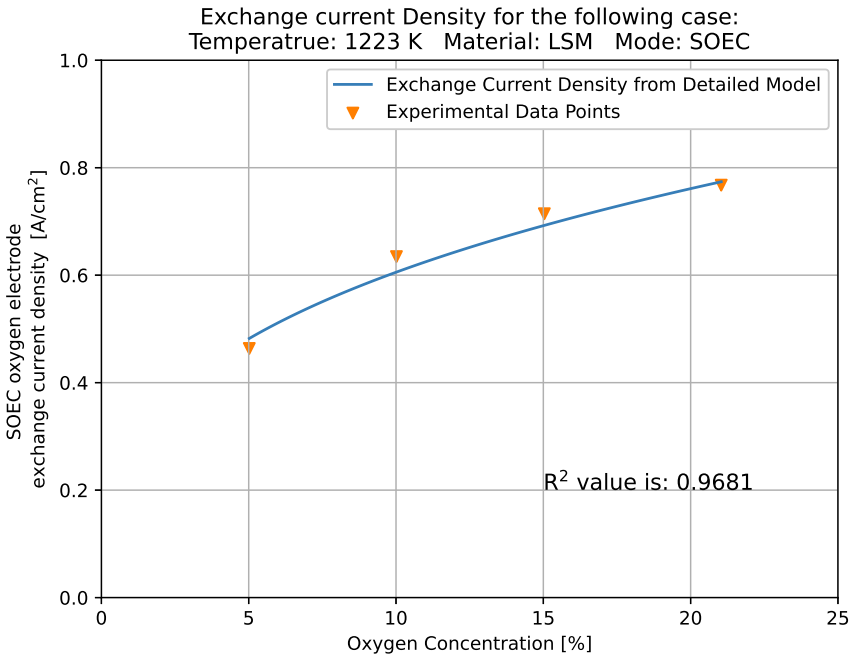

Figure 4.4: Plot showing relation between oxygen concentration and electrode exchange current density. The solid line is the exchange current density the detailed model produces. The exchange current density model used by the activation model are the same as the curve fit model from [49]. The individual data points are taken from [49], Figure 2, for the oxygen electrode of an SOEC at 1223 K for the electrode cermet LSM

4.3.3. Verification Ohmic Model

The model used to describe the ohmic overpotential is presented in subsubsection 3.1.2.3. For this model, the conductivity of the membrane material at various temperatures is the driving factor in determining the overpotential. Similar to the activation overpotential model, conductivity of an electrolyte is typically done experimentally as differences in manufacturing processes can have a large impact on the overall conductivity. As no experimental setup was available to determine the values for conductivity, data from literature was used instead. Specifically, data was taken from [52]. For verification, the values taken from [52] compared to the calculated conductivity of the ohmic model. The results of this can be seen in Figure 4.5. The R^2 values between the model and the data points are shown in Table 4.1.

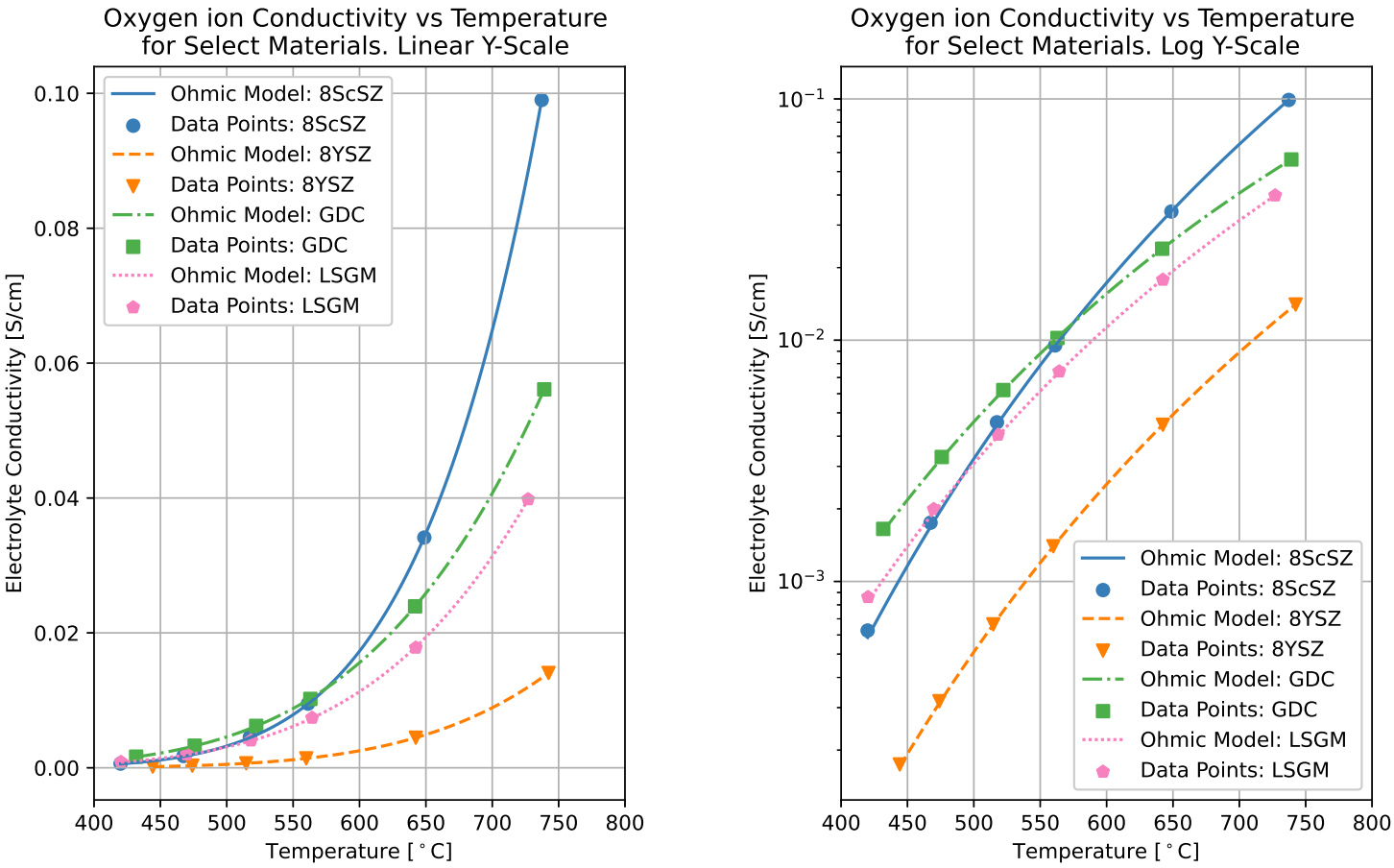

Figure 4.5: Plot of oxygen ion conductivity vs temperature comparing conductivity between "Data Point" values taken from [52] and the ohmic model's computed values. Showing both linear and log Y-axis scale

Table 4.1: R^2 values of the data and model for the conductivity shown in Figure 4.5. Values to four significant figures

Material	R^2 Value
8ScSZ	0.9999
8YSZ	0.9999
GDC	0.9999
LSGM	0.9999

4.4. Verification Balance of Plant Models

Verification of the BOP models can be done using software already used for process engineering modelling as the BOP components are typical systems used in process engineering. DWSIM is an open source software package used to model chemical and process engineering which is a viable free alternative to commercial software like ASPEN Plus [69]. DWSIM will be the software used to verify the Balance of Plant (BOP) in the SOEC system model.

To determine the validity of the results from the BOP models compared to DWSIM, the relative error of relevant quantities (e.g. power) between the two models will be used. If the relative errors are less than 1e-3 (0.1%), the model will be considered verified. All DWSIM models will be run using the standard CoolProp thermodynamic model available in DWSIM.

4.4.1. Verification Heat Exchanger

Table 4.2 shows the results from the SOEC system model and DWSIM verification for the following fluid flow case:

- Flow 1:
  - Temperature in: 1000 K
  - Pressure in: 101325 Pa
  - Fluid: Nitrogen
  - Molar flow rate: 1000 mols/s (28.01 kg/s)
- Flow 2:
  - Temperature in: 300 K
  - Pressure in: 101325 Pa
  - Fluid: Nitrogen
  - Molar flow rate: 1000 mols/s (28.01 kg/s)

Table 4.2: SOEC system model heat exchanger model compared to DWSIM heat exhanger model

	SOEC system model	DWSIM	Relative Error [-]
Fluid 1 Output Temperature [K]	482.8208	482.81	$2.071 \cdot 10^{-5}$
Fluid 2 Output Temperature [K]	833.697	833.697	0

4.4.2. Verification Vaporiser

There is no vaporiser model pre-loaded in DWSIM. However, as explained in subsection 3.2.6, the SOEC system vaporiser model just converts a liquid to a gas via an enthalpy change at a given efficiency and then a further increase in enthalpy via temperature change to a given temperature value above boiling point at a given efficiency. This can be modelled in DWSIM by using a heater which heats up the incoming flow until a vapor quality of one is reached, and then heated up in a heater until the desired temperature is reached. The powers for these two processes can then be added to return the power required to vaporise the flow.

Table 4.3 shows results the from the SOEC system model and DWSIM verification for the following fluid flow case:

- Temperature in: 300 K
- Pressure in: 101325 Pa
- Fluid: Water
- Molar flow rate: 1000 mols/s (18.02 kg/s)
- Vaporiser efficiency of 85%

Table 4.3: SOEC system model vaporiser compared to DWSIM equivalent vaporiser model

Model	SOEC system Model	DWSIM	Relative Error
Power Required [kW]	54 755.33	54 755.37	$7.305 \cdot 10^{-7}$

4.4.3. Verification Trim Heater

Table 4.4 shows the results from the SOEC system model and DWSIM verification for the following fluid flow case:

- Temperature in: 800 K
- Pressure in: 101325 Pa
- Fluid: Water
- Molar flow rate: 1000 mol/s (18.02 kg/s)
- Heater efficiency of 85%

Table 4.4: SOEC system model trim heater compared to DWSIM trim heater

	SOEC system Model	DWSIM	Relative Error [-]
Power Required [kW]	13 004.39	13 004.41	$1.5379 \cdot 10^{-6}$

4.4.4. Verification Pumps

Table 4.5 shows the results from the SOEC system model and DWSIM verification for the following fluid flow case:

- Temperature in: 400 K
- Pressure in: 1 bar
- Pressure increase: 6000 Pa
- Fluid: Oxygen
- Molar flow rate: 1000 mols/s (32.0 kg/s)
- Pump Efficiency: 75%

Table 4.5: SOEC system model pump compared to DWSIM pump

	SOEC system Model	DWSIM	Relative Error [-]
Power Required [kW]	260.3965	260.48	$3.2056 \cdot 10^{-4}$

5

Model Results

This chapter is a discussion of the output from the models presented in chapter 3. In section 3.2, two different control methods are discussed, in this chapter an individual discussion of both control methods will be given as well a comparison between the different methods.

For the discussion of all results presented in this chapter, it should be remembered that the results pertain to the system design presented in Figure 3.1 for a given cell design. As such, various systems settings and cell design options are possible. The system settings and cell design parameter used to produce the figures presented in this chapter can be seen in Appendix D.

In this section, references to ”thermal energy” or ”thermal flow” refers to the energy/flow provided by other industrial processes which is utilisable by the SOEC system through the ”industry heat exchanger” seen in Figure 3.1. Additionally, ”cathode flow” refers to the flow going through the balance of plant system, towards the cathode side of the SOEC stack system.

5.1. Cell Design

Before an analysis on the system control methods can be given, it is important to understand the cell design used inside the stacks, as the cell design impacts the thermodynamics of the system. The V-I curve of the cell design can be seen in Figure 5.1. For the cell design specified in Figure 5.1, it can be seen that the current density at which the thermoneutral voltage is reached is **0.589** A/cm^2. The thermonetural voltage at the operational temperature is **1.286** V.

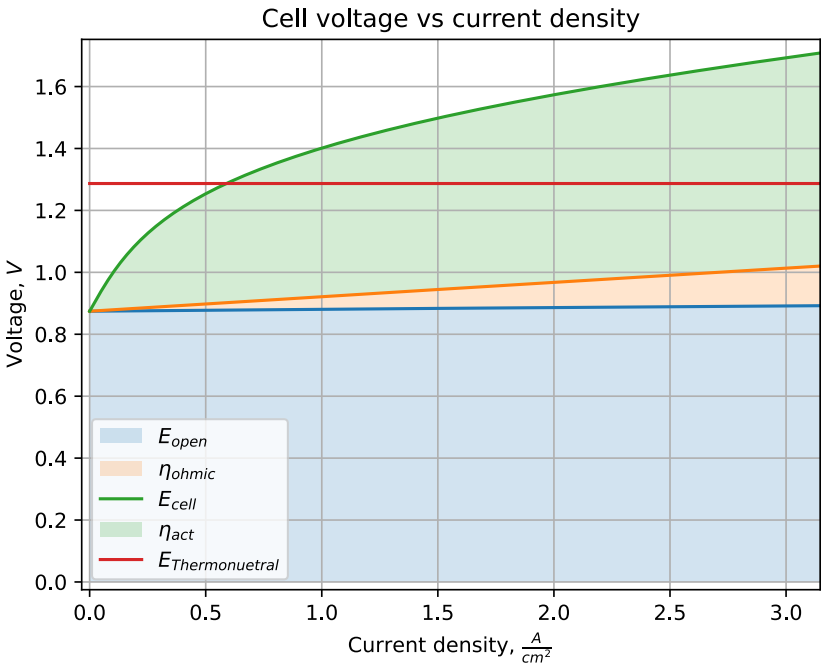

Figure 5.1: The Voltage-Current density curve of the cell design used in the SOEC model. This cell is an anode supported cell type, utilising an 8YSZ electrolyte with a Ni-YSZ cathode and LSM anode operating at a temperature of 1073 K. Further cell design properties are presented in Appendix D.

5.2. Irho design control method

This control method's operation is described in subsection 3.2.8. In essence, it involves turning on more stacks as the system power level increases while keeping the current density of all cells which are in use, as close to the design current density as possible. The impact of the control method can be seen when comparing the system efficiency curve vs system power to the current density vs system power curve for the system, which can be seen in Figure 5.2. The saw tooth pattern seen in Figure 5.2b is indicative of more stacks turning "on" (from standby mode) as system power increases, decreasing the current density of all active stacks. Typically, the lower the current density, the more electrically efficient a stack is. This impacts the overall system efficiency, which can be seen in Figure 5.2a, where the "saw tooth" pattern again can be seen, with increases in efficiency occurring when the current density reduces as new stacks turn on. The "logarithmic like" shape of the efficiency curve can be explained by the fact that as the system power increases, more stacks can be turned on and less power is required to maintain "off" stacks in standby mode, which consumes power.

In Figure 5.2a, the impact of thermal energy being provided to the system to improve overall system efficiency, which is discussed in subsection 2.4.2, is not included. The impact of additional thermal energy input is a function of the temperature and flow rate. For various temperature and flow rates of thermal energy, the impact on system efficiency can be seen in Figure 5.3 and Figure 5.4.

To explain Figure 5.3, it can be seen that for a flow rate of 0 m^3/s, all efficiency curves are the same; this is expected as with a flow rate of 0 m^3/s, there is no enthalpy exchange possible. For increasing flow rates, specifically flow rates of 0.09 m^3/s and 0.179 m^3/s, it can be seen that for all temperatures, the efficiency increases to some degree when compared to the "base" regime, but with increasing system power, the efficiency gains are reduced. This is due to the fact that for higher system powers, the amount of energy which can be transferred between the "thermal flow" and "cathode flow" can become limited depending on flow rates and temperatures due to changes in flow enthalpy values. As a result, the "cathode flow" is heated to a lower temperature by the "thermal flow" for increasing system power values, thereby resulting in the cathode trim heater consuming more power in order to maintain correct inflow temperature of the cathode side flow into the electrolyser stacks.

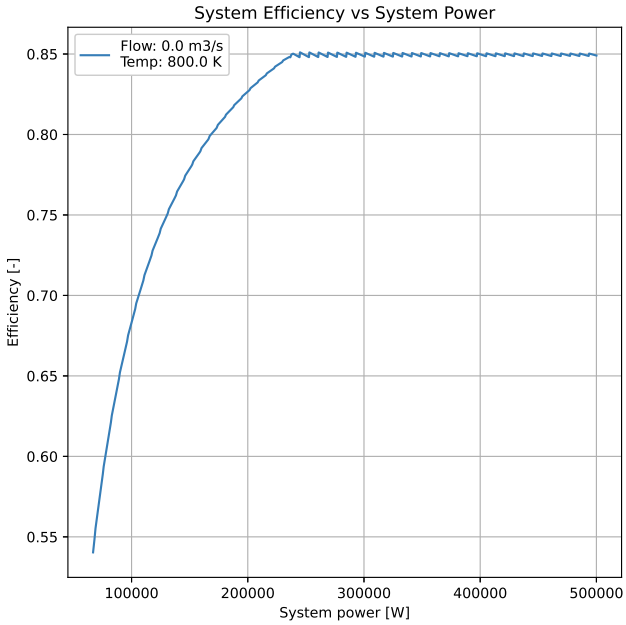

(a) System efficiency vs system power for a system operating at the following inputs: Cathode inflow temperature: 400 K, Anode inflow temperature: 300 K

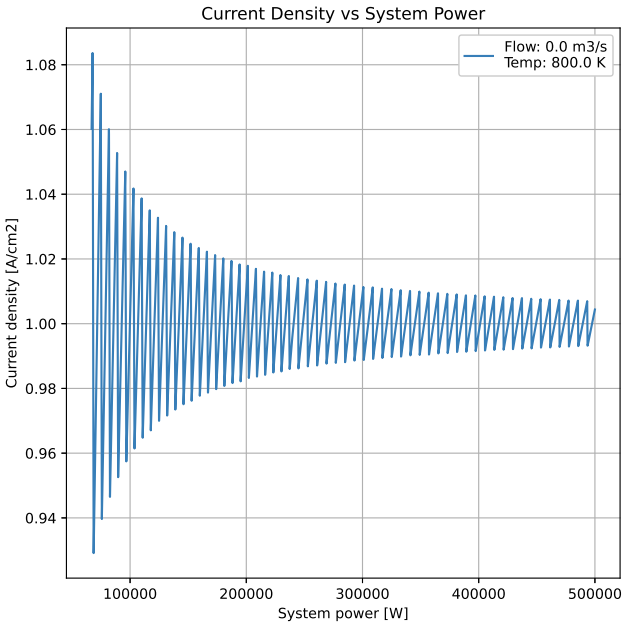

(b) Operating cell current density vs system power for a system operating at the following inputs: Cathode inflow temperature: 400 K, Anode inflow temperature: 300 K

Figure 5.2: System electrical efficiency vs system power and active cell current density vs system power for the **irho design** control method. Industry inflow does not impact the efficiency curve as the flow rate is zero. Cathode side inflow temperature is 400 K while anode side inflow temperature is 300 K

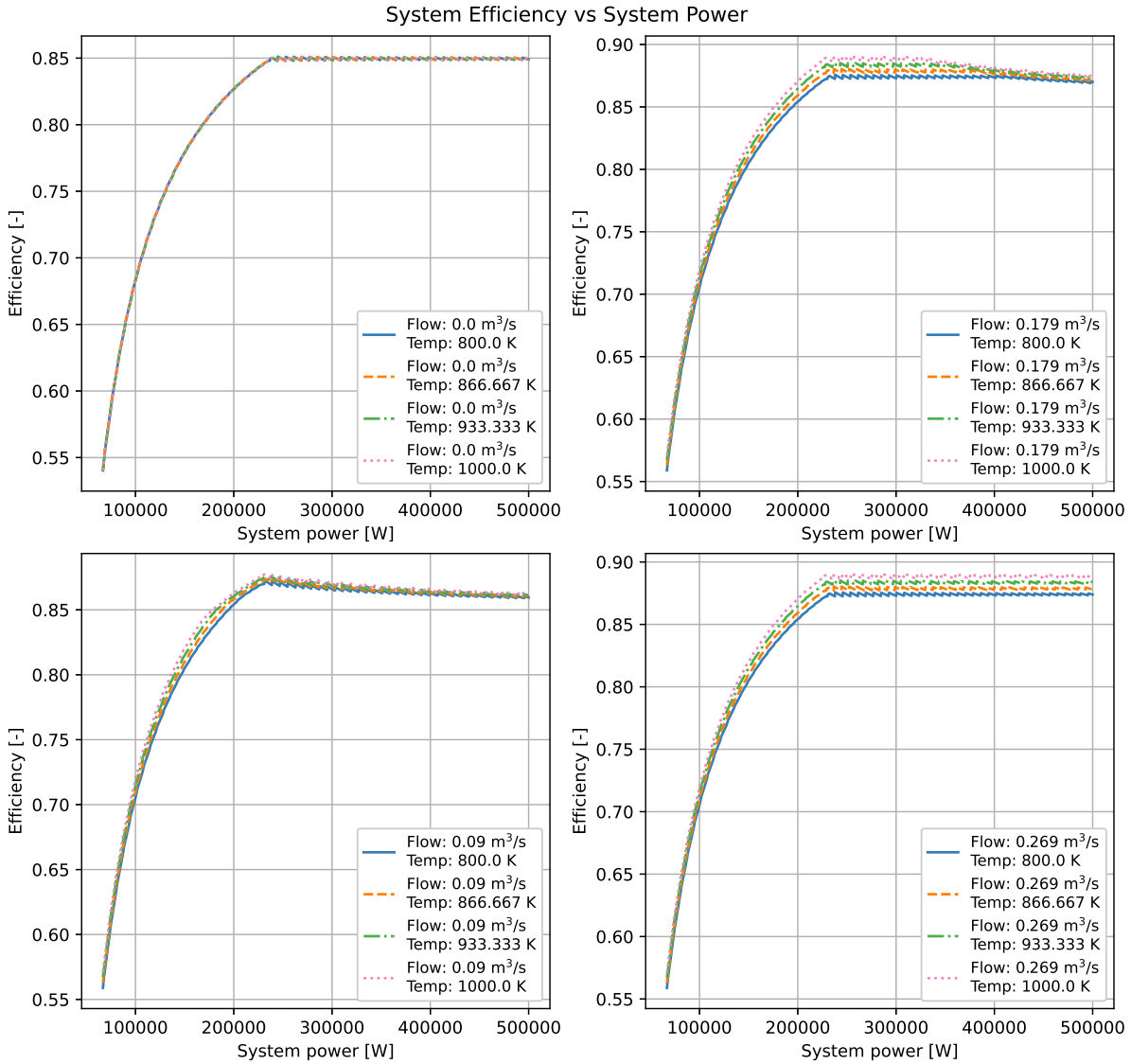

Figure 5.3: System efficiency vs system power for various flow rates for a range of temperatures. Control method is **irho design**. Cathode side inflow temperature is 400 K while anode side inflow temperature is 300 K

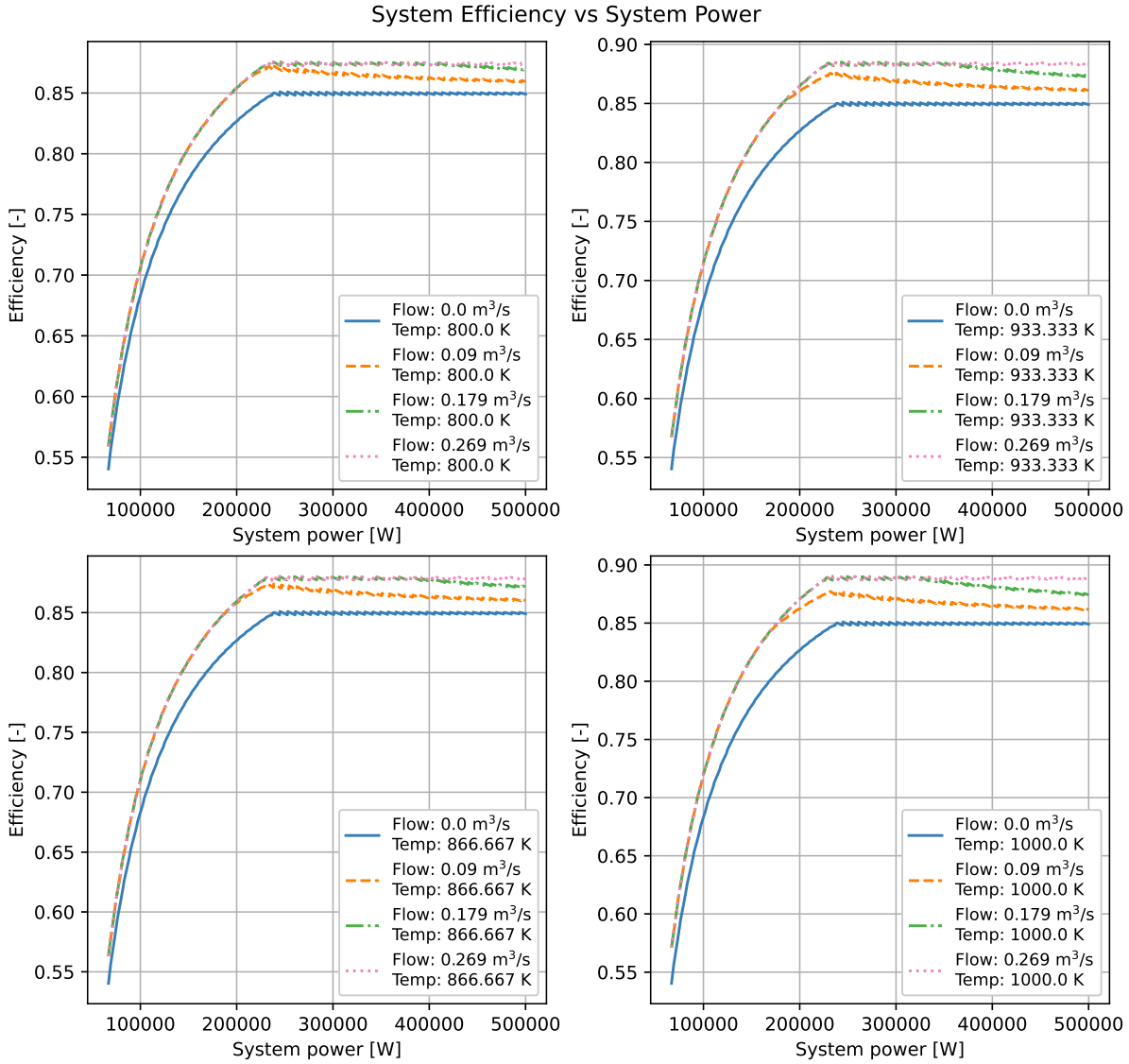

Figure 5.4: System efficiency vs system power for various temperature for a range of flow rates. Control method is **irho design**. Cathode side inflow temperature is 400 K while anode side inflow temperature is 300 K

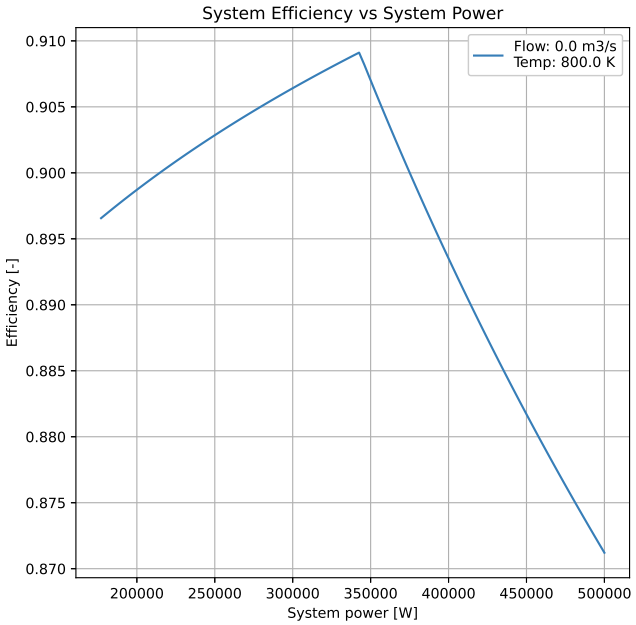

(a) System efficiency vs system power for a system operating at the following inputs: Cathode inflow temperature: 400 K, Anode inflow temperature: 300 K

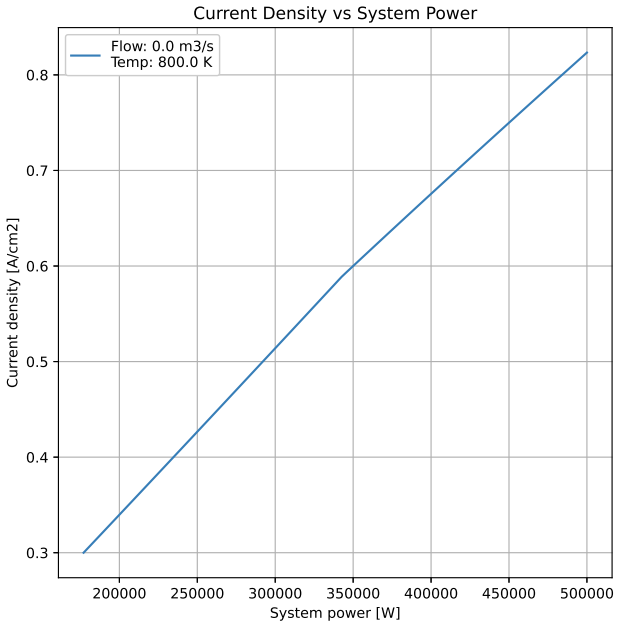

(b) Operating cell current density vs system power for a system operating at the following inputs: Cathode inflow temperature: 400 K, Anode inflow temperature: 300 K

Figure 5.5: System electrical efficiency vs system power and active cell current density vs system power for the **stacks same** control method. Industry inflow does not impact the efficiency curve as the flow rate is zero. Cathode side inflow temperature is 400 K while anode side inflow temperature is 300 K

To explain Figure 5.4, in all plots, there is a case in which there is no impact of the ”thermal flow” on the overall system efficiency as the flow rate is 0 m^3/s. For fixed ”thermal flow” temperatures for increasing flow rates, system efficiency increases. With increasing system power levels however, the impact of these increasing flow rates reduces as the amount of ”cathode flow” coming into the system increases with increasing system power. At some point, the limit for enthalpy transfer between the ”thermal flow” and ”cathode flow” is reached and a discontinuity in the efficiency curve can be seen. For the highest flow rate (0.269 m^3/s) for all temperature cases, there is no discontinuity in the efficiency curve, indicating the ”limit” of enthalpy transfer is never reached.

5.3. Stacks same control method

This control method’s operation is described in subsection 3.2.8. In short, all cells in all stacks are operated the same way at a given power level; that is, all cells experience the same current density at all times. It can be seen in Figure 5.5a that from minimum system power until around 343 kW system power, the efficiency of the system increases. After 343 kW, the system efficiency decreases with increasing system power. This power level occurs around a current density value of 0.589 A/cm^2, as can be seen in Figure 5.5b. As mentioned in section 5.1, this is the current density at which the thermoneutral value occurs. Therefore after this point, an increasing percentage of input electrical power is being turned into ”waste” heat and not used for hydrogen production.

In the figures shown in Figure 5.5, the impact of thermal energy on the system is not shown. The impact of various temperature and flow rates for the ”thermal flow” on system efficiency can be seen in Figure 5.6 and Figure 5.7.

To explain Figure 5.7, it can be seen that for when there is a non zero flow rate, regardless of ”thermal flow” temperature, the efficiency is the same. In both Figure 5.7 and Figure 5.6, there is a discontinuity in the efficiency curves between 330 kW and 345 kW. This is due to the system reaching the

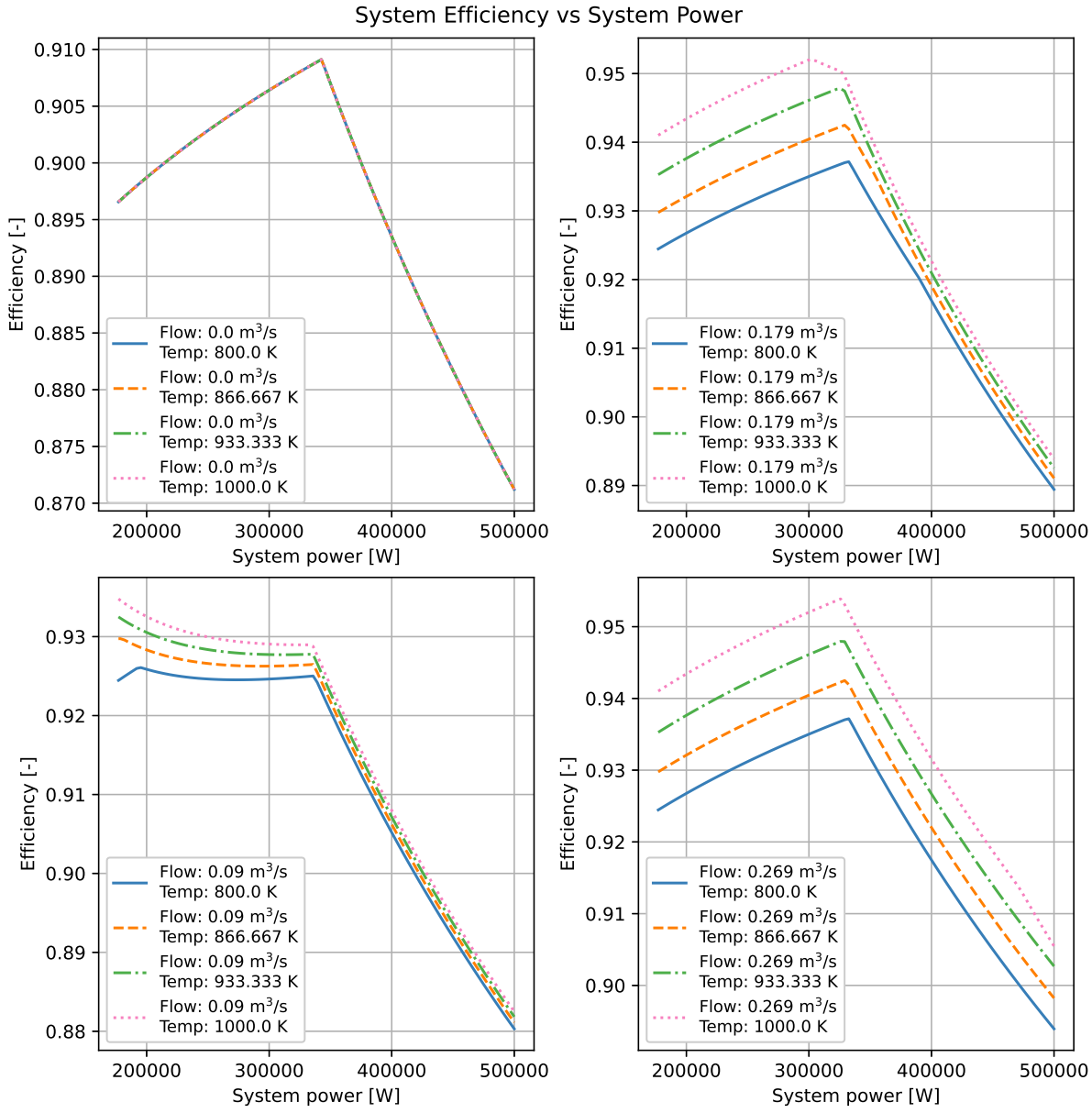

Figure 5.6: System efficiency vs system power for various flow rates for a range of temperatures. Control method is **stacks same**. Cathode side inflow temperature is 400 K while anode side inflow temperature is 300 K

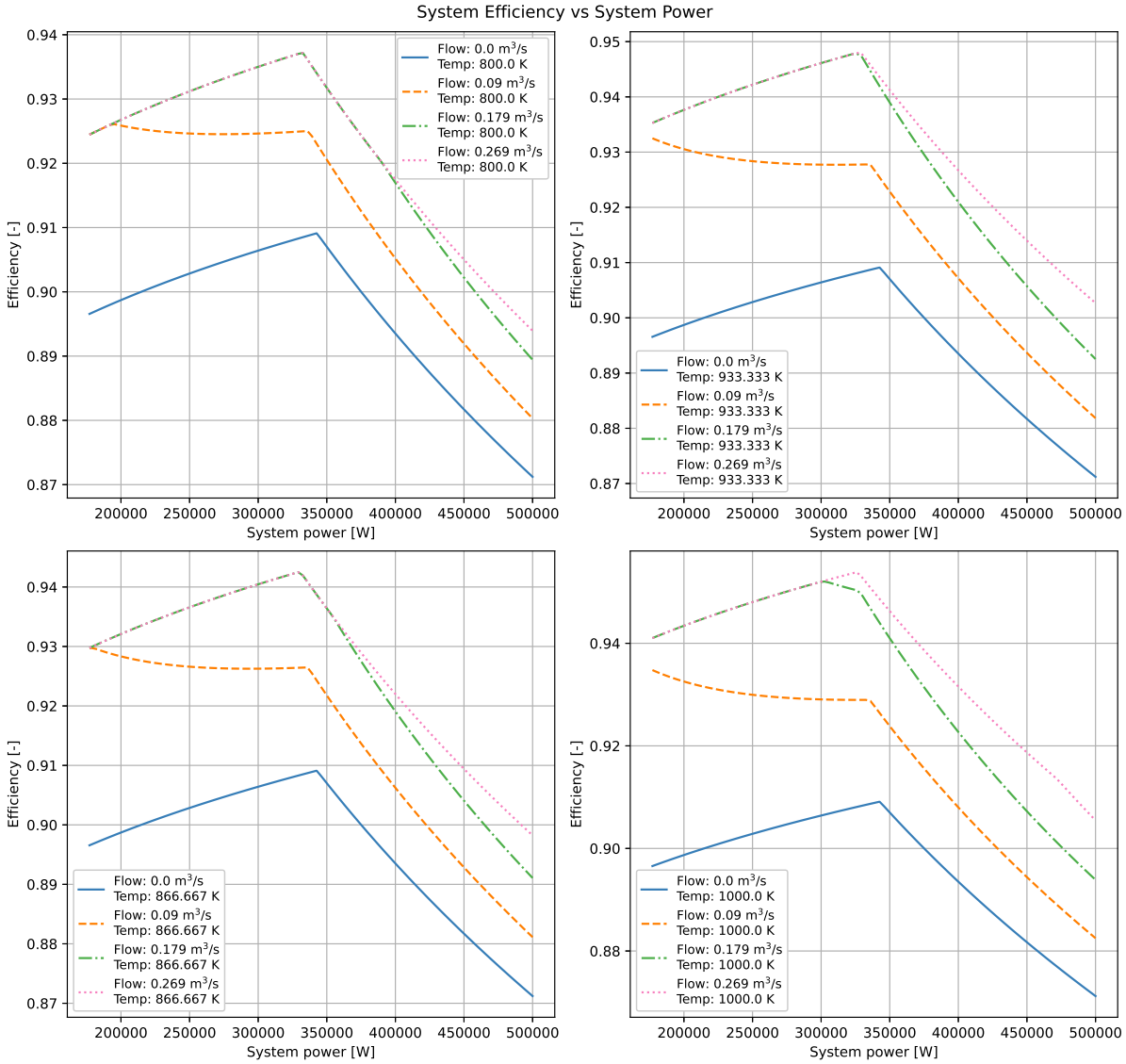

Figure 5.7: System efficiency vs system power for various temperature for a range of flow rates. Control method is **stacks same**. Cathode side inflow temperature is 400 K while anode side inflow temperature is 300 K

thermoneutral current density, as described previously. The reason for the changing system power at which thermoneutral current density occurs is that with increasing energy from the ”thermal flow”, less power is required for the cathode trim heater, resulting in more power being available for the electrolyser stacks, thereby providing a greater percentage of system power to producing hydrogen, increasing system efficiency and lowering the power level at which thermoneutral current density occurs.

In almost all other curves in which the mass flow is not 0 m^3/s, for all temperatures it can be seen that each efficiency curve has another discontinuity in it. This discontinuity occurs as a result of a the capacity of the ”thermal flow” to transfer enthalpy to the ”cathode flow” reaching the limit imposed by the heat exchanger. After this point, no more energy can be utilised from the ”thermal flow”, thereby for increasing system power, a greater proportion of the energy required for electrolysis is coming from the electrical power supplied to the system, resulting in a gradient change for efficiency versus system power. For specific efficiency curves, namely curves with the following parameters:

- Flow 0.09 m^3/s, Temp: 933.33 K
- Flow 0.09 m^3/s, Temp: 1000.0 K

It can be seen such a discontinuity does not occur. This is because the enthalpy transfer from the ”thermal flow” to the ”cathode flow” is unlimited at all power levels in that for the entire system power range, the outflow temperature from the ”thermal flow” is always decreasing and not plateauing at a temperature value for which further heat transfer is not possible, as seen in Figure 5.8. Enthalpy transfer limits from the ”thermal flow” to the ”cathode flow” also explain the discontinuities which are seen in efficiency curves in Figure 5.6 (which are not the result of the thermoneutral power level being reached).

5.4. Comparison of Control Methods

Logically, different control methods result in different efficiency curves for the SOEC system. A comparison between the **irho design** and **stacks same** strategies is given in this section. Additionally, for all other system settings being the same, expect for a cathode inflow temperature of 300 K, the efficiency curves for this system case can be seen in Figure 5.9 for constant flow rates of the ”thermal flow” various temperatures.

The most noticeable impact on efficiency between Figure 5.9a and Figure 5.3 is the drop in peak efficiency value of around 26 percentage points. It is similar for the difference in peak efficiency between Figure 5.9b and Figure 5.6 with a reduction in peak efficiency of around 29 percentage points. These drops in efficiency values occurs because in the 300 K inflow case, the water present in the ”cathode flow” initially is in the liquid phase and therefore needs to be converted into the gas phase before it can be used in the system.

When comparing Figure 5.2a and Figure 5.5a, or Figure 5.9a and Figure 5.9b, it can be seen that the ”stacks same” method leads to overall higher efficiency values, as a result of the lower current densities the control method uses. However this is at the expense of a higher minimum operating power level. With both systems, it can be seen that increasing waste temperature or waste flow rate, higher electrical efficiencies can be obtained, this is logical given more energy required to sustain electrolysis is coming from thermal sources, as indicated is possible in Figure 2.10.

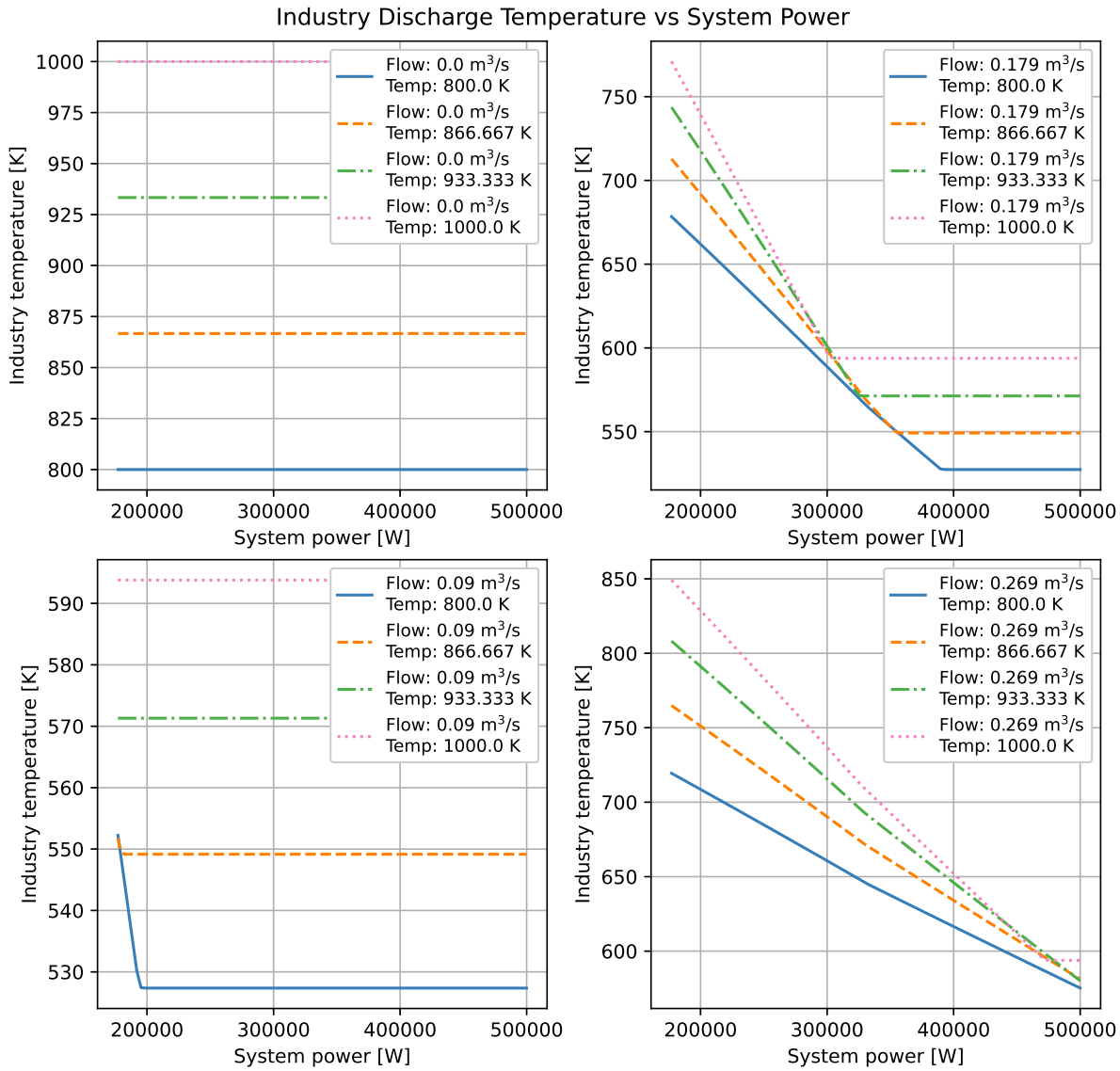

Figure 5.8: Industry flow discharge temperature vs system power for various flow rates for a range of temperatures. Control method is **stacks same**. Cathode side inflow temperature is 400 K while anode side inflow temperature is 300 K

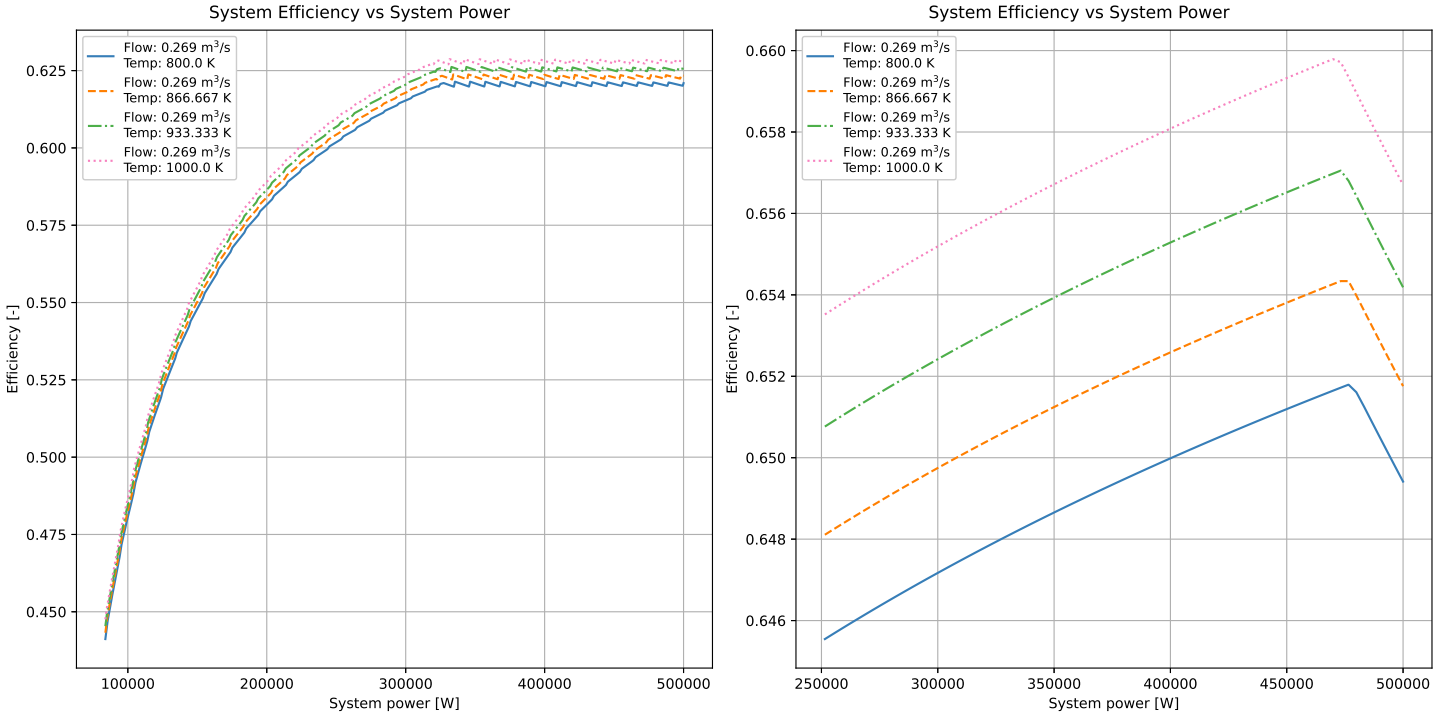

(a) irho design control strategy. 3588 cells present in the system over 78 stacks. Operating temperature is 1073 K

(b) stacks same control strategy. 3570 cells present in the system. Operating temperature is 1073 K

Figure 5.9: System electrical efficiency vs system power for different control system designs for a 500 kW SOEC system. Cell design is identical along with BOP settings. Cathode fluid inflow temperature is 300 K. Figures shows the impact of a constant ”thermal flow” temperature value for a range of ”thermal flow” flow rate values on system electrical efficiency

6 Recommendations

This chapter covers suggestions for future work on modelling of Solid Oxide Cells (SOCs) and solid oxide systems at HyCentA. Specifically, suggestions for improvements and upgrades to the numerical models produced for HyCentA will be given along with suggestions for future research topics

6.1. Model Improvements

While the purpose of the thesis was to only create a numerical model describing the operation of solid oxide electrolyse systems, the decision was made at the beginning to make the produced code expandable and upgradable with new or refined sub-models as easily as possible. Therefore, the following coding recommendations are what could be of benefit to HyCentA in the future with regards to SOC modelling.

Improvements to be made to the detailed model include:

- Add support for the dusty gas model for diffusion modelling
- Improve the exchange current density model to account for variations in exchange current density of electrodes based off manufacturing method, catalyst particle density and other relevant factors
- Additional model to account for carbon build up (coking) on electrodes when running with carbon based fuels
- Extend the ohmic model to allow for the use of layered electrolytes and co-doped electrolytes
- Expand the options for different cathode and anode materials
- Extend model capabilities to also include co-electrolysis operation (electrolysis of water and carbon dioxide simultaneously)
- Add a consumption API to the detailed model to allow for future uses of the code to easily determine, based off a voltage-current curve, the power available from a SOFC along with the reactant consumption rates and produced product rates.

Improvements to be made to the SOEC system model include:

- Extend user options for different implementing different system layout designs by adding a graphical user interface for easier system design
- Extend the operation mode to allow the Hydra model to work in SOFC mode along side the currently implemented SOEC mode
- Design and implement more advanced stack operation strategies such that optimised operation conditions of a SOEC system can be obtained according to the desired operation case
- Extend the balance of plant models to allow for two-phase flow rather than only single phase flow

Of the above improvements, adding support for the dusty gas model will enable the the models to be more readily accepted by the scientific community when publishing the results. However, allowing different system designs to be investigated more easily, it will be easier to determine more efficient system design options.

6.2. Future Research

No technology is ever fully ”finished”; there is always more which could be done to improve usability, improve profitability, improve reliability etc. After spending eight months researching SOCs, the future topics of further research in SOCs, I believe, which would be beneficial to expanding the capabilities of the technology are:

- Development of models which can simulate degradation effects on SOCs. This can be used to make a digital twin of existing SOC systems and therefore can be useful to predict the maintenance and changes i performance of SOC systems, allowing for preventative maintenance and to enable the development of operational strategies to extend SOC system life
- Development of lower temperature electrolytes for SOC operation in combination with development of materials which are stable in the operating conditions and when in contact with other system materials. This will enable the development of more durable and easier to operate SOCs

References

1. IPCC. in *Climate Change 2022: Impacts, Adaptation, and Vulnerability. Contribution of Working Group II to the Sixth Assessment Report of the Intergovernmental Panel on Climate Change* (eds Pörtner, H. O. *et al.*) In Press, In Press (Cambridge University Press, Cambridge, UK, 2022).
2. Andrews, J. & Shabani, B. Re-envisioning the role of hydrogen in a sustainable energy economy. *International Journal of Hydrogen Energy* **37,** 1184–1203. ISSN: 03603199. https://www.sciencedirect.com/science/article/pii/S0360319911022841 (2012).
3. Ginsberg, M. *et al.* Integrating Solar Energy, Desalination, and Electrolysis. *Solar RRL* **6,** 2100732. ISSN: 2367-198X. https://onlinelibrary.wiley.com/doi/full/10.1002/solr.202100732 (2022).
4. Minke, C., Suermann, M., Bensmann, B. & Hanke-Rauschenbach, R. Is iridium demand a potential bottleneck in the realization of large-scale PEM water electrolysis? *International Journal of Hydrogen Energy* **46,** 23581–23590. ISSN: 03603199. https://www.sciencedirect.com/science/article/pii/S0360319921016219 (2021).
5. Nagpal, M. S. Electrolytic Cells. *Mrs Shilpi Nagpal.* https://classnotes.org.in/class12/chemistry12/electro-chemistry/electrolytic-cells/ (6/07/2019).
6. Atkins, p. & de paula, J. *Physical Chemistry for the Life Sciences* ISBN: 0-1992-8095-9 (Oxford University Press, United Kingdom, 2006).
7. Mohammadi, A. & Mehrpooya, M. A comprehensive review on coupling different types of electrolyzer to renewable energy sources. *Energy* **158,** 632–655. ISSN: 03605442. https://www.sciencedirect.com/science/article/pii/S0360544218311381 (2018).
8. Li, C. & Baek, J.-B. The promise of hydrogen production from alkaline anion exchange membrane electrolyzers. *Nano Energy* **87,** 106162. ISSN: 2211-2855. https://www.sciencedirect.com/science/article/pii/S2211285521004183 (2021).
9. Hartvigsen, J., Elangovan, S., Elwell, J. & Larsen, D. Oxygen Production from Mars Atmosphere Carbon Dioxide Using Solid Oxide Electrolysis. *ECS Transactions* **78,** 2953–2963. ISSN: 1938-5862 (2017).
10. Lenser, C. *et al.* in *Advanced ceramics for energy conversion and storage* (ed Guillon, O.) 387–547 (Elsevier, Amsterdam, 2019). ISBN: 9780081027264.
11. NI, M., LEUNG, M. & LEUNG, D. Technological development of hydrogen production by solid oxide electrolyzer cell (SOEC). *International Journal of Hydrogen Energy* **33,** 2337–2354. ISSN: 03603199 (2008).
12. *Solid Oxide Fuel Cell Market Size US$ 14.8 Billion by 2030* 11/04/2023. https://www.precedenceresearch.com/solid-oxide-fuel-cell-market.
13. Mukerjee, S., Leah, R., Selby, M., Stevenson, G. & Brandon, N. P. in *Solid oxide fuel cell lifetime and reliability* (ed Brandon, N. P.) 173–191 (Academic Press, Amsterdam, 2017). ISBN: 9780081011027.
14. Tucker, M. C. Progress in metal-supported solid oxide electrolysis cells: A review. *International Journal of Hydrogen Energy* **45,** 24203–24218. ISSN: 03603199. https://www.sciencedirect.com/science/article/pii/S0360319920325106 (2020).
15. Institute of Thermal Engineering, T. G. *Online Call* Personal Communication. 2022.
16. Wang, J., Du, A., Di Yang, Raj, R. & Conrad, H. Grain Boundary Resistivity of Yttria-Stabilized Zirconia at 1400°C. *Journal of Ceramics* **2013,** 1–4. ISSN: 2090-8628 (2013).
17. Hannink, R. H. J., Kelly, P. M. & Muddle, B. C. Transformation Toughening in Zirconia-Containing Ceramics. *Journal of the American Ceramic Society* **83,** 461–487. ISSN: 00027820 (2000).

18. Zakaria, Z. & Kamarudin, S. K. Advanced modification of scandia–stabilized zirconia electrolytes for solid oxide fuel cells application—A review. *International Journal of Energy Research* **45,** 4871–4887. ISSN: 1099-114X (2021).
19. Jaiswal, N. *et al.* A brief review on ceria based solid electrolytes for solid oxide fuel cells. *Journal of Alloys and Compounds* **781,** 984–1005. ISSN: 0925-8388. https://www.sciencedirect.com/science/article/pii/S0925838818345626 (2019).
20. Bernadet, L., Moncasi, C., Torrell, M. & Tarancón, A. High-performing electrolyte-supported symmetrical solid oxide electrolysis cells operating under steam electrolysis and co-electrolysis modes. *International Journal of Hydrogen Energy* **45,** 14208–14217. ISSN: 03603199. https://www.sciencedirect.com/science/article/pii/S0360319920311101 (2020).
21. Grether-Murray, T. *Using Solid Oxide Electrolysis Cells to Scale Green Hydrogen Production* 2022. https://medium.com/@tobias_gm/using-solid-oxide-electrolysis-cells-to-scale-green-hydrogen-production-2055a1770304.
22. Jiang, Y., Chen, F. & Xia, C. A review on cathode processes and materials for electro-reduction of carbon dioxide in solid oxide electrolysis cells. *Journal of Power Sources* **493,** 229713. ISSN: 03787753. https://www.sciencedirect.com/science/article/pii/S0378775321002548 (2021).
23. *Advanced ceramics for energy conversion and storage* (ed Guillon, O.) ISBN: 9780081027264 (Elsevier, Amsterdam, 2019).
24. Li, N. *et al.* Ni-cermet with straight pore paths as cathode for solid oxide electrolysis cell enabling energy-efficient and coking-resistant conversion of CO2. *Journal of Power Sources* **518,** 230787. ISSN: 03787753. https://www.sciencedirect.com/science/article/pii/S0378775321012787 (2022).
25. Khan, M. S., Xu, X., Knibbe, R. & Zhu, Z. Air electrodes and related degradation mechanisms in solid oxide electrolysis and reversible solid oxide cells. *Renewable and Sustainable Energy Reviews* **143,** 110918. ISSN: 13640321. https://www.sciencedirect.com/science/article/pii/S1364032121002112 (2021).
26. P. Fragiacomo, F. Piraino, M. Genovese, O. Corigliano, G. De Lorenzo. Strategic Overview on Fuel Cell-Based Systems for Mobility and Electrolytic Cells for Hydrogen Production. **200,** 1254–1263 (2022).
27. Yokokawa, H. *et al.* Recent Achievements of NEDO Durability Project with an Emphasis on Correlation Between Cathode Overpotential and Ohmic Loss. *Fuel Cells* **17,** 473–497. ISSN: 1615-6854. https://onlinelibrary.wiley.com/doi/10.1002/fuce.201600186 (2017).
28. Ng, K. H., Rahman, H. A. & Somalu, M. R. Review: Enhancement of composite anode materials for low-temperature solid oxide fuels. *International Journal of Hydrogen Energy* **44,** 30692–30704. ISSN: 03603199. https://www.researchgate.net/publication/329565103_Review_Enhancement_of_composite_anode_materials_for_low-temperature_solid_oxide_fuels (2019).
29. Hotflex, M. *Site Visit* Personal Communication. 2022.
30. Shiraki, M., Yakabe, H. & Uchida, H. Efficiency Calculations for SOFC/SOEC Reversible System and Evaluations of Performances of Button-Size Anode-Supported Cell. *ECS Transactions* **57,** 3261–3267. ISSN: 1938-5862 (2013).
31. Daneshpour, R. & Mehrpooya, M. Design and optimization of a combined solar thermophotovoltaic power generation and solid oxide electrolyser for hydrogen production. *Energy Conversion and Management* **176,** 274–286. ISSN: 01968904 (2018).
32. Jolly, S., Tang, E. & Casteel, M. VII.C.4 Modular SOEC System for Efficient Hydrogen Production at High Current Density. https://www.semanticscholar.org/paper/VII.C.4-Modular-SOEC-System-for-Efficient-Hydrogen-Jolly/bdbe5f908712398a11e69cf3b227e9f3a084819c (2018).
33. Tang, E. *et al. Solid Oxide Based Electrolysis and Stack Technology with Ultra-High Electrolysis Current Density (>3A/cm²) and Efficiency* 2018.

34. Fischer, K. & Seume, J. R. Impact of the Temperature Profile on Thermal Stress in a Tubular Solid Oxide Fuel Cell. *Journal of Fuel Cell Science and Technology* **6.** ISSN: 1550-624X (2009).

35. Rathore, S. S., Biswas, S., Fini, D., Kulkarni, A. P. & Giddey, S. Direct ammonia solid-oxide fuel cells: A review of progress and prospects. *International Journal of Hydrogen Energy* **46,** 35365–35384. ISSN: 03603199. https://www.sciencedirect.com/science/article/pii/S0360319921032870 (2021).

36. You, H., Abuliti, A., Ding, X. & Zhou, Y. Reactions of low and middle concentration dry methane over Ni/YSZ anode of solid oxide fuel cell. *Journal of Power Sources* **165,** 722–727. ISSN: 03787753. https://www.sciencedirect.com/science/article/pii/S0378775306025596 (2007).

37. Clarke Energy. *Synthesis gas / syngas* 18/06/2020. https://www.clarke-energy.com/applications/synthesis-gas-syngas/.

38. Brownstein, A. M. in *Renewable motor fuels* (ed Brownstein, A. M.) 33–46 (Elsevier/Butterworth-Heinemann, Amsterdam, 2015). ISBN: 978-0-12-800970-3. https://www.sciencedirect.com/science/article/pii/B9780128009703000042.

39. Muruganandam Loganathan & Murthy Shekhar Shantha. A Review of the Water Gas Shift Reaction Kinetics. *International Journal of Chemical Reactor Engineering.* ISSN: 1542-6580. https://www.degruyter.com/document/doi/10.2202/1542-6580.2238/html (2238).

40. Subotić, V. *et al.* On the origin of degradation in fuel cells and its fast identification by applying unconventional online-monitoring tools. *Applied Energy* **277,** 115603. ISSN: 03062619. https://www.sciencedirect.com/science/article/pii/S0306261920311107 (2020).

41. Bell, I. H., Wronski, J., Quoilin, S. & Lemort, V. Pure and Pseudo-pure Fluid Thermophysical Property Evaluation and the Open-Source Thermophysical Property Library CoolProp. *Industrial & Engineering Chemistry Research* **53,** 2498–2508. eprint: http://pubs.acs.org/doi/pdf/10.1021/ie4033999. http://pubs.acs.org/doi/abs/10.1021/ie4033999 (2014).

42. Chung-Nin Mak, P. *Thermodynamic Properties From Cubic Equations Of State* Master's dissertation (The University of British Columbia, Vancouver, 1985). https://open.library.ubc.ca/media/download/pdf/831/1.0058883/2.

43. Haynes, W. M., Lide, D. R. & Bruno, T. J. *CRC Handbook of Chemistry and Physics* ISBN: 9781315380476. https://www.taylorfrancis.com/books/mono/10.1201/9781315380476/crc-handbook-chemistry-physics-william-haynes (CRC Press, 2016).

44. EPA, U. S., OAQPS & CATC. Nitrogen Oxides (NOx), Why and How They are Controlled. https://www3.epa.gov/ttncatc1/dir1/fnoxdoc.pdf.

45. Hamann, C. H. & Vielstich, W. *Elektrochemie* 4., vollständig überarbeitete und aktualisierte Auflage. ISBN: 3527310681 (Wiley-VCH-Verlag GmbH & Co. KGaA, Weinheim, 2005).

46. Ba, L. *et al.* A study on solid oxide electrolyzer stack and system performance based on alternative mapping models. *International Journal of Hydrogen Energy* **47,** 12469–12486. ISSN: 03603199 (2022).

47. Marina, O. A. *et al.* Electrode Performance in Reversible Solid Oxide Fuel Cells. *Journal of The Electrochemical Society* **154,** B452. ISSN: 1945-7111. https://www.researchgate.net/publication/234895058_Electrode_Performance_in_Reversible_Solid_Oxide_Fuel_Cells (2007).

48. NI, M., Leung, M. K. H. & Leung, D. Y. C. An Electrochemical Model of a Solid Oxide Steam Electrolyzer for Hydrogen Production. *Chemical Engineering & Technology* **29,** 636–642. ISSN: 0930-7516 (2006).

49. Fukumoto, T. *et al. Exchange current density of reversible solid oxide cell electrodes* https://reader.elsevier.com/reader/sd/pii/S0360319922012708?token=19822255767C3C1E4F3F8ACC4C0DBEC1941A58F2A07C9B824293A3D8C2AB3B2B917D3ED5E1484CBFF6C1722B622B73DD&originRegion=eu-west-1&originCreation=20221021075129 (2022).

50. Menon, V., Fu, Q., Janardhanan, V. M. & Deutschmann, O. A model-based understanding of solid-oxide electrolysis cells (SOECs) for syngas production by H2O/CO2 co-electrolysis. *Journal of Power Sources* **274,** 768–781. ISSN: 03787753. https://www.sciencedirect.com/science/article/pii/S0378775314015778 (2015).

51. Pawel Stempien, J., Sun, Q. & Hwa Chan, S. Solid Oxide Electrolyzer Cell Modeling: A Review, 216–246. https://papers.itc.pw.edu.pl/index.php/jpt/article/download/443/557/0 (2013).
52. Shi, H., Su, C., Ran, R., Cao, J. & Shao, Z. Electrolyte materials for intermediate-temperature solid oxide fuel cells. *Progress in Natural Science: Materials International* **30,** 764–774. ISSN: 1002-0071. https://www.sciencedirect.com/science/article/pii/S1002007120304925 (2020).
53. *PlotDigitizer by PORBITAL* https://plotdigitizer.com/app. 2023.
54. KAKAC, S., PRAMUANJAROENKIJ, A. & ZHOU, X. A review of numerical modeling of solid oxide fuel cells. *International Journal of Hydrogen Energy* **32,** 761–786. ISSN: 03603199 (2007).
55. Hajimolana, S. A., Hussain, M. A., Daud, W. A. W., Soroush, M. & Shamiri, A. Mathematical modeling of solid oxide fuel cells: A review. *Renewable and Sustainable Energy Reviews* **15,** 1893–1917. ISSN: 13640321 (2011).
56. Bertei, A. & Nicolella, C. *Common inconsistencies in modeling gas transport in porous electrodes: The dusty-gas model and the Fick law* https://reader.elsevier.com/reader/sd/pii/S0378775315000087?token=9EC0296C190F3616EBA03E39107FC38BC64FA1E17E968602B989E237A70347FEF16DA3179B5251481585CEB864193A8F&originRegion=eu-west-1&originCreation=20230419135217 (2015).
57. Bove, R. & Ubertini, S. Modeling solid oxide fuel cell operation: Approaches, techniques and results. *Journal of Power Sources* **159,** 543–559. ISSN: 03787753 (2006).
58. Krishna, R. & van Baten, J. M. Investigating the validity of the Bosanquet formula for estimation of diffusivities in mesopores. *Chemical Engineering Science* **69,** 684–688. ISSN: 0009-2509. https://www.sciencedirect.com/science/article/pii/S0009250911008256 (2012).
59. James R. Welty, Charles E. Wicks, Robert E. Wilson, Gregory L. Rorrer. *Wilson and Rorrer, Fundamentals of Momentum, heat and Mass Transfer. Fifth Edition* 5th ed. ISBN: 978-0470128688 (Wiley, 2008).
60. Fu, Y. *et al.* Multicomponent Gas Diffusion in Porous Electrodes. *Journal of The Electrochemical Society* **162,** F613–F621. ISSN: 1945-7111 (2015).
61. Cox, K. R. & Chapman, W. G. The Properties of Gases and Liquids, 5th Edition By Bruce E. Poling (University of Toledo), John M. Prausnitz (University of California at Berkeley), and John P. O'Connell (University of Virginia). McGraw-Hill: New York. 2001. 768 pp. $115.00. ISBN 0-07-011682-2. *Journal of the American Chemical Society* **123,** 6745. ISSN: 0002-7863 (2001).
62. Engineering Units. *Log Mean Temperature Difference Calculator - Engineering Units* 2020. https://engineeringunits.com/log-mean-temperature-difference-calculator/.
63. Perry, R. H. & Green Don W. *Perry's Chemical Engineers' Handbook* 7th ed. (McCraw-Hill, New York, 1997).
64. Cai, Q., Adjiman, C. S. & Brandon, N. P. Optimal control strategies for hydrogen production when coupling solid oxide electrolysers with intermittent renewable energies. *Journal of Power Sources* **268,** 212–224. ISSN: 03787753. https://www.sciencedirect.com/science/article/pii/S0378775314008817 (2014).
65. AlZahrani, A. A. & Dincer, I. Modeling and performance optimization of a solid oxide electrolysis system for hydrogen production. *Applied Energy* **225,** 471–485. ISSN: 03062619. https://reader.elsevier.com/reader/sd/pii/S030626191830686X?token=9783FD895931064FBCE69FB5722DFA77271B05B752DC71569130587439538 6B5F485F389FFF76D63B10F4242D3299CAC&originRegion=eu-west-1&originCreation=20230202103121 (2018).
66. Fragiacomo, P., Piraino, F., Genovese, M., Corigliano, O. & de Lorenzo, G. *Strategic Overview on Fuel Cell-Based Systems for Mobility and Electrolytic Cells for Hydrogen Production* https://reader.elsevier.com/reader/sd/pii/S1877050922003350?token=1DBF1A90DFA55DC0952376889A89A398B9243CAF510D20AAC2D548D60E8C52FE909B0CACBEF4661EAFCC1D316880A895&originRegion=eu-west-1&originCreation=20221208161701 (2022).

67. Hernández-Pacheco, E., Singh, D., Hutton, P. N., Patel, N. & Mann, M. D. A macro-level model for determining the performance characteristics of solid oxide fuel cells. *Journal of Power Sources* **138,** 174–186. ISSN: 03787753. https://www.sciencedirect.com/science/article/pii/S0378775304007098 (2004).

68. Iwata, M. Performance analysis of planar-type unit SOFC considering current and temperature distributions. *Solid State Ionics* **132,** 297–308. ISSN: 0167-2738. https://www.sciencedirect.com/science/article/pii/S0167273800006457 (2000).

69. Tangsriwong, K. *et al. Modeling of chemical processes using commercial and open-source software: A comparison between Aspen Plus and DWSIM* in *IOP Conference Series: Earth and Environmental Science* **463** (2020), 012057.

A

Appendix A - Ohmic Overpotential Comparison

This appendix contains a worked out proof that in the ohmic overpotential, the electrolyte overpotential dominates and electrical overpotential can be neglected. This can be done by comparing the area resistance of both the electrode and electrolyte to each other.

The resistance of an electrical conductor as a function of its geometry can be described by:

$$R = \frac{\rho \cdot l}{A} \tag{A.1}$$

Where:
R is the resistance of the conducting material [Ω]
ρ is the electrical resistivity of the conducting material [Ωm]
l is the length of the conducting material [m]
A is the cross sectional area of the conducting materials [m^2]

The electrical resistivity, ρ, of a material changes with temperature. The equation for this is:

$$\rho = \rho_0 \cdot (1 + \alpha \cdot (T - T_0)) \tag{A.2}$$

Where:
ρ is the electrical resistivity of the conducting material [Ωm]
ρ_0 is the reference electrical resistivity of the conducting material [Ωm]
α is the temperature coefficient of resistance for the conducting material [Ω/m K]
T is the operating temperature [K]
T_0 is the reference temperature [K]

Assuming the connection between the electrode and bipolar plate is achieved via the metallic particles contained in the electrode, which are typically made from nickle, the the following values can be used:

What	Value
α_{Ni}	0.005866 [Ωm/K]
ρ_0	7x10^{-8} [Ωm]
T_0	293.15 [K]

Assume 1% the surface area of a reference cell (i.e. active area is 1 m^2) is nickle particles, with the electrode thickness being 50 μm. Then letting the electrical paths being four times longer than the thickness of the electrode, for the operating temperature of SOC, $\pm$1073 K, the the electrical resistance can be calculated:

$$\rho = \rho_0 \cdot (1 + \alpha \cdot (T - T_0))$$
$$\rho = 7 \cdot 10^{-8} \cdot (1 + 0.005866 \cdot (1073 - 293.15))$$
$$\rho = 3.9022 \cdot 10^{-7}\ \Omega\text{m}$$
$$R = \frac{\rho \cdot l}{A}$$
$$R = \frac{3.9022 \cdot 10^{-7} \cdot (4 \cdot 50 \cdot 10^{-6})}{1\%}$$
$$R = 9.44692 \cdot 10^{-9}\ \Omega\text{m}^2$$

For an electrolyte material, say 8YSZ, the data for which can be taken from Table 3.3, the area resistance can be determined using the method provided in subsubsection 3.1.2.3 (the equations for which will be repeated here for convince). Assume the thickness of the electrolyte is 200 μm and the cell operates at 1073 K.

Material	σ_0 [S/m]	E_{el} [J/mol]
8YSZ	133 117 255.5	96 611.97

$$\sigma_{mem} = \frac{\sigma_0}{T} \cdot \exp\left(\frac{-E_{el}}{R \cdot T}\right)$$

Where:
σ_{mem} is the conductivity of the membrane [S/m]
σ_0 is the pre-exponential factor of the conductivity [S/m]
T is the temperate of the membrane [K]
E_{el} is the activation energy for ion transport [J/mol]
R is the universal gas constant [J/mol K]

$$R_{mem} = \frac{l_{mem}}{\sigma_{mem}}$$

Where:
R_{mem} is the ohmic resistance of membrane [Ωm^2]
l_{mem} is the thickness of the membrane [m]
σ_{mem} is the membrane conductivity [S/m]

Calculating the electrolyte resistance:

$$\sigma_{mem} = \frac{\sigma_0}{T} \cdot \exp\left(\frac{-E_{el}}{R \cdot T}\right)$$
$$\sigma_{mem} = \frac{133117255.5}{1073} \cdot \exp\left(\frac{-96611.97}{8.3145 \cdot 1073}\right)$$
$$\sigma_{mem} = 2.45791\ \text{S/m}$$
$$R_{mem} = \frac{l_{mem}}{\sigma_{mem}}$$
$$R_{mem} = \frac{200 \cdot 10^{-6}}{2.45791}$$
$$R_{mem} = 8.1370 \cdot 10^{-5}\ \Omega\text{m}^2$$

Comparing the values from electrical resistance and electrolyte resistance, it can be seen that the resistance value for the membrane/electrolyte is orders of magnitude higher than for the electrical resistance. As such, the overpotential from the electrolyte will be the dominant ohmic overpotential.

B

Appendix B - Exchange Current Density Verification Plots

All figures shown in this appendix show the relation between humidity or oxygen concentration and electrode exchange current density. The solid line is the exchange current density values the detailed model uses. The model used to determine the exchange current density is the same as the curve fit model from [49]. The individual data points are taken from [49]. The equation which the data points are curve fit to in [49] is shown in subsubsection 3.1.2.2, and a generalised form of the equation is and repeated here for convince:

$$i_{0,w} = r_w \cdot \Pi_{k=1} \left(\frac{y_{q_k}}{y_{q_k,ref}} \right)^{A_k} \cdot \exp\left(-\frac{E_{a,w}}{RT} \right) \tag{B.1}$$

Where:
$i_{0,w}$ is the exchange current density at the w electrode [A/cm^2]
w is the electrode. Can either be fuel or oxygen electrode
r_w is the reaction rate constant for the w electrode [-]
y_{q_k} is the molar fraction of species q_k [-]
k is a numerical indication of a species at an electrode [-]
$y_{q_k,ref}$ is the molar fraction of q_k in the reference conditions [-]
A_k is a gas concentration exponent which is determined by fitting the equation to data [-]
$E_{a,w}$ is the activation energy of the species reacting at the w electrode [J/mol]
R is the universal gas constant [J/mol K]
T is the temperature [K]
k is a reference to a species which exists at electrode w

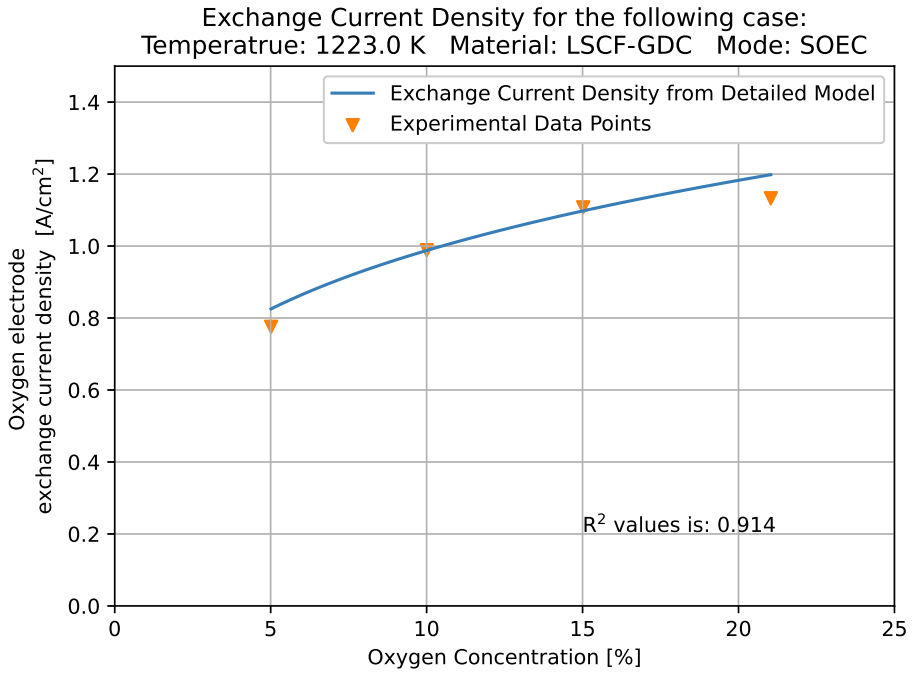

Figure B.1

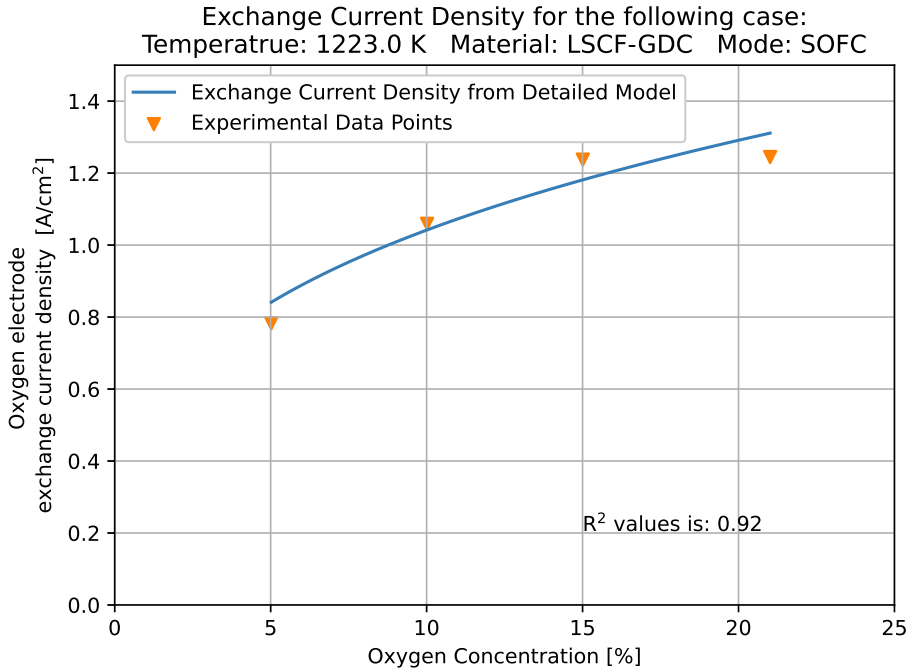

Figure B.2

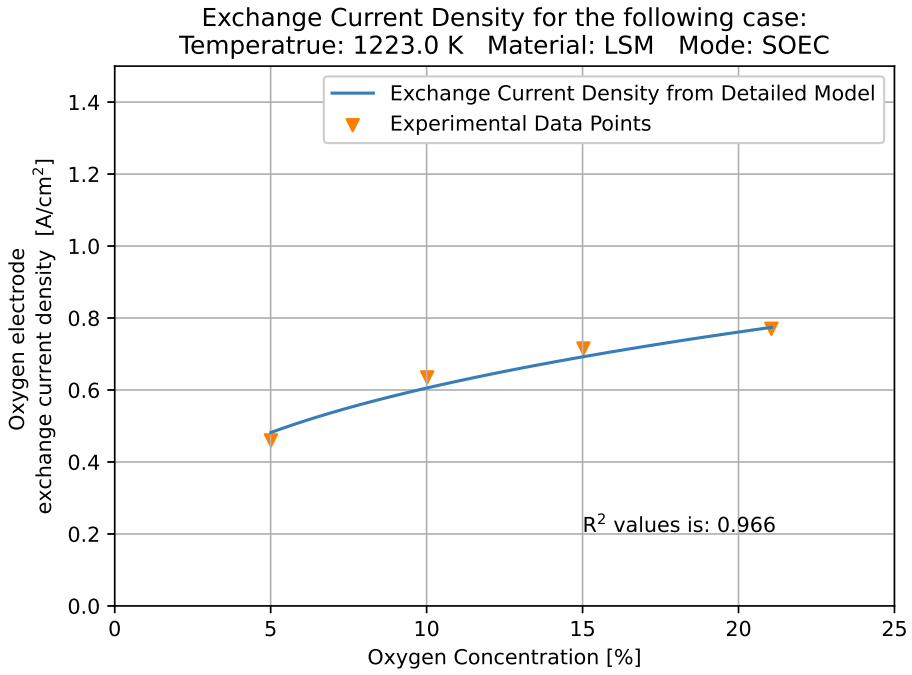

Figure B.3

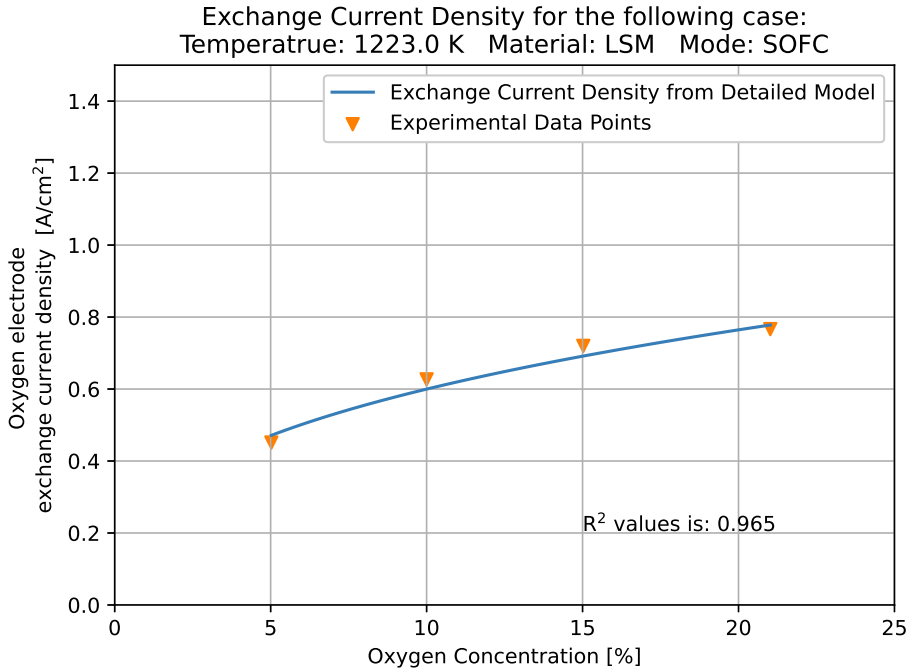

Figure B.4

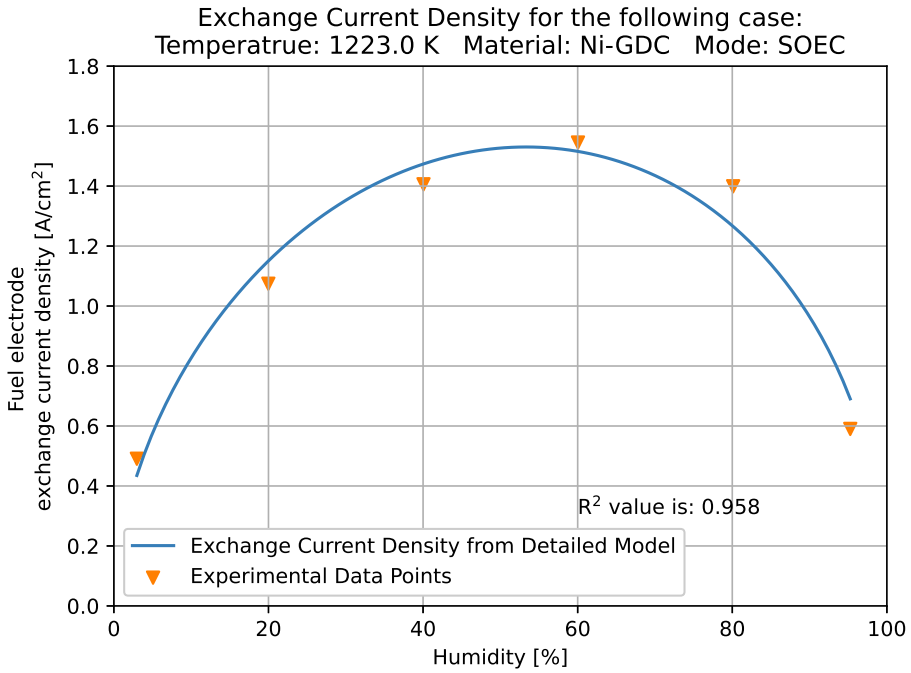

Figure B.5

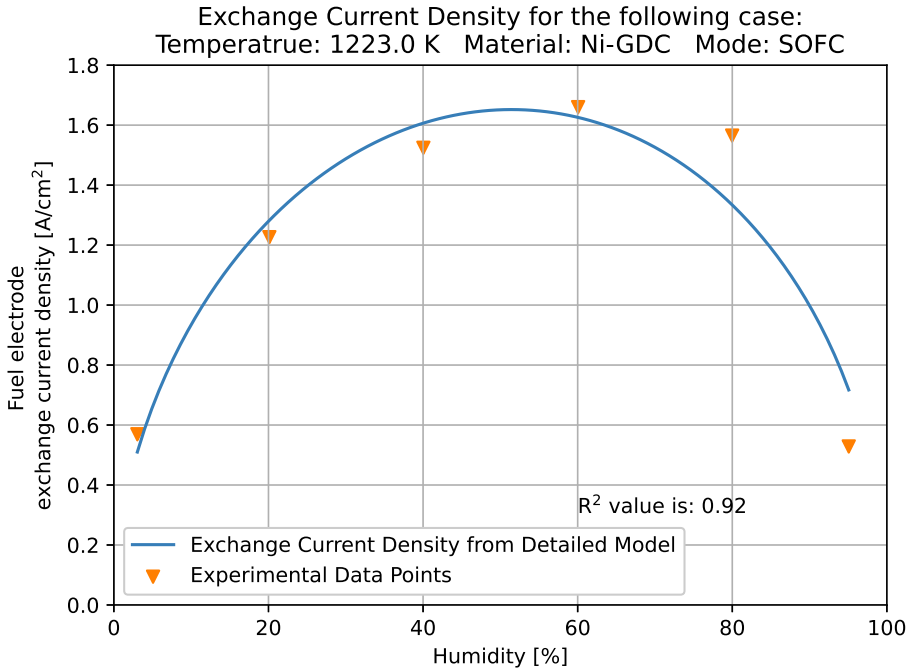

Figure B.6

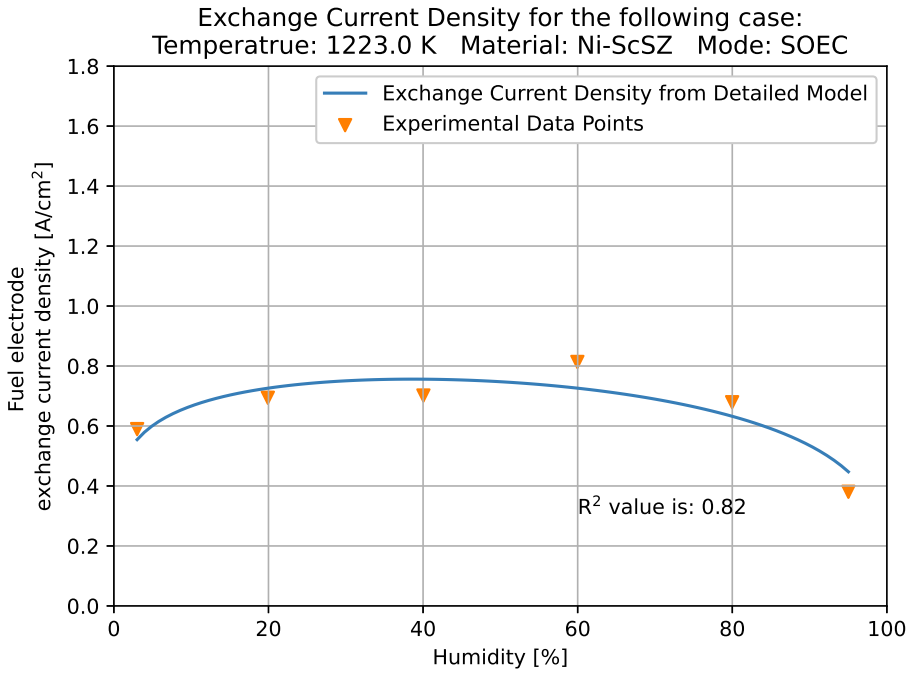

Figure B.7

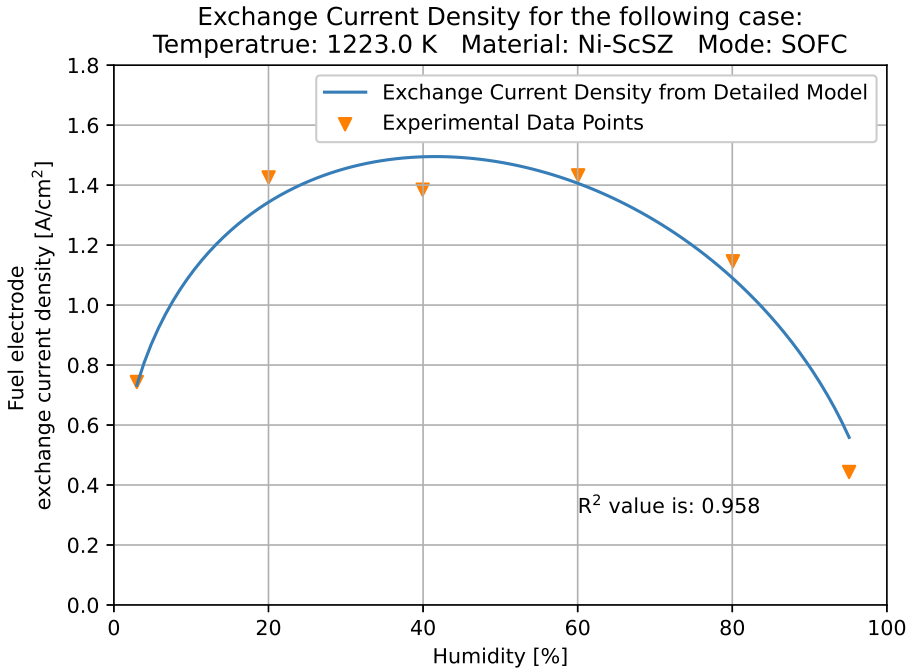

Figure B.8

C

Appendix C - Impact of Charge Transfer Coefficient Variation

In the Butler-Volmer equation, typical values for the charge transfer coefficients used are 0.5 for both the anodic and cathodic reactions at both electrodes, as explained in subsubsection 3.1.2.2. While this is the standard approach to activation overpotential modelling, this appendix will quantify the order of magnitude in error in deviating from this value. The activation overpotential from both the cathode and anode for various charge transfer coefficient values can be seen in Figure C.1. It should be noted that the overpotential is calculated in electrolysis mode and therefore the overpotentials are negative. If the activation overpotentials were for fuel cell mode, the overpotentials would be positive. The exchange current density values used for the cathode and anode are 0.0466 A/cm^2 and 0.0591 A/cm^2 respectively. The temperature of operation is 1073 K.

As can be seen in Figure C.1, the smallest activation overpotential for the cathode and anode electrode (at 1.5 A/cm^2), is (-)0.178 V and (-)0.167 V respectively. The maximum activation overpotential for the cathode and anode electrode (at 1.5 A/cm^2) is (-)1.6 V and (-)1.5 V respectively. The default case (charge transfer coefficients equal at 0.5) for the cathode and anode (at 1.5 A/cm^2) is (-)0.32 V and (-0.299) V. For the presented range of charge transfer coefficients, the variation in overpotential can be seen in Table C.1. As the Nernst equation gives a minimum voltage for electrolysis of water, which at 800°C is (-)0.977 V, the variations in activation overpotential for changing charge transfer coefficients are significant.

Table C.1: Difference in activation overpotential for various charge transfer coefficients

	Default case [V]	Minimum overpotential case [V]	Absolute difference between default and minimum case [V]	Maximum overpotential case [V]	Absolute difference between default and maximum case [V]
Cathode	(-)0.32	(-)0.178	(-)0.142	(-)1.6	(-)1.28
Anode	(-)0.299	(-)0.167	(-)1.371	(-)1.5	(-)1.201

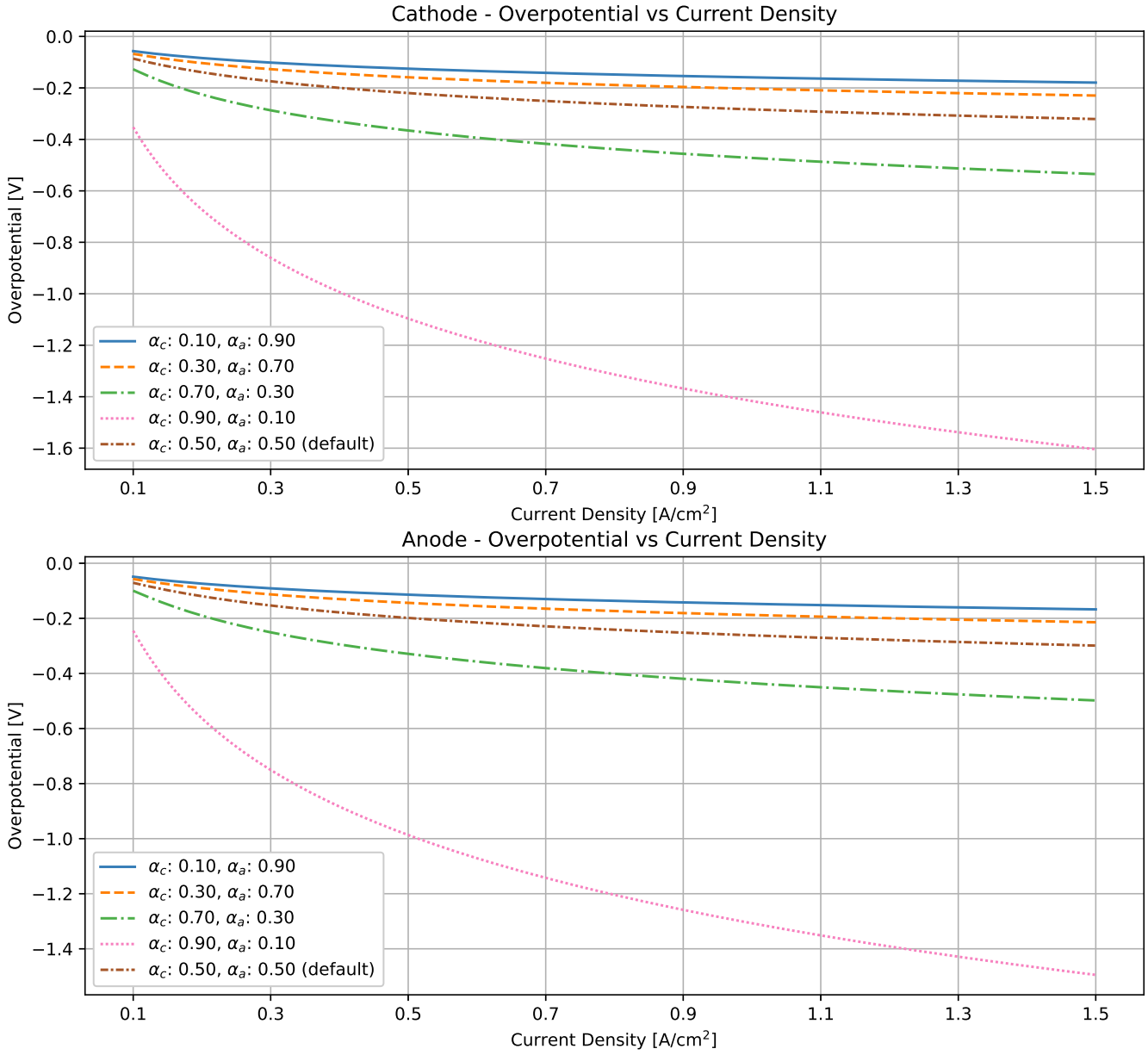

Figure C.1: Overpotential (in electrolysis mode) at the cathode and anode for various charge transfer coefficients. α_c and α_a are the charge transfer coefficients for the cathodic and anodic reactions at the electrodes respectively. The exchange current density values used for the cathode and anode are 0.0466 A/cm^2 and 0.0591 A/cm^2 respectively. The temperature of operation is 1073 K.

D

Appendix D - SOEC System Run Settings

The system operation conditions for the efficiency curves shown in subsection 3.1.4.

Settings which are constant between all four cases

- Cell settings:
  - Operation temperature: 1073 K
  - Operation pressure: 1.0 bar
  - Mode: Water electrolysis mode
  - Membrane thickness: 10 μm
  - Membrane material: 8YSZ
  - Cathode thickness: 10 μm
  - Cathode porosity: 0.25
  - Cathode tourtorosity: 15
  - Cathode pore radius: 0.4
  - Anode thickness: 40 μm
  - Anode porosity: 0.34
  - Anode tourtorosity: 10
  - Anode pore radius: 0.5 μm
  - Diffusion model: Fick's Diffusion
  - Diffusion modelled for activation overpotential: True
- System settings:
  - Maximum System power: 500 000 W
  - Anode inflow temperature: 300 K
  - Design current density: 1.0 A/cm^2
  - Overflow (how much additional flow is provided over what is minimally required for electrolysis): 2
  - Cell area: 100 cm^2
  - Standby power %: 5
  - Reference Temperature: 300 K
  - Industry flow pressure: 101325 Pa
  - Pump pressure difference: 6000 Pa
  - Anode pump efficiency: 70%
  - Cathode pump efficiency: 70%
  - Anode trim heater efficiency: 85%
  - Cathode trim heater efficiency: 85%
  - Anode heat exchanger efficiency: 70%
  - Cathode heat exchanger efficiency: 70%

  - Vaporiser efficiency: 70%

Settings which changed between runs are:

- Cathode inflow temperature:
  - 300 K
  - 400 K
- Control method:
  - Stacks same
  - irho design
- Minimum current density:
  - 0.3 A/cm^2 for stacks same method
  - 0.8 A/cm^2 for irho design
- Maximum current density:
  - 1.0 A/cm^2 for stacks same method
  - 1.2 A/cm^2 for irho design